Eirik Haneset Nygård

Method Development for Rapid Determination of Organophosphorus Flame Retardant Exposure in Harbor Porpoises Along the Norwegian Coast

June 2020

NTNU
Norwegian University of
Science and Technology

NTNU
Norwegian University of
Science and Technology

NTNU
Norwegian University of Science and Technology

Method Development for Rapid Determination of Organophosphorus Flame Retardant Exposure in Harbor Porpoises Along the Norwegian Coast

Eirik Haneset Nygård

Abstract

Utilizing UHPLC-QqQ-MS/MS and liquid-liquid extraction as rapid and efficient methods of determining chemical occurrence, this study aims to shed light on the marine spread of organophosphorus flame retardants, PFRs, a flame retarding additive often used in polymers. The liver of harbor porpoises caught as bycatch along the Norwegian coast were in this study analyzed the presence of 21 different PFRs and metabolites.

Due to COVID-19 large parts of the planned activities could not be carried out, hence methods used in this study has room for improvement that is necessary to more accurately describe the occurrence of PFRs in the marine environment and harbor porpoises. However, this study offers insight into the possible presence of tri-n-butyl phosphate, TnBP, triphenyl phosphate, TPP, and the metabolite of tris(2-butoxyethyl) phosphate, TBOEP, bis(2-butoxyethyl)hydroxyethyl phosphate BBOEHEP, in the liver of the porpoises. There are some weak indications that IDPP, TCIPP, TBOEP and BPA-BDPP might be present in the matrix. This study also offers insight in the presence of TEHP, TDCIPP and EHDP in the instrument, and that TMP, TEP, RDP, TTBPP, DPMP and maybe TBOEP pollution may occur during the extraction process due to large reagent blank peaks. These are common additives in laboratory plastic equipment, which might be the origin of the pollution. All of these insights should be more thoroughly investigated. During sample preparation it was found that ethylacetate is superior to DCM:HEX for liquid-liquid extraction of PFRs.

Finally, this study also includes proposed fragment ion structures for all PFRs included in this research project, and recommendations for quantification and confirmation ions for high throughput PFR chemical analysis.

Keywords: Organophosphorus Flame Retardants, Liquid-liquid extraction, MS/MS Product Ion Structure Elucidation, Method Development, Harbor Porpoises.

Sammendrag

Ved å bruke UHPLC-QqQ-MS/MS og væske-væske ekstraksjon som raske og effektive metoder for å bestemme kjemisk tilstedeværelse, sikter denne studien på å utvikle feltet rundt marin spredning av organofosforerte flammehemmere, PFR, et flammehemmende tilsetningstoff som ofte blir brukt i polymerer. Leveren til niser fra utilsiktet fangst fra norskekysten ble i denne studien analysert for 21 forskjellige PFRer og metabolitter.

På grunn av COVID-19 ble store deler av de planlagte aktivitetene kansellert, så metoden brukt i denne studien har store muligheter for utvikling som er nødvendig for en mer nøyaktig beskrivelse av tilstedeværlesen av PFR i det marine miljøet og niser. Likevel, gir studien insikt rundt den mulige tilstedeværelsen av tri-n-butyl fosfat, TnBP, trifenyl phosphate, TPP, og metabolitten til tris(2-butoxyetyl) fosfat, TBOEP, bis(2-butoxyetyl) fosfat, BBOEHEP, i leveren til niser. Det ble funnet svake indikasjoner at IDPP, TCIPP, TBOEP and BPA-BDPP også kan være tilstede i matrisen. Denne studien gir også innsikt i tilstedeværelsen av IDPP, TCIPP, TBOEP og BPA-BDPP i analyse instrumentent, og at TMP, TEP, TTBPP, DPMP og kanskje TBOEP forurensning skjer under ekstraksjons prosessen på grunn av store signaler i reagens blindprøve. Disse er vanlige tilsetningstoffer i plastutstyr på labaratorier, noe som kan være årsaken til denne forurensningen. Alle disse innsiktene burde studeres nøyere. Fra prøve forberedelse metodeutviklingen ble det funnet at etylacetat er bedre enn DCM:HEX for væske-væske ekstraksjon av PFRer.

Til slutt inkluderer denne studien forslag til produkt fragment ion strukturer for alle PFRene inkludert i dette forskningsprosjektet, og hvilke ioner som burde brukes som kvantifikasjon og kvalifikasjons ioner i høykapasitets PFR kjemisk analyse.

Contents

1 Introduction

The spread of microplastics and other pollutants in the marine environment has seen a resurgence in the public domain in recent years. Whereas previously the main focus was on heavy metals, microplastics and other polymer originating pollutants are now gaining traction. Organophosphorus flame retardants, PFRs, is a polymer additive that is used to increase the material's flame retardancy and was one of the types of flame retardants recommended to substitute polybrominated diphenyl ethers, PBDEs, after the Stockholm Convention restricted and banned their usage based on toxicity and persistence in nature in the early 2000s. (POPRC, 2008). However, PFRs might be a regrettable subsititute as new discoveries offers insights into the unfortunate toxicity and persistence of PFRs. (Blum et al., 2019)

The aim of this project is to investigate the spread of PFRs in the marine environment by determining their presence in harbor porpoises along the Norwegian coast using UHPLC-MS/MS and liquid-liquid extraction. Unfortunately, COVID-19 cancelled large parts of planned activites, including using the optimized extraction method to analyze liver, blubber or muscle from 124 individual harbor porpoises depending on which matrix yielded better results from planned preliminary testing.

This is the second part of a two part project, where the first optimized a rapid LC-MS/MS method and the second part was initially planned to determine the concentration of PFRs in harbor porpoises from the Norwegian coast by optimizing an extraction method. The results from the first part of the project are described in Nygård (2019) and determined the LC-MS/MS method used in the analyzation of PFRs in this second part. Two liquid-liquid extraction methods were tested, where ethylacetate yielded better results than DCM:HEX (1:1).

This study offer insight into the possible presence of TnBP, TPP and BBOEHEP in the liver of harbor porpoises. IDPP, TCIPP, TBOEP and BPA-BDPP might also be found in the same matrix. TEHP, TDCIPP and EHDP should be further investigated in other instruments or with another method in order to shed insight into whether the instrument contains these compounds, making the determination of these compounds in matrices difficult. TMP, TEP, RDP, TTBPP, DPMP and TBOEP seem to present during the extraction method and pollutes the samples.

Major parts of this study also involves suggestions for daughter ion structure elucidation based on MS spectra for all PFRs analyzed. These suggested structures are paired with recommendations for quantification and confirmation ions for assisting future high throughput PFR chemical analysis.

This second part of the project concludes my master thesis in the university program Industrial Chemistry and Biotechnology at NTNU, Trondheim, Norway.

2 Background

2.1 Polymer Additives and Emerging Contaminants

Synthethic polymers has been around for more than a hundred years, starting with Bakelite by the chemist Leo Baekeland in 1907. Since then development of new types of polymers has become an abundance and there's a type of polymer fitting for just about any application necessary. One of the reasons polymers can be used in such a variety of applications are polymer additives such as stabilizers, lubricants, plasticizers and flame retardants because their properties are very adjustable to fit each purpose. These additives can protect the polymer from thermal or light-assisted oxidation, alter the overall rheology or increase the flame retardancy. (Hunt, 2000)

These additives are not always chemically bound to the polymer and can therefore be extractable, through for instance thermal desorption or leaching, by being in the presence of water, oil, salts or other organic compounds. Leaching of polymer additive compounds are of major concern to the polymer industry and society as many of the these compounds show hazardous effects in humans such as endocrine disruption, suspected carcinogenic effects and more. (Bolgar et al., 2015)

As many polymer additives and other Persistant Organic Pollutants (POPs) have adverse effects in humans the Stockholm Convention banned and restricted the use of many compounds that had showed toxic effects and persistence in nature. Among the compounds restricted in the Stockholm convention are pesticides such as dieldrin and aldrin, and flame retardants such as poly brominated diphenyl ethers (PBDEs). Decabromodiphenyl ether (decaBDE), a PBDE, was one of the flame retardants banned in the stockholm convention in 2001. Flame retardants are required to adhere to fire regulations for different materials. When decaBDE and several other PBDEs were banned or restricted, Bisphenol A bis(diphenyl phosphate) (BPA-BDP), Resorcinol bis(diphenyl phosphate) (RDP), Triphenyl phosphate (TPP) and aluminium trihydroxide (ATH), most of which are Organophosphorus Flame Retardants (PFRs), were recommended as substitute flame retardants. (UNEP/POPS/POPRC, 2015). Since then production of additional forms of PBDEs has been restricted or voluntarily phased out by industry. (Dodson et al., 2012)

2.2 Organophosphate Flame Retardants, PFRs

PFRs consist of a core phosphorus atom connected to three, often identical, ester groups. Due to the variety in ester groups attached the Log K_{ow} values differ significantly. The smallest compound TMP (Trimethyl Phosphate) has a Log K_{ow} value of -0.60, while TTBPP (Tris(4-*tert*-butylphenyl) Phosphate) has a Log K_{ow} value of 10.43. This large range of Log K_{ow} significantly impact their behaviour in a marine environment. See fig. 1 for general structure of PFRs and table 1 for specific structures.
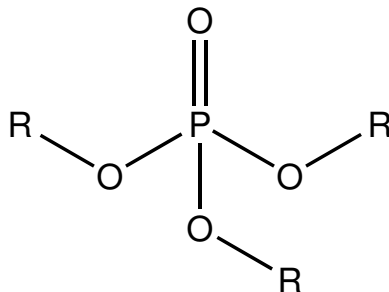
Figure 1: General structure of PFRs, a core phosphorus atom with three ester groups.

2.2.1 Use and Production

As many regions around the world adopt increasingly stringent fire safety policies, production volumes of flame retardants (FR) are increasing to meet demand. Between 2009 and 2018 global demand for flame retardants rose from 1.7 to 2.6 million tonnes, making it a 4.5% annual increase. It is expected to continue growing by 3.7% annually to 3.1 million tonnes by 2023, where PFRs are estimated to account for 16% of market share, while in 2006 PFRs accounted for 20%. (Thomas et al., 2017; Freedonia, 2011; McWilliams, 2018; van der Veen and de Boer, 2012).
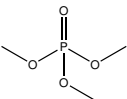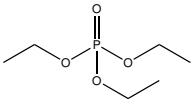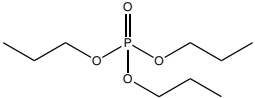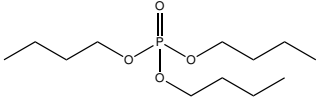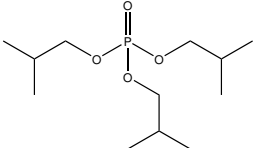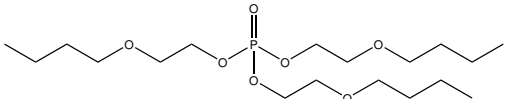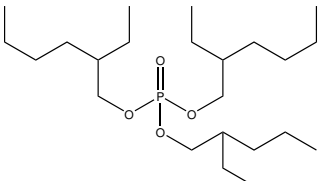
2.2.2 Exposure and Effects

Several studies document human exposure to PFRs in indoor environment where leaching, volatilization and abrasion all constitute pathways to exposure. (Wensing et al., 2005; Marklund et al., 2003). Waste water treatment plants (WWTP) and other industrial discharge of PFRs to the aquatic environment have also been documented. (Cristale et al., 2016; Meyer and Bester, 2004).
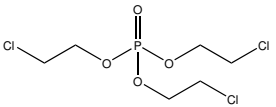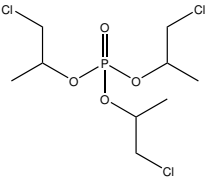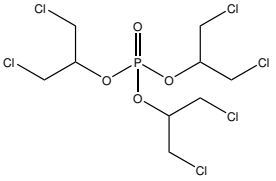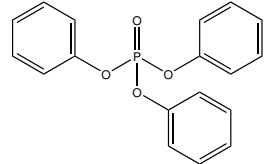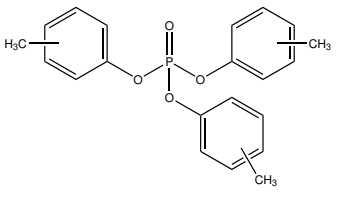
Chlorinated-PFRs have been called a regrettable substitution to PBDEs because of indications of their toxic effects and persistence in water. It has also been suggested that PFRs should be classified as persistent mobile organic compounds (PMOC). (Blum et al., 2019).

Organophosphorus compounds are linked to oxidative stress, acetylcholinesterase inhibition and can cause releases of β-glucuronidase into plasma. (Soltaninejad et al., 2007; Banerjee et al., 1999). Decrease in full scale IQ scores and working memory of children at 7 years have been linked to elevated DPP concentrations of their birthing mother during pregnancy. (Castorina et al., 2017). Other life-long effects of PFR exposure are also indicated in multiple other studies. (Hoffman et al., 2018; Alzualde et al., 2018).
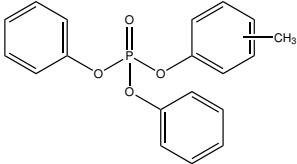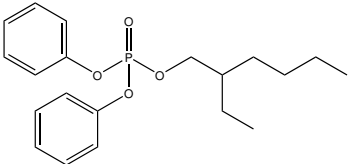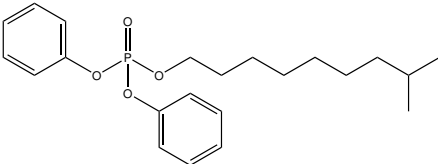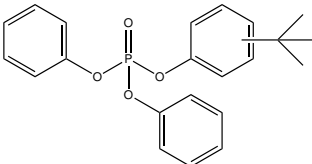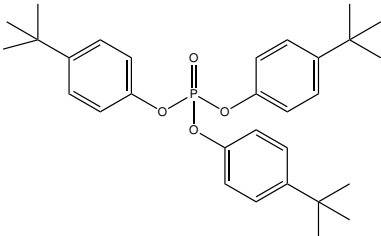
Table 1: Name (abbr.), molecular structure, molecular formula, molecular weight, solubility factor and CAS number of all analytes tested in this project.

Chemical	Molecular Structure	Molecular Formula	Molecular weight (g mol^{-1})	Log K$_{ow}$	CAS number
Trimethyl Phosphate (TMP)		$C_3H_9O_4P$	140.07	-0.60	512-56-1
Triethyl Phosphate (TEP)		$C_6H_{15}O_4P$	182.15	0.87	78-40-0
Tri-*n*-propyl Phosphate (TnPP)		$C_9H_{21}O_4P$	224.23	2.35	513-08-6
Tri-*n*-butyl Phosphate (TnBP)		$C_{12}H_{27}O_4P$	266.31	3.82	126-73-8
Triisobutyl Phosphate (TiBP)		$C_{12}H_{27}O_4P$	266.31	3.60	126-71-6
Tris(2-butoxyethyl) Phosphate (TBOEP)		$C_{18}H_{39}O_7P$	398.47	3.00	78-51-3
Tris(2-ethylhexyl) Phosphate (TEHP)		$C_{24}H_{51}O_4P$	434.63	9.49	78-42-2
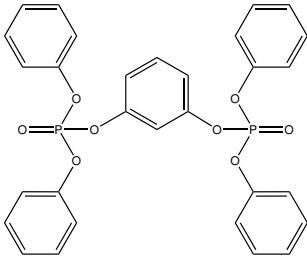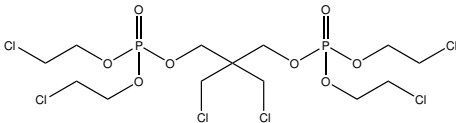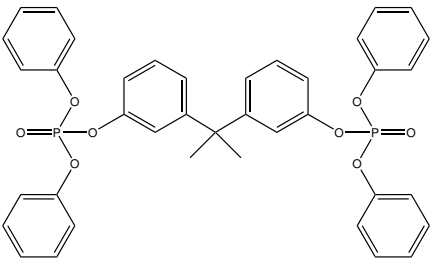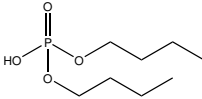
(Continued)

Chemical	Molecular Structure	Molecular Formula	Molecular weight (g mol^{-1})	Log K$_{ow}$	CAS number
Tris(2-chloroethyl) Phosphate (TCEP)		$C_6H_{12}Cl_3O_4P$	285.49	1.63	115-96-8
Tris(1-chloro-2-propyl) Phosphate (TCIPP)		$C_9H_{18}Cl_3O_4P$	327.57	2.89	13674-84-5
Tris(1,3-dichloro-2-propyl) Phosphate (TDCIPP)		$C_9H_{15}Cl_6O_4P$	430.90	3.65	13674-87-8
Triphenyl Phosphate (TPP)		$C_{18}H_{15}O_4P$	326.28	4.70	115-86-6
Tritolyl Phosphate (TMPP)		$C_{21}H_{21}O_4P$	368.37	6.34	1330-78-5

(Continued)

Chemical	Molecular Structure	Molecular Formula	Molecular weight (g mol^{-1})	Log K$_{ow}$	CAS number
Diphenyltolyl Phosphate (DPMP)		C$_{19}$H$_{17}$O$_4$P	340.32	5.25	26444-49-5
2-Ethylhexyldiphenyl Phosphate (EHDP)		C$_{20}$H$_{27}$O$_4$P	362.40	6.30	1241-94-7
Isodecyldiphenyl Phosphate (IDPP)		C$_{22}$H$_{31}$O$_4$P	390.46	7.28	29761-21-5
tert-Butylphenyldiphenyl Phosphate (BPDP)		C$_{22}$H$_{23}$O$_4$P	382.40	6.61	56803-37-3
Tris(4-*tert*-butylphenyl) Phosphate (TTBPP)		C$_{30}$H$_{39}$O$_4$P	494.60	10.43	78-33-1

(Continued)

Chemical	Molecular Structure	Molecular Formula	Molecular weight (g mol^{-1})	Log K$_{ow}$	CAS number
Tetraphenylrecorcinol bis(diphenyl Phosphate) (RDP)		$C_{30}H_{24}O_8P_2$	574.45	7.41	57583-54-7
2,2-Bis(chloromethyl)-1,3-propandiol bis[bis(2-chloroethyl) Phosphate] (V6)		$C_{13}H_{24}Cl_6O_8P_2$	582.99	3.31	38051-10-4
Bisphenol A bis[(diphenyl) Phosphate] (BPA-BDPP)		$C_{39}H_{34}O_8P_2$	692.63	4.5	5945-33-5
Metabolites					
Di-*n*-butyl Phosphate (DnBP)		$C_8H_{19}O_4P$	210.21	2.29	107-66-4

(Continued)
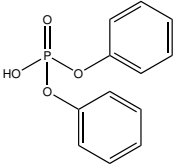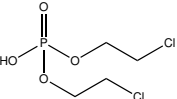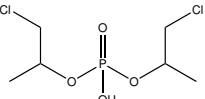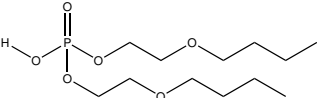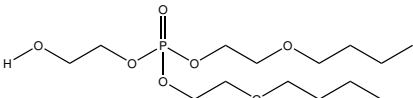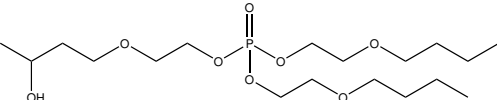
Chemical	Molecular Structure	Molecular Formula	Molecular weight (g mol^{-1})	Log K$_{ow}$	CAS number
Diphenyl Phosphate (DPP)		$C_{12}H_{11}O_4P$	250.19	2.28	838-85-7
Bis(2-chloroethyl) Phosphate (BCEP)		$C_4H_9Cl_2O_4P$	222.99	0.83	3040-56-0
Bis(2-chloropropyl) Phosphate (BCIPP)		$C_6H_{13}Cl_2O_4P$	251.04	Missing	789440-10-4
Bis(2-butoxyethyl) Phosphate (BBOEP)		$C_{12}H_{27}O_6P$	298.31	1.74	14260-97-0
Bis(2-butoxyethyl) hydroxyethyl Phosphate (BBOEHEP)		$C_{14}H_{31}O_7P$	342.37	Missing	1477494-86-2
Bis(2-butoxyethyl) hydroxy-2-butoxyethyl Phosphate (3OH-BOEP)		$C_{18}H_{39}O_8P$	414.47	Missing	1477494-87-3

Table gathered from the pre-project. (Nygård, 2019)

2.3 Study Population: Harbor Porpoises (Phocoena phocoena)

PFRs have been investigated in cetaceans before. Papachlimitzou et al. (2015) detected 6 out of 20 PFRs tested in harbor porpoises in the UK from 2012. The highest quantified concentration was found to be $246\,\mu\mathrm{g\,kg^{-1}}$ lw in the blubber.

Sala et al. (2019) detected PFRs in all 11 tested individuals of (*Delphinus delphis*) in the Alboran Sea, Spain, and found the presence of 12 of the 16 PFRs tested. The concentration levels found reached up to $24.7\,\mu\mathrm{g/g}$ lw and the highest concentration of dry weight was found in the blubber. Since PFRs has lower biomagnification potential and lower production volumes than other halogenated flame retardants, the concentration of PFRs should be expected to be significantly lower in the same individuals, however this is not the case. Sala et al. (2019) indicated therefore that there might be an additional source of PFR pollution in addition to their flame retardant usage.

Harbor Porpoises (*Phocoena phocoena*) is a cetacean and top predator with a high trophic level and have been shown to accumulate pollutants such as PBDEs and heavy metals in their fatty tissue. (Strand et al., 2005; Pierce et al., 2008) As harbor porpoises generally reside in coastal regions and don't migrate a lot they are exposed to several negative antrophogenic effects such as chemical pollution, ship traffic, overfishing and noise. Another way harbor porpoises are affected by human activities is bycatch, of which there is a high incidental occurrence. However, *Phocoena phocoena* are categorized as a species of least concern due to their large population, which is estimated at 300,000 to 700,000 individuals worldwide. (Bjørge and Tolley, 2018; Hammond et al., 2008)

2.4 Method Development

Method development in chemical bioanalysis can generally be separated into three main developmental sections - MS/MS method, LC method and Sample preparation method - generally developed in that order. (Waters, 2008).

2.4.1 Mass Spectrometry (MS/MS Method)

The first part in developing a method for chemical bionalysis is to create a method that will yield high specificity and sensitivity. This can be done by determining how a compound will ionize and what mass per charge *(m/z)* will be optimal for quantitative analysis. Determining the optimal *m/z* for a compound can be done manually, but there exists several automatic programs that aid in the this search as many parameters must be adjusted correctly for optimal results. Ionization mode, cone voltage, collision energy, source temperature and desolvation gas flow are all parameters that affect the abundance of different *m/z* ions.

Ionization Source
In order to detect a compound in a MS system it has to be ionized. The most common ways to ionize a compound in MS is to either use electrospray ionization (ESI) or atmospheric pressure chemical ionization (APCI).

ESI is a method using electrical energy to transfer ions to gaseous phase from the solution followed by desorption by heat/gas. Neutral analytes can also become ionized, generally

by protonation/cationzation in positive mode and deprotonation/anionization in negative mode.

APCI is a method using heat energy to vaporize neutral analytes, and subsequently charge transfer through a reagent ion formed at a charged corona needle to the target ion. APCI is generally only used for small nonpolar compounds, while ESI is used for the majority of other compounds. (Verplaetse and Tytgat, 2011).

Mass Analyzers
In order to optimize sensitivity in the detector a variety of mass analyzers can be used. The most commonly used analyzers are triple quadrupole (QqQ), ion trap and time-of-flight (TOF) analyzers. These analyzers separate different m/z ions by applying a electrical field/pulse in different ways. Hybrids of several of these analyzers also exist.

QqQ consist of a series of three quadrupoles in a row. Each quadrupole has four parallell rods where each of the two pairs are located in opposite corners. Each pair of rods apply either an oscillating radiofrequency or static direct current potentials to generate a oscillating electrical field that filters out all but one m/z as this m/z is the only ion that will have a stable oscillatory pathway with constant amplitude. All other ions will experience an unstable amplitude and will not pass on to the next quadrupole, hence the quadrupole is utilized as a mass filter. While the first and third quadrupole is assigned to mass filtration the second quadrupole is designed as a collision cell where product/daughter ions are produced by collision with a neutral gas, such as nitrogen, which is called collision-induced dissociation.

There are several types of **ion trap** mass analyzers, however they all utilize the same principle of a static and oscillating electrical field. In contrast to a quadrupole, an ion trap traps the ion in place rather than generating a stable oscillatory pathway.

TOF analyzers separate different m/z ions based on another principle. The ions are accelerated with an identical electrical charge/potential, i.e. kinetic energy, and separated in time based on velocity gained from that kinetic energy pulse. Low m/z ions will gain higher velocity than a higher m/z ions from the same kinetic energy, and by letting both ions travel the same distance, the faster velocity ion will reach the detector ahead of the slower ion. (Waters-Corporation, 2020; ThermoFisher-Scientific, 2020).

MS Parameters
Ionization mode is a binary parameter, i.e. it can either be in positive or negative mode. This is a parameter which determines whether the compound of interest is analyzed as a cation or anion. It is possible to make an educated guess based on the structure whether the compound should be analyzed in positive or negative mode, protonation/deprotonation properties are often heavily influential factors. However, both modes are generally tested anyways.

In positive mode the ion becomes ionized by protonation, making the parent ion m/z equal $[M+H]^+$ meaning Molecular ion + Hydrogen weight, with a charge of +1. While in negative mode the parent ion is usually $[M-H]^-$. Adduct formation is not uncommon in MS, for positive the most commonly formed adducts are Na (+23 m/z), NH_4 (+18 m/z) and K (+39 m/z) while in negative mode the most commonly formed adducts are Cl (+35/37

m/z). (Mortier et al., 2004; Zhu and Cole, 2000).

Cone Voltage is a major factor in determining which fragments of a compound are visible in the final spectrum. By increasing the cone voltage, a stronger electrical potential is applied, hence increasing the kinetic energy of the ion. With a larger kinetic energy, the **Collision Energy** of the ion with a neutral molecule in the collision cell is increased. When colliding some of the kinetic energy is transferred into internal energy which results in bond breakage or rearrangement of the ion. This means a low cone voltage will yield a larger abundance of the parent ion as not enough energy is applied to break the bonds in the ion when colliding, while a higher cone voltage will yield higher abundance of more fragmented product ions (low *m/z*) in the spectrum as enough energy to break stronger bonds are applied. (Ho et al., 2003; Kazakevich et al., 2007)

Source Temperature and **Desolvation Gas Flow** both assist in the reduction of the radius of the charged droplets generated by the ion source by evaporation of the solvent. This droplet size-reduction causes an increase in charge density on the surface of the droplets which concludes in the droplets reaching the Rayleigh limit and the analyte ions entering the gaseous phase before entering the mass analyzer. (Ho et al., 2003; Bruins, 1998).

2.4.2 Liquid Chromatography (LC Method)

Liquid chromatography is a method of separating analytes in a mixture based on their affinity to different phases. This is based on the principle that a mobile phase transport the mixture along a stationary phase, i.e. the column, which has different affinity to the different analytes. This difference in affinity retards each analyte's individual transport through the column differently. With increasing affinity to the stationary phase, the time spent passing the analyte through the column is increased, which means that retention time is longer. In most analytical experiments it is common to use a reversed-phase column, this is a non-polar stationary and a polar mobile phase. Optimizing the LC method is done by adjusting the polarity of the mobile phase to push out the more retarded analytes through the column after the initial analytes has been eluted so that the experiment time is decreased. (Lundanes et al., 2014).

2.4.3 Sample Preparation Method

Within the field of bioanlaysis it is important to be aware of possible metabolic effects that may alter the structure of xenobiotics when analyzed in the matrix. In order to counteract this effect **Enzymatic Digestion** can be utilized as it breaks bonds of some conjugated compounds. β-glucuronidase is an enzyme that breaks the glucuronide conjugate bonds that can be formed as part of the phase II metabolic pathway. This way the compounds of interest are readily available in the form needed to be analyzed and more accurately detect exposure. In combination with **Ultrasonication** these two methods can liberate compounds of interest from the studied matrix while maintaining chemical integrity as the cavity frequencies generated by ultrasonication enhances the transfer of compounds across cell membranes by damaging them without destroying them. (Liu et al., 2020; Freiser and Jiang, 2009; Bermejo et al., 2004; Al-Jitan et al., 2018).

Liquid-Liquid Extraction is a process which extracts a solute by bringing the solvent into contact with a second solvent in which the solute is soluble while the solvents are immiscible. The solvent used for extraction of should be selective for the analyte to reduce the amount of extraction steps necessary, this way the analyte will partition favorably into the second extraction solvent. (Thornton, 2011).

Solid-Phase Extraction uses the same chromatographic principle as liquid chromatography. See section 2.4.2. However, as a sample preparation method it is used to simplify the sample matrix and help with compound purification as whole classes of compounds can easily be isolated by adjusting the solvent strength. (Waters, 2020; Supelco, 1998).

2.5   Analytical Parameters

2.5.1   Internal Standard

By spiking the sample with known amount of an analog compound with very similar characteristics to the analyte, usually an isotope-labeled analog, results becomes more reliable as inconsistency due to loss and other irregularities are reduced. Adding such an analog is called an internal standard (IS), and is generally done during the beginning of the sample preparation part. This increase in reliability is based on the assumption that the loss/gain of target analyte signal should be proportional to the loss/gain of the IS signal. This way operational fluctuations between samples are minimized. (Dass, 2007). Equation (1) shows the calculation of the peak area ratio of the target analyte.

$$Area\ Ratio = \frac{Area\ of\ Analyte}{Area\ of\ Internal\ Standard} \tag{1}$$

2.5.2   Retention Time (RT) and Relative Retention Time (RRT)

Retention time is the time required, given a set of parameters, for a specific analyte to elute through a column. These paramaters are flow rate, temperature, injection method and stationary and mobile phase. However, retention time may vary as inter- and intra-lab variations does occur as a result of fluctuations in flow rate or column degradation. In order to maintain experimental reproducibility, a relative retention time factor is introduced. This factor removes the uncertainty caused by these variations as the standard used will be affected similarly to the analyte. The standard used should have similar characterestics to the analyte, and not too much of a difference in retention time, hence the IS is a commonly used standard for this reason. See eq. (2) for the calculation of Relative Retention Time. t_{Rj} is the retention time of the standard and t_{Ri} is analyte of interest's retention time. (Ettre, 1980).

$$RRT = \frac{t_{Ri}}{t_{Rj}} \tag{2}$$

2.5.3 Limit of Quantification (LOQ) and Limit of Detection (LOD)

LOD and LOQ determines the lowest concentration level of detection and the lowest level of concentration determinable for a compound. In order to obtain the highest accuracy and precision for trace level analysis it is therefore important to achieve as low values as possible for these parameters. There are many different ways of determining LOD and LOQ values, but the core principle is that LOD should require a signal-to-noise ratio (S/N) ≥ 3 and LOQ should have a S/N ratio of ≥ 10. (Dass, 2007). See eqs. (3) and (4) for LOD and LOQ calculations.

$$LOD = [Calculated\,Concentration\,of\,Peak] \times \frac{3 \times Highest\,Noise\,Signal\,Height}{Peak\,Height} \quad (3)$$

$$LOQ = [Calculated\,Concentration\,of\,Peak] \times \frac{10 \times Highest\,Noise\,Signal\,Height}{Peak\,Height} \quad (4)$$

2.5.4 Ion Ratio

In order to reduce the likelihood of false positives it is possible to use use an analytical parameter called ion ratio. Ion ratio is a ratio of two product ions and should remain the same between experiments. The reason this ratio reduce the probability of false positives is because it is far less likely for two different product ions to be retained for the same amount of time in the chromatographic system and with the same abundance ratio than just one. It is therefore possible to detect inconsistent results by observing the ratio between the quantification and confirmation ion. (Berendsen et al., 2013). See eq. (5) for the calculation of ion ratios.

$$Ion\,Ratio = \frac{Confirmation\,Ion\,Peak\,Area}{Quantification\,Ion\,Peak\,Area} \quad (5)$$

2.5.5 Matrix Effects (ME)

In matrix analysis co-eluting residual matrix component can affect the ionization of the target analyte causing suppression or enhancement of the signal. It is therefore important to perform matrix effect analysis in order to take this into account when performing quantitative analysis in order to obtain accurate results. One method to determine the ME is to spike a sample set after extraction and another clean solution without the matrix, and calculate the ratio. (Dams et al., 2003; Wang et al., 2007; Matuszewski et al., 2003)

2.5.6 Recovery (R%)

Recovery is another important analytical parameter that gives an indication of loss of analyte of interest through the extraction process. It is calculated based on ratio of signal of a pre-extraction spiked sample vs the signal of a post-extraction spiked sample. Generally only R% values between 40-120% are considered acceptable.

2.6 Previous Studies

Table 2 contains quantification and confirmation ions used in previous studies of PFRs. Table 3 contains several previous studies of PFRs in biota and abiotic matrices including analytical technique, sample preparation method and analytical parameters.

Table 2: Literature quantification and confirmation ions for analytes. Parent ion > daughter ion, where different studies use different ions, a "/" separates them. From Giulivo et al. (2016); Chen et al. (2012); Chu et al. (2011); Santín et al. (2016); Brandsma et al. (2013); Gustavsson et al. (2017); D'Agostino and Provost (1994); Ionas (2016); García-López et al. (2010); Quintana et al. (2006); Mariani et al. (2017)

Compound	Quantification Ion	Confirmation Ion
TMP	140>110	140>79
TEP	182>155	182>127/138
TnPP	225>99	225>183/141
TnBP	267>99	267>155/210
TiBP		
TBOEP	399>299	399>199
TEHP	435>99	435>80/133
TCEP	285>223	285>99/63
TCIPP	327>99	327>250/175/125
TDCIPP	431>99	431>320/209
TPP	327>77	327>152/215
TMPP	369>165	369>99
DPMP	341>152	341>99/228
EHDPP	363>251	363>151/77
IDPP	391>251	391>151/77
BPDP		
TTBPP	494>479	494>367
RDP	575>481	575>419
V6	535>361	583>235
BPA-BDPP	693>367	693>327
DnBP*	209>79	209>153
DPP*	249>93	249>155
BCEP*	221>35	223>37**
BCIPP*	249>35	251>37**
BBOEP*	297>79	297>197
BBOEHEP		
3OH-TBOEP		
TEP-d15	198>135	198>167
TnBP-d27	294>102	294>166/82
TCEP-d12	297>102	297>82
TDICPP-d15	445>102	445>331/201

*For ESI(-) mode, **Isotope Cl
Gathered from (Nygård, 2019)

Table 3: Overview of some previous analytical studies on PFRs

Analytical Technique(s)/ Time required	Matrix	Sample pretreatment/ column(s)/ solvents	Clean-up Technique(s)/ Solvents	Column(s)/ Mobile Phase	Analytical parameters	Reference
LC	*Biota*					
LC-QqLIT-TISI-MS/MS/ 37 minutes	Dolphins	USE/ HEX:Acetone (1:1)	SPE basic alumina + C18/acetonitrile	Guard C18(4mm x 2.0mm) Purosphere Star RP-C18 (2.0mm x 125mm, 5μm)/ H$_2$O:MeOH (0.1% formic acid in H$_2$O, 10 mM ammonium acetate in MeOH)	LOD: 0.34-116ng/g lw LOQ: 1.12-38.8ng/g dw R%: 48-102% RSD: <10%	Sala et al. (2019)
TFC-LC-(H-ESI)-MS/MS/ 29 minutes	Fish(River)	USE/ HEX:Acetone (1:1)	Concentrated and reconstituted in HEX:MeOH (1:3)	Precolumn, Cyclone^{TM}-P (0.5mm x 50mm), precolumn, C18-XL(0.5 mm x 50mm), Purosphere Star RP-C18 (0.2mm x 125mm)/ H$_2$O:MeOH (0.1% formic acid)	Linear range: 0.1-250pg/μL R^2: 0.998-0.999 mLOD: 0.19-19.3ng/g dw mLOQ: 0.97-24.8ng/g dw R%: 51-96% RSD: 2.4-16%	Giulivo et al. (2016)
TFC-LC-(H-ESI)-MS/MS/ Not Reported	Fish(River)	USE/ HEX:Acetone (1:1)		Precolumn, Cyclone^{TM}-P (0.5mm x 50mm), precolumn, C18-XL(0.5 mm x 50mm), Purosphere Star RP-C18 (0.2mm x 125mm)/ H$_2$O:MeOH (0.1% formic acid)	R%: 49-99% mLOD: 0.002-19.3ng/g dw mLOQ: 0.008-24.8ng/g dw	Giulivo et al. (2017)
LC-QqLIT-MS/MS/ 36 minutes	Fish(River)	USE/15 min/ HEX:Acetone (1:1)	SPE/Tandem basic silica + C18	Precolumn, C18(2mm x 4mm), Pureosphere Star RP-18 (2mm x 125mm, 5μm) H$_2$O:MeOH 0.1% Formic acid in H$_2$O 10mM Ammonium acetate in MeOH	R% 45-15% RSD <25% mLOD 0.34-11.6ng/g lw mLOQ 1.12-38.8ng/g lw Linear range: 0.1-240pg/μL	Santín et al. (2016)
LC-(ESI(+))-QqQ-MS/MS/ 44 minutes	Eight arctic species	PLE/ASE350(Dionex)/ DCM:HEX (1:1)	SPE/ OASIS HLB DCM:Isooctane (3:1)	Luna C18 (3mm x 150mm, 3μm) H$_2$O:MeOH 0.1% Formic acid	LOD: 3.16-2198ng/g lw	Hallanger et al. (2015)
HPLC-(ESI(+))-QqQ-MS/MS/ 61 minutes	Herring gull egg	PLE/ASE200(Dionex)/ DCM:HEX (1:1)	SPE/1g ISOLUTE aminopropyl silica Supelclean	Waters Xterra phenyl (2.1mm x 100mm, 3.5μm)/ H$_2$O:MeOH (0.1% formic acid)	RSD <8% IDL 0.01-0.12ng/mL R% 67-104% mLOQ 0.6-2.0ng/g lw	Chen et al. (2012)
HPLC-(ESI(+))-QqQ-MS/MS/ Not reported	Benthic and Pelagic organisms	PLE/ASE350(Dionex)/ DCM:Acetone(1:1,v/v)	SPE/NH$_2$ (Discovery^R DSC-NH)	Luna C18 (3mm x 150mm, 3μm	R% 43-134% STD <20%	Brandsma et al. (2015)
LC-(ESI(+))-QqQ-MS/MS/ 35 minutes	Rat liver microsomes			Precolumn, Luna C18 (2mm x 4mm) Luna C18(Phenomex) (2mm x 50mm, 3μm)/ H$_2$O:MeOH (2mM ammonium acetate)	R^2 0.995 Linear range: 0.2-1000ng/g lw LOD 0.2-0.14ng/mL LOQ 0.07-0.46ng/mL %ME 99.2-103.3% RSD <10%	Chu et al. (2011)

(Continued)

Analytical Technique(s)/ Time required	Matrix	Sample pretreatment/ column(s)/ solvents	Clean-up Technique(s)/ Solvents	Column(s)/ Mobile Phase	Analytical parameters	Reference
	Non-biota					
UPLC-(ESI(+))-MS/MS/ 12 minutes	River	0.45 µm cellulose acetate membrane	SPE/ACN	Waters BEH C8 (2.1 mm x 50 mm, 1.7 µm)/ H_2O:ACN (0.1% formic acid in both)	R%: 69-110% R^2: 0.992-0.999 LOQ: 2-6 ng L RSD%<10%	Wang et al. (2011)
LC-(ESI(+/-))-MS/MS/ 35 minutes	River and wastewater samples	0.45 µm nitrocellulose filter	SPE/MeOH:TBAHS methanolic solution	Luna C18 (2 mm x 100 mm, 3 µm with same supplier guard H_2O:MeOH (5 mM ammonium acetate in both)	R^2: >0.991 LOQ: 0.3-1 ng mL^{-1}	García-López et al. (2010)
TFC-LC-(ESI(-))-MS/MS >28 minutes	Wastewater	0.45 µm cellulose acetate filters	SPE/H_2O:MeOH	Luna Phenyl-hexyl (2 mm x 150 mm, 3 µm) MeOH:H_2O (1 mM TrBA and acetic acid in both)	R^2: >0.998 RSD%: <5.3% LOQ: 7-14 ng L^{-1}	Quintana et al. (2006)
UPLC-(ESI(+))-QqQ-MS/MS/ 7 minutes	Milk powder	Dissolved in water at 50 °C/ 0.5% formic acid in ACN	QuEChERS PSA(50/100)/ ACN with 0.5% formic acid	Phenomenex Kinetex PFP (2.1 mm x 50 mm, 2.6 µm) H_2O:ACN (0.1% formic acid in water)	R^2: >0.994 LOD: 0.1-0.25 µg kg^{-1} LOQ: <1.5 µg kg^{-1} R%: 78-102%	Guo et al. (2016)
TFC-LC-(H-ESI)-MS/MS/ 29 minutes	Sediment	PLE/ASE350(Dionex)/ Cu + Hydromatrix in HEX:Acetone (1:1)	Concentrated and redesolved in MeOH	Precolumn, Cyclone^{TM}-P (0.5mm x 50mm), precolumn, C18-XL(0.5 mm x 50mm), Purosphere Star RP-C18 (0.2mm x 125mm)/ H_2O:MeOH (0.1% formic acid)	Linear range: 0.1-250pg/µL R^2: 0.998-0.999 mLOD: 0.2-1.25ng/g dw mLOQ: 0.07-3.44ng/g dw R%: 49-112% RSD: 1.3-8,8%	Giulivo et al. (2016)
TFC-LC-(H-ESI)-MS/MS/ Not reported	Sediment	PLE/ASE350(Dionex)/ Cu + Hydromatrix in HEX:Acetone (1:1)		Precolumn, Cyclone^{TM}-P (0.5mm x 50mm), precolumn, C18-XL(0.5 mm x 50mm), Purosphere Star RP-C18 (0.2mm x 125mm)/ H_2O:MeOH (0.1% formic acid)	R%: 48-114% mLOD: 0.0001-1.65ng/g dw mLOQ: 0.0003-5.49ng/g dw	Giulivo et al. (2017)
HPLC-(ESI(+))-MS/MS/ Not reported	Dust	USE/(Vortex mixing)/ Acetone:Toluene	SPE/Florisil DCM:Diethylether	Luna C18 (3mm x 150mm, 3µm)		Brandsma et al. (2013)
HPLC-(ESI(+))-MS/MS/ >8 minutes	Dust	USE/(Vortex mixing)/ Acetone:Toluene	SPE/Florisil DCM:Diethylether	Precolumn, Acquity C18 VanGuard (2.1mm x 5mm, 1.8µm) Acquity C18 (2.1mm x 100mm, 1.8µm)/ H_2O:MeOH (0.2% formic acid in both)		Brandsma et al. (2013)
LC-MS/MS/ >23 minutes	Dust	USE/(Vortex mixing)/ Acetone:Toluene				Brandsma et al. (2014)
GC	*Biota*					
GC-MS/MS	Harbor Porpoises	Drying, Soxhlet extraction Acetone:HEX	SPE/Isolute amino-silicate/ DCM,HEX	DB-5MS Ultrainert (15mm x 0.25mm, 0.1µm)	R% 69-101%	Papachlimitzou et al. (2015)
GC-MS	Hair and nails	Digestion/ HNO_3:H_2O_2	SPE/Florisil	DB-5MS Ultrainert (30mm x 250mm, 0.25µm) High purity He	R% 106-143% RSD <10% Linear range: 4-320ng/mL LOQ 150ng/g	Liu et al. (2015)

Table gathered and expanded from the pre-project. (Nygård, 2019)

3 Experimental and Method

3.1 Standards and Reagents

Standards of all the organophosphorus esters, namely, Trimethyl Phosphate (TMP), Triethyl Phosphate (TEP), Tri-*n*-propyl Phosphate (TnPP), Tri-*n*-butyl Phosphate (TnBP), Triisobutyl Phosphate (TiBP), Tris(2-butoxyethyl) Phosphate (TBOEP), Tris(2-ethylhexyl) Phosphate (TEHP), Tris(2-chloroethyl) Phosphate (TCEP), Tris(1-chloro-2-propyl) Phosphate (TCIPP), Tris(1,3-dichloro-2-propyl) Phosphate (TDCIPP), Triphenyl Phosphate (TPP), Tritolyl Phosphate (TMPP), Diphenyltolyl Phosphate (DPMP), 2-Ethylhexyldiphenyl Phosphate (EHDP), Isodecyldiphenyl Phosphate (IDPP), *tert*-Butylphenyldiphenyl Phosphate (BPDP), Tris(4-*tert*-butylphenyl) Phosphate (TTBPP), Tetraphenylrecorcinol bis(diphenyl Phosphate) (RDP), 2,2-Bis(chloromethyl)-1,3-propandiol bis[bis(2-chloroethyl) Phosphate] (V6), Bisphenyl A bis(diphenyl) Phosphate (BPA-BDPP), Di-*n*-butyl Phosphate (DPhP), Bis(2-chloroethyl) Phosphate (BCEP), Bis(2-chloropropyl) hydrogen Phosphate (BCIPP), Bis(2-butoxyethyl) Phosphate (BBOEP), Bis(2-butoxyethyl) hydroxyethyl Phoshate (BBOEHEP), Bis(2-butoxyethyl) hydroxy-2-butoxyethyl Phosphate (3OH-TBOEP), Triethyl Phosphate -d15 (TEP-d15), Tri-*n*-butyl Phosphate -d27 (TnBP-d27), Tris(2-chloroethyl) Phosphate -d12 (TCEP-d12), Tris(1,3-dichloro-2-propyl) Phosphate -d15 (TDCIPP-d15) were purchased from Chiron AS (Trondheim, Norway). β-Glucuronidase from Helix pomatia (type HP - 2, aqueous solution, $\geq$ 100,000 units/mL) were purchased from Sigma - Aldrich (Steinheim, Germany)

3.2 LC-MS/MS Analysis Instrument

Separation was performed in a Acquity UHPLC system (Waters, Milford, US) with a Kinetex C18 (2.1 mm x 30 mm, 1.3 µm, 100Å Phenomenex) with a Phenomenex C18 guard column. The aqueous phase (A) was water with 0.1% formic acid, while the organic phase (B) was acetonitrile with 0.1% formic acid. Flow rate was set to 0.4 mL/min and injection rate was 4 µL. The analysis was performed in ESI(+) on a Xevo TQ-S, Triple Quadrupole Mass analyser (QqQ), including a ZSpray ESI function (Waters, Milford, US).

3.3 LC Method

Analytes were solved in 50/50 ACN/H_2O with 4 µL as injection volume, 0.4 mL/ min as flow rate and 45 °C as the temperature. The aquatic phase was H_2O with 0.1% formic acid (A), and the organic phase was ACN with 0.1% formic acid (B). The gradient elution program was used: 0 min (10% B), 0.2 min (10% B), 3 min (100% B), 3.5 min (100% B), 3.6 min (10% B), 4 min (10% B). The method was developed during the first phase of this two part project. (Nygård, 2019).

3.4 Sampling Harbor Porpoises

Liver, blubber and muscle samples were cut from 124 individual porpoises as part of the pre-project. They were cut and put in aluminum foil before being refrozen until sample

preparation and extraction assumed. The scalpel used to cut was cleaned with methanol, and a clean tissue between each sample, and samples were cut on a board wrapped in aluminum foil.

All individuals were caught as bycaught from the Norwegian coast between 2016 and 2017 and stored frozen.

3.5 Sample Preparation

General Preparation
Ammonium acetate (2.31 g) was dissolved in MilliQ Water (30 mL) to make a 1 M solution. β-Glucuronide enzyme (25 µL) was added to another ammonium acetate solution (1 M, 50 mL) to create an activated enzyme salt solution. Pooled matrices from 12 porpoise liver sample (0.1 g) was added to an ammonium acetate solution (2 mL) with internal standard (IS), sonicated for 30 minutes and shaken for 45 minutes. Activated enzyme solution was added (2 mL) and the mixture was left to incubate overnight at 37 °C while shaking.

Ethylacetate Extraction
After incubation ethylacetate (5 mL) was added, before being shaken for 45 minutes, sentrifuged for 5 minutes and the supernatant was decanted. This ethylacetate addition and subsequent shaking and sentrifugation before decantation was performed once more.

MilliQ Water (1 mL) was introduced to the two combined supernatant before being vigorously shaken and sentrifuged. The new supernatant was concentrated by evaporation and reconstituted in ACN:H$_2$O to 1 mL and put in the fridge until analyzation.

DCM:HEX Extraction
After incubation DCM:HEX (1:1, v/v, 5 mL) was added, before being shaken for 45 minutes, sentrifuged for 5 minutes and the supernatant was decanted. This DCM:HEX addition and subsequent shaking and sentrifugation before decantation was performed once more, and one final time with ethylacetate.

MilliQ Water (1 mL) was introduced to the three combined supernatant before being vigorously shaken and sentrifuged. The new supernatant was concentrated by evaporation and reconstituted in ACN:H$_2$O to 1 mL and put in the fridge.

The following day some of the cold mixtures were sentrifuged and decanted into fresh LC vials and stored cold until analyzation.

Spiking
10 vials were prepared before extraction, 1 reagent blank (RB), 3 unspiked samples (S), 4 pre-extraction spiked samples (SP), 2 post-extraction samples (MM). See table 4 for where in the extraction process samples were spiked. Target analyte (TA) pre-extraction was added at the same time as IS addition. TA post-extraction was added as the final step before analyzation.

Table 4: Overview of target analyte (TA) and internal standard (IS) addition during extraction.

	IS Pre-extraction	TA Pre-extraction	TA Post-extraction
RB	X		
S1	X		
S2	X		
S3	X		
S4	X		
SP1	X	X	
SP2	X	X	
SP3	X	X	
SP4	X	X	
MM1	X		X
MM2	X		X

Matrix Comparison

10 liver and blubber samples (0.1 g) from the same 10 individuals followed general preparation with IS addition and ethylacetate extraction with 3 extractions. 10 minutes of sonication and 30 minutes of shaking was done instead of 45 minutes of shaking.

The extraction process was stopped just before the concentration step due to the lab-shutdown. Muscle tissue would've been the next matrix tested. Depending on which matrix yielded the best results of the 10 samples from each matrix the rest of the remaining 114 samples of that matrix would've been analyzed.

3.6 Quantification and Confirmation Ions

Table 5 contains the quantification and confirmation ions used in this study. The quantification and confirmation ions are selected based on their analytical parameters. Due to COVID-19 the metabolites that were supposed to be analyzed in negative mode ions were not analyzed. BPDP was not analyzed because a LC-MS/MS method was not generated before labs were shut down.

Table 5: Quantification and confirmation ions used in this project. Parent ion > daughter ion.

Compound	Quantification Ion	Confirmation Ion
TMP	141>79	140>109
TEP	183>127	183>155
TnPP	226>99	NA
TnBP	267>155	267>211
TiBP	267>211	267>155
TBOEP	399>299	399>199
TEHP	435>99	435>71
TCEP	285>99	285>223
TCIPP	327>99	NA
TDCIPP	429>99	NA
TPP	327>152	327>215
TMPP	369>165	369>99
DPMP	341>152/165*	341>229
EHDPP	363>273	NA
IDPP	391>153	391>77/95*
BPDP	NA	NA
TTBPP	495>152	495>439
RDP	575>419/152*	575>481
V6	535>359	NA
BPA-BDPP	693>367	693>327
DnBP	NA	NA
DPP	NA	NA
BCEP	NA	NA
BCIPP	NA	NA
BBOEP	NA	NA
BBOEHEP	344>243/99*	344>99/243*
3OH-TBOEP	415>199	415>243
TEP-d15	198>134	198>102
TnBP-d27	294>102	NA
TCEP-d12	299>102	297>130
TDICPP-d15	444>216	444>102

*Ethylacetate selected ion / DCM selected ion.

4 Results and Discussion

4.1 Sample Preparation Method Development

Liver sample extractions with DCM:HEX and ethylacetate seem to form 3 separate phases. The bottom water layer was transparent with a bit of white foggyness. The middle layer, which is assumed to be a lipid layer, had a strong red color and some coagulation might have occurred as it seemed quite viscous and had some solid chunks. The top layer, consisting of the extraction solution, was clear without any coloration.

The DCM:HEX extraction had issues with 6 of the samples becoming foggy when cooled down. It is possible that some of the bottom layer followed in the decantation process as not all of the samples became foggy after cooling down. However, this happened to 6 out of the 10 samples during the DCM:HEX extraction and none of the samples extracted with ethylacetate experienced this issue with the same operator.

Having to reconstitute the solution a second time must be considered when comparing these two extraction methods and it most likely affected the analytical parameters negatively. Hence, the ethylacetate extraction method is recommended when using liquid-liquid extraction when optimizing for high throughput.

Comparing ethylacetate liquid-liquid extraction with SPE DCM:HEX, HEX:Acetone and ethylacetate intralab would be a natural next step in sample preparation optimization.

4.2 Analytical Parameters

There seem to be either significant difference in carry-over or interday fluctuations between the signal area of the ethylacetate and DCM extractions as the instrumental blank (IB) is significantly larger during the DCM extracted sample analysis. Compare IB in tables 7 and 9. When observing R% range, IR stability and LOD/LOQ ethylacetate seem to outperform DCM significantly as an extraction solvent. See tables 6 and 8.

TEHP, TDCIPP and EHDP might possibly be in the instrument as the IB signals were just as large as the post-extraction spiked samples. From the results it seems likely that TMP, TEP, RDP, TTBPP, DPMP and maybe also TBOEP pollution occur sometime during the sample preparation as they all have small instrument blank signals but large reagent blank signals.

However, the most interesting results yields insight into possible presence of TnBP/TiBP, TPP and BOEHEP in the samples. IDPP, TCIPP, TBOEP and BPA-BDPP are also show some sign of being present in the sample matrix as well, but are not as clear. Especially large and significant are the results of TnBP in the samples.

Only one calculated concentration was found to be above LOD, TDCIPP. However, this is not very reliable as all the analysis' of TDCIPP yielded the same signal area, whether it be a post extraction spike or an instrumental blank.

Matrix effect was not calculated for the liver as the spiked clean solvent match was not analyzed before the shut-down.

Table 6: Experimental results for extraction with ethylacetate: Calculated Concentration ($\text{ng\,g}^{-1}$ w.w), Limit of Detection, LOD, ($\text{ng\,g}^{-1}$ w.w), Limit of Quantification, LOQ, ($\text{ng\,g}^{-1}$ w.w), Recovery, R%, (%), Ion Ratio of the confirmation ion (%) $\pm$ standard deviation for each analyte in the developed method.

	Concentration	LOD	LOQ	R%	IR
TMP	4.4×10^{-2}	7.4×10^{-2}	2.5×10^{-1}	42	481 ± 105
TEP	0			87	94 ± 11
TnPP	6.1×10^{-3}	2.2×10^{-2}	7.3×10^{-2}	141	NA
TnBP	1.1×10^{-1}	8.9×10^{-2}	3.0×10^{-1}	98	93 ± 9
TiBP	1.8×10^{-2}	6.3×10^{-2}	2.1×10^{-1}	95	82 ± 11
TBOEP	7.2×10^{-3}	3.5×10^{-3}	1.2×10^{-2}	103	96 ± 5
TEHP	0			44	6 ± 1
TCEP	6.3×10^{-3}	1.0×10^{-2}	1.5×10^{-1}	93	NA
TCIPP	6.2			366	NA
TDCIPP	0				NA
TPP	8.9×10^{-2}	8.4×10^{-2}	2.8×10^{-1}	22	381 ± 119
TMPP	1.4×10^{-2}	8.2×10^{-2}	2.7×10^{-1}	36	NA
DPMP	2.2×10^{-4}	5.0×10^{-4}	1.7×10^{-2}	22	88 ± 54
EHDP	0			846	NA
IDPP	9.6×10^{-2}	1.4×10^{-1}	4.8×10^{-1}	83	85 ± 6
TTBPP	0			52	202 ± 29
RDP	8.3×10^{-3}	1.4×10^{-2}	4.6×10^{-2}	17	115 ± 20
V6	7.2×10^{-4}	4.8×10^{-3}	1.6×10^{-2}	148	NA
BPA-BDPP	4.2×10^{-3}	1.6×10^{-1}	5.3×10^{-1}	42	37 ± 44
BBOEHEP	3.9×10^{-1}	4.7×10^{-1}	1.6	142	386 ± 63
3OH-TBOEP	1.4×10^{-3}	5.2×10^{-3}	1.7×10^{-2}	242	86 ± 40

Due to the high instrumental blank signals it was not possible to determine LOD or LOQ for a lot of the compounds. For the compounds where only one daughter ion was analyzed or only yielded one with applicable results it was not possible to deteremine IR. See table 5 for used daughter ions.

Table 7: Experimental results for the instrumental blank (IB), reagent blank (RB) and average sample signal area for ethylacetate extraction.

	IB	RB	Average Sample
TMP	2.6×10^1	4.2×10^2	5.2×10^2
TEP	8.7×10^1	1.3×10^3	9.3×10^2
TnPP	1.4×10^1	1.7×10^1	5.4×10^1
TnBP	5.3×10^3	6.8×10^3	1.0×10^4
TiBP	5.5×10^3	7.4×10^3	8.1×10^3
TBOEP	2.9×10^2	9.3×10^2	1.5×10^3
TEHP	1.8×10^3	2.1×10^3	2.1×10^3
TCEP	5.7×10^1	3.0×10^1	9.3×10^1
TCIPP	2.2×10^1	5.3×10^1	1.1×10^3
TDCIPP	8.9×10^3	7.2×10^3	8.9×10^3
TPP	2.7×10^3	2.9×10^3	3.8×10^3
TMPP	3.2×10^2	4.8×10^2	9.2×10^2
DPMP	7.5×10^2	7.4×10^2	7.5×10^2
EHDP	5.5×10^4	6.3×10^4	5.3×10^4
IDPP	9.6×10^2	8.5×10^2	1.5×10^3
TTBPP	0	2.6×10^3	1.0×10^3
RDP	7.8×10^1	1.4×10^2	1.6×10^2
V6	1.4	2.2	1.5×10^1
BPA-BDPP	1.4×10^1	1.6×10^1	9.3×10^1
BBOEHEP	8.3	1.0×10^2	8.5×10^2
3OH-TBOEP	6.2×10^{-1}	2.1	5.4×10^1

Only TEHP seemed to yield better results when extracted with DCM:HEX. Even though the instrumental blank signal was significantly less, the RB signal was still to high to be able to determine the concentration. Only TnPP and TMPP had sample signals that were not matched or lower than the RB signals in DCM:HEX extracted samples.

Table 8: Experimental results for extraction with DCM:HEX: Calculated Concentration ($ng\,g^{-1}$ w.w), Limit of Detection, LOD, ($ng\,g^{-1}$ w.w), Limit of Quantification, LOQ, ($ng\,g^{-1}$ w.w), Recovery, R%, (%), Ion Ratio of the confirmation ion (%) $\pm$ standard deviation for each analyte in the developed method.

	Concentration	LOD	LOQ	R%	IR
TMP	2.8×10^{-2}	1.2×10^{-1}	4.1×10^{-1}	84	676 ± 440
TEP	2.3×10^{-2}	1.1×10^{-1}	3.7×10^{-1}	137	79 ± 46
TnPP	1.8×10^{-1}	6.2	2.1×10^{1}	580	NA
TnBP	9.9×10^{-2}	1.4×10^{-1}	4.6×10^{-1}	185	88 ± 22
TiBP	2.5×10^{-2}	7.2×10^{-2}	2.3×10^{-1}	159	65 ± 19
TBOEP	4.2×10^{-1}	1.3	4.5	79	102 ± 27
TEHP	9.7×10^{-1}	4.4×10^{-1}	1.5	51	NA
TCEP	1.2×10^{-1}	2.0×10^{1}	6.7×10^{1}	42	95 ± 58
TCIPP	3.9×10^{-2}	4.0×10^{-2}	1.3×10^{-1}	69	NA
TDCIPP	4.3×10^{-1}	5.4×10^{-2}	1.8×10^{-1}	920	NA
TPP	1.9×10^{-1}	2.9×10^{-1}	9.8×10^{-1}	88	273 ± 86
TMPP	0				NA
DPMP	9.4×10^{-1}	1.6	5.3	45	350 ± 533
EHDP	1.3	8.0	2.7×10^{1}		NA
IDPP	0			965	194 ± 219
TTBPP	2.7	4.0×10^{2}	1.3×10^{3}		NA
RDP	4.3×10^{-1}	4.4×10^{-1}	1.5	8	83 ± 13
V6	0				NA
BPA-BDPP	0			19	NA
BBOEHEP	6.4×10^{-1}	4.6	1.5×10^{1}	89	22 ± 10
3OH-TBOEP	0				NA

It is worth mentioning that it seems likely that one of the DCM extracted unspiked samples in fact were spiked with some of the compounds pre-extraction as some of compounds in one sample yielded signals parity of the samples that were spiked pre-extraction. This causes a large increase in average unspiked sample signal which makes some compounds seem present in the matrix. When the outlier sample is excluded from the average, the RB signal vs unspiked sample signal resemble the ethylacetate results more.

Table 9: Experimental results for the instrumental blank (IB), reagent blank (RB), average sample signal area and average sample signal area excluding outlier sample for DCM:HEX extraction.

	IB	RB	Average Sample	Average w/o Outlier
TMP	1.4×10^2	5.2×10^2	6.5×10^2	5.5×10^2
TEP	4.0×10^1	4.0×10^2	7.9×10^2	7.1×10^2
TnPP	1.1×10^2	6.4×10^1	2.6×10^2	3.0×10^2
TnBP	2.3×10^3	1.9×10^3	4.2×10^3	2.0×10^3
TiBP	1.6×10^3	2.3×10^3	3.2×10^3	2.3×10^3
TBOEP	5.9×10^2	3.3×10^2	2.4×10^3	1.0×10^3
TEHP	5.9×10^3	4.0×10^3	6.0×10^3	5.2×10^3
TCEP	0	8.5×10^1	5.1×10^2	2.4×10^2
TCIPP	2.6×10^4	2.0×10^4	2.1×10^4	1.8×10^4
TDCIPP	1.8×10^4	1.7×10^4	1.9×10^4	1.7×10^4
TPP	3.9×10^3	4.8×10^3	6.1×10^3	4.4×10^3
TMPP	1.2×10^2	2.0×10^3	6.1×10^3	5.2×10^2
DPMP	7.7×10^2	5.7×10^3	9.8×10^2	8.3×10^2
EHDP	6.5×10^4	5.5×10^4	5.1×10^4	6.4×10^4
IDPP	4.4×10^3	3.7×10^3	2.7×10^3	2.7×10^3
TTBPP	6.7×10^2	9.3×10^2	1.3×10^3	3.9×10^2
RDP	3.2×10^2	3.9×10^2	6.8×10^2	4.1×10^2
V6	0	4.0×10^1	1.9×10^1	1.9×10^1
BPA-BDPP	3.9×10^2	3.3×10^2	4.8×10^2	2.5×10^2
BBOEHEP	1.6×10^2	8.1×10^2	3.2×10^3	3.4×10^3
3OH-TBOEP	0	1.6×10^2	6.7×10^1	6.7×10^1

4.2.1 Individual Analyte Discussion

TMP
Due to the high RB signal it is hard to determine whether TMP is found at elevated levels in porpoises based on as few samples and the fact that the calculated concentration is lower than LOD. It is however more clear that pollution occurs sometime during the extraction step as the IB and RB signal difference is in the order of magnitude. The R% is a bit small in ethylacetate and the IR has a quite large standard deviation, however the IR in DCM:HEX is significantly larger.

TEP
Due to the high RB signal it is hard to determine whether TEP is found at elevated levels in porpoises, at least when extracted with ethylacetat. DCM extraction did showed some indications that it might be present. DCM:HEX did not yield as high RB signal for the quantification ion, however the confirmation ion had large IB and RB signals. The R% and IR was decent for ethylacetate, but inadequate for DCM.

TnPP
Due to quite low overall signals of TnPP it is seem possible that it was not detected. There's however larger signals in the samples than the blanks, but the larger sample signals might

just be due to the high R%. Having a confirmation ion could give more insight in whether the sample contains TnPP or not.

TnBP

Porpoises do seem to have elevated levels of TnBP as the calculated concentration is above LOD. Extractions with ethylacetate shows high sample signals and all the analytical parameters are consistent and good. There seem to be indications of some pollution occurring during the extraction process for TnBP, but not so much that RB signals overcome sample signals. The analytical parameter results from the DCM extracted samples are considerably worse.

TiBP

TnBP and TiBP are analyzed separately in this project, however, due to the fact that they are not separated sufficiently in the LC system, and are isomers, i.e. cannot be distinguished in the MS, their concentrations cannot be individually separated. It is therefore peculiar that their calculated concentrations are an order of magnitude apart.

TBOEP

Both DCM and ethylacetate seem to extract TBOEP from the matrix and ethylacetate yields excellent analytical parameters. In fact TBOEP is almost found at levels exeeding LOQ. As both TBOEP and it's metabolite BBOEHEP, are found above or just beneath LOD levels with decent analytical parameters and significantly larger average sample signals than RB. All these observation build a strong indication that TBOEP can be transferred through the food chain and should therefore be further investigated.

TEHP

Like EHDP and TDCIPP, TEHP is another compound with matching and exeedingly large IB and post-extraction spiked signals.

TCEP

Due to low overall signal of TCEP it seems to not be detected in the samples. There's however larger signals in the samples than the blanks with DCM. R% was good in ethylacetate, but a bit low in DCM. IR was not very consistent in DCM and not applicable in ethylacetate as the confirmation ion was not detected in many of the samples.

TCIPP

The calculated concentration seem to indicate that there's a large concentration of TCIPP found in the samples when extracted with ethylacetate. This is not observed in DCM as the integrated peaks are not the same. There's a small peak at 1.89 minutes instead of 2.00 minutes that significantly increases in height for the sample from non-spiked to pre-extraction spiked to post-extraction spikes. However, the integrated area does not increase the same way. This increase in height is only observed for ethylacetate extraction. Either way due to the very large signal at 2.00 minutes in both solvents for all IBs it seems probable that there's TCIPP in the instrument. It is also worth mentioning that the R% for the peak at 1.89 in ethylacetate is very large. It is possible the 2.00 minute peak should've been integrated as well to see if the R% was better.

TDCIPP
Like EHDP and TEHP, TDCIPP has very large IB signals making it difficult to analyze. As even the IB signals match the size of post-extraction spiked signals any other conclusion than that they might originate from the instrument themselves is difficult to reach unless the fragments analyzed are wrong.

TPP
TPP is found at levels above LOD in ethylacetate and has decent analytical parameters. All three product ions tested seem to indicate the presence of TPP in the matrix. DCM did not yield similar results, as the analytical parameters are acceptable, a bit large variation in IR, but R% is good and calculated levels below LOD. Without the outlier sample the sample average signal is not above RB levels.

TMPP
Unspiked TMPP samples do have a higher average signal with ethylacetate than RBs, however, most were at RB levels, while one outlier significantly increased the average. TMPP should therefore not be considered to be found in the samples. The analytical parameters for TMPP poor.

DPMP
Due to the high RB signal and very poor analytical parameters with both ethylacetate and DCM it is hard to determine whether DPMP is found at elevated levels in porpoises.

EHDP
EHDP has been difficult to analyze throughout the entire method development process. Due to it's exeedingly large IB signals it seems likely that the EHDP signal originate from the instrument somewhere. The anlalytical parameters are otherwise useless or not applicable.

IDPP
IDPP shows decent analytical parameters when extracted with ethylacetate, and there are indications that the matrix might contain trace levels of the compound. However, the levels are just below LOD. DCM did not seem to extract IDPP from the matrix at all as the analytical parameters makes analysis unreliable.

TTBPP
TTBPP was all around difficult to analyze due to large RB signals in ethylacetate and large IB signals in DCM as well as poor analytical parameters. R% and IR are alright for ethylacetate, but the large RB values yield a negative calculated concentration as well as LOD and LOQ as they are dependent on the calculated concentration.

RDP
RDP had medium sized IB and RB signals that matched average sample signals and very low R% with both ethylacetate and DCM making it hard to analyze.

V6
V6 was difficult to analyze due to its overall very small signals, though the average sample signal was larger than RB with ethylacetate.

BPA-BDPP

There's weak indications that BPA-BDPP can be extracted from the matrix as there's consistent larger peaks in unspiked samples than IB and RBs. However, the signals are very small and must be further investigated, and it is important to take note of the poor analytical parameters.

BBOEHEP

Even though BBOEHEP was not found at concentration levels above LOD, the signal is almost an order of magnitude larger in the unspiked ethylacetate extracted samples than the RB, and significantly larger in the DCM extracted samples as well. R% is a bit high when extracted with ethylacetate and IR vary a bit much with DCM.

3OH-TBOEP

Even though 3OH-TBOEP is also a metabolite of TBOEP, the analytical parameters are not as great, and it is difficult to determine whether it is present in the matrix studied due to the small size of the signals even though the average sample signals seem to be larger than RB.

As the LC method time is so rapid, not all compounds are separated and can therefore elute approximately at the same time. Common fragment ions should therefore be avoided in order to avoid compounds interfering with each others analysis. Hence, common ions such as 99, 81, 77, 152 m/z should be avoided whenever possible. In addition ions such as 77 m/z is not unique for TPP, i.e. 3 equal ions yield the same m/z which can be problematic for quantitative analysis.

4.3   Proposed General Fragmentation Mechanism

Schwarzenberg et al. (2013) proposed a fragmentation mechanism for organophosphorus diesters. The proposed fragmentation mechanism is supported by the TEP and its analog internal standard TEP-d15 ion fragments in this project. See Figure 2 and Figure 3. In Figure 3 it is observed that the initial ionization of the compound is protonated with a non-deuterated hydrogen atom from the solution/ESI source, while the rest of the alcohols on the compound remain deuterated due to the elimination reaction with the cleaved ethane cation.
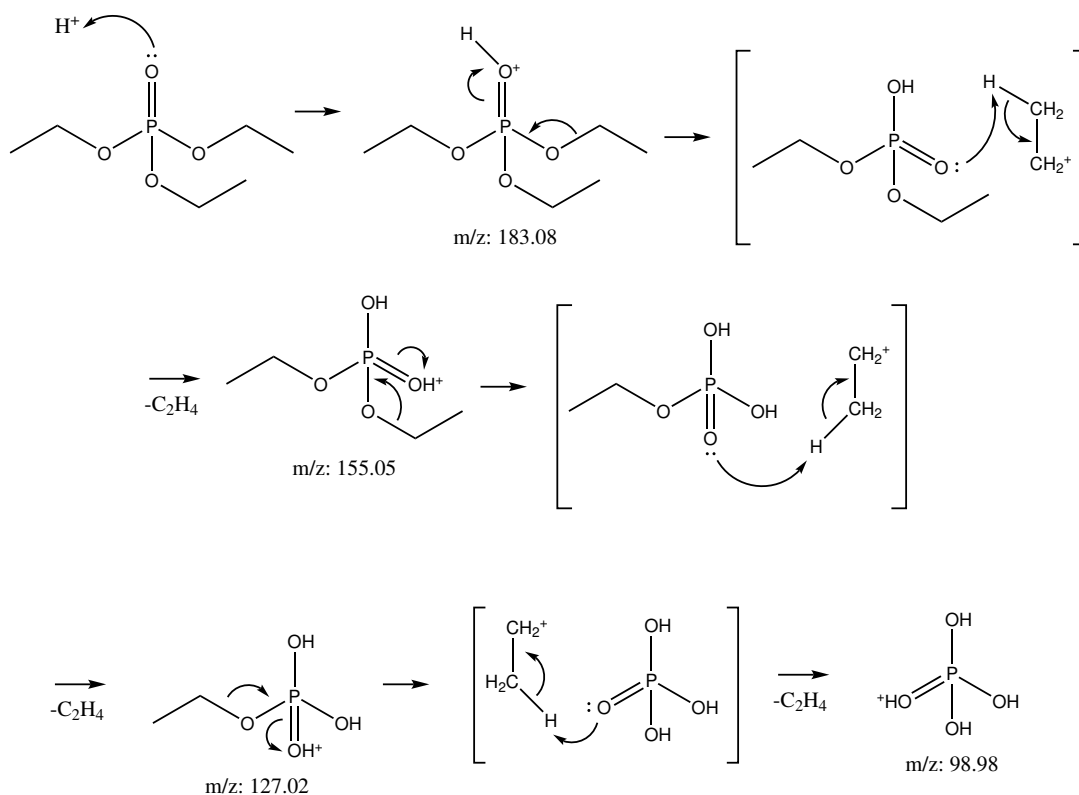
Figure 2: Proposed mechanism for fragmentation of organophosphorus triesters with TEP as reference.

4.4 Fragmentation

Several of the following suggested fragment structures have their chemical formula supported by the database created by Schulze (2020). The following suggested structures are clustered by their abundance ratio from several optimized spectra, and can therefore be compared in relation to stability and hence whether or not it is should be considered as potential candidate for quantitative analysis.

Some of the metabolites were based on the preliminary results in Nygård (2019) assumed to work better in ESI(-) mode as they have a freely available OH group to be deprotonated, yet some of them are in the following section both tested in ESI(+) and ESI(-) mode.

IDPP is missing in the following section as the MS spectra data couldn't be found after COVID-19 lockdown, and BPDP was not analyzed before the lockdown.
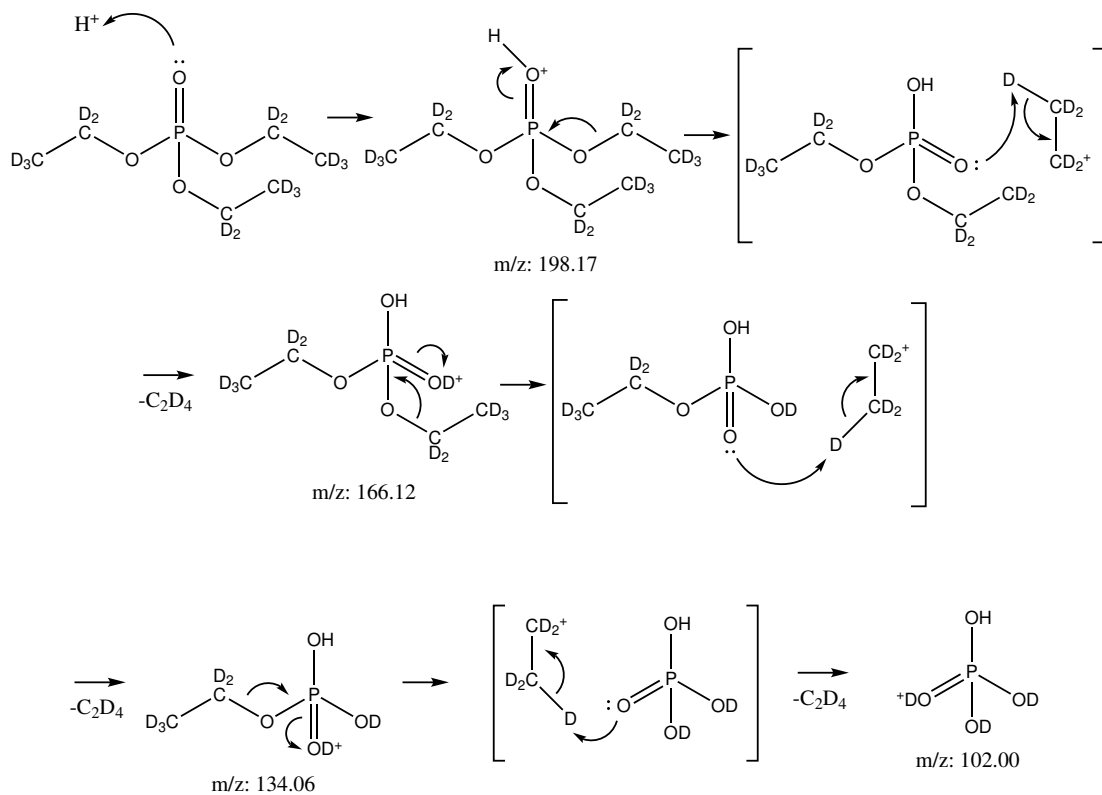
Figure 3: Proposed mechanism for fragmentation of organophosphorus triesters with TEP-d15 as reference.

4.4.1 TMP

TMP's fragmentation differ from the rest of the compounds as the phosphorus atom seem to experience a reduction in its oxidation number, from +5 to +3 see ion 47 m/z. Few other compound tested in this project behave this way during the fragmentation. It is worth noting that the ion 47 m/z has very low abundance. TMP also differ by cleavage of the oxygen atom. The general pathway most of the other compounds experience do not cleave the P-O bond, but rather the C-O bond. This may be due to the instability of a methyl fragment as its ability to disperse the charge is very low, hence giving rise to the P-O bond cleavage fragments. This P-O cleavage also require more energy, as the optimized cone voltage and collision energy is a bit higher than most C-O cleavage observed in other compounds. Based on the optimized spectrum it would seem the 109 m/z fragment should be the quantification ion and 79 m/z should be the confirmation ion. These ions do not overlap m/z with any other fragments from other compounds either. See figs. 4, 6 and 7 for spectra and suggested structures of the major daughter fragments found.

Optimized Daughter Spectrum (at Collision Energy 18eV)
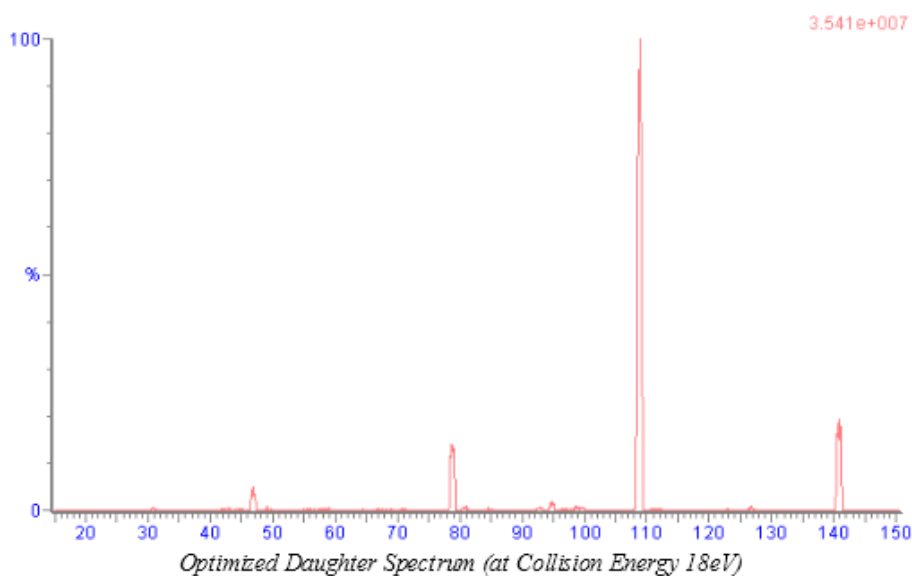
Compound	Formula/Mass		Parent m/z	Cone Voltage	Daughters	Collision Energy	Ion Mode
TMP	C3H9O4P	1	140.86	32	108.86	16	ES+
		2	140.86	32	78.90	22	ES+
		3	140.86	32	46.98	14	ES+
		4	140.86	32	94.82	18	ES+

Figure 4: Spectrum and fragments generated with IntelliStart
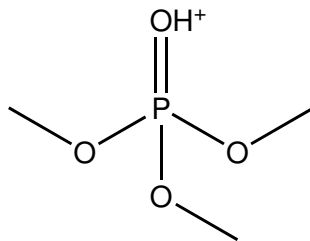
m/z: 141.03

Figure 5: TMP precursor ion
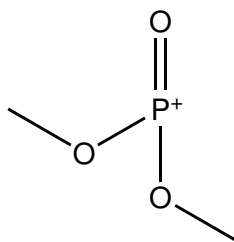
m/z: 109.01

Figure 6: TMP daughter ions with more than 80% abundance.

m/z: 78.99   m/z: 46.97   m/z: 94.99   m/z: 94.99
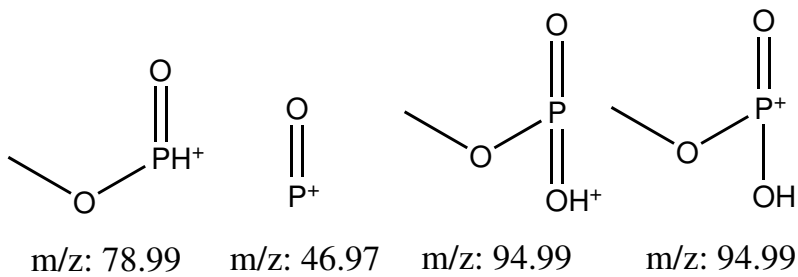
Figure 7: TMP daughter ions with more than 10% abundance.

4.4.2 TEP

According to the proposed general fragmentation mechanism proposed in Section 4.3 the peak observed at m/z 142 does not belong to the spectrum. This ion is believed to be [M-C_2H_4-C_2H_4+NH_3]$^+$ adduct and its structure can be observed in Figure 10. Based on the optimized spectrum 127 m/z should be the quantification ion and 155 m/z should be the confirmation ion. Even though 99 and 142 m/z are higher prioritized on the IntelliStart table recommendation, the 99 m/z ion is shared between almost all PFR compounds, and 142 m/z is a NH_3 adduct which which could lead to inconsistencies, especially because TEP-d15 does not have an analogus peak. See figs. 8 to 10 for spectra and suggested daughter ion structures.

Optimized Daughter Spectrum (at Collision Energy 10eV)
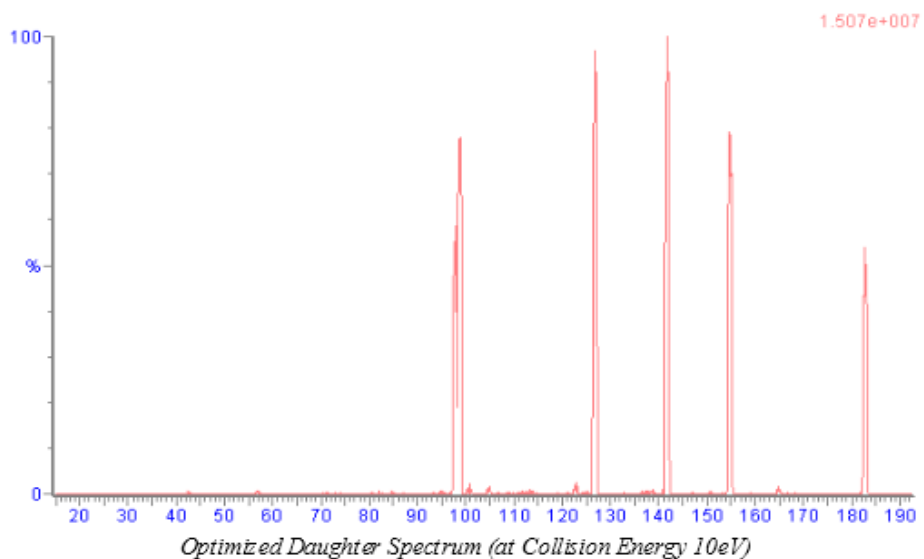
Compound	Formula/Mass		Parent m/z	Cone Voltage	Daughters	Collision Energy	Ion Mode
TEP	C6H15O4P	1	182.85	22	98.65	18	ES+
		2	182.85	22	141.80	6	ES+
		3	182.85	22	126.85	10	ES+
		4	182.85	22	154.86	8	ES+

Figure 8: Spectrum and fragments generated with IntelliStart

m/z: 183.08
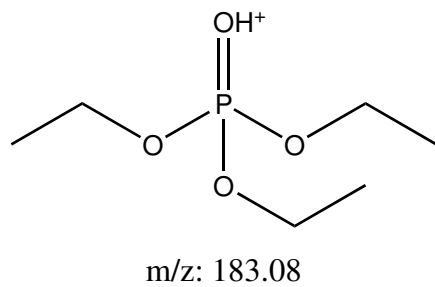
Figure 9: TEP precursor ion

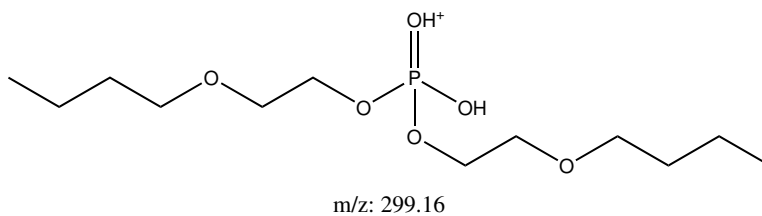
m/z: 98.98   m/z: 142.03

m/z: 127.02   m/z: 155.05
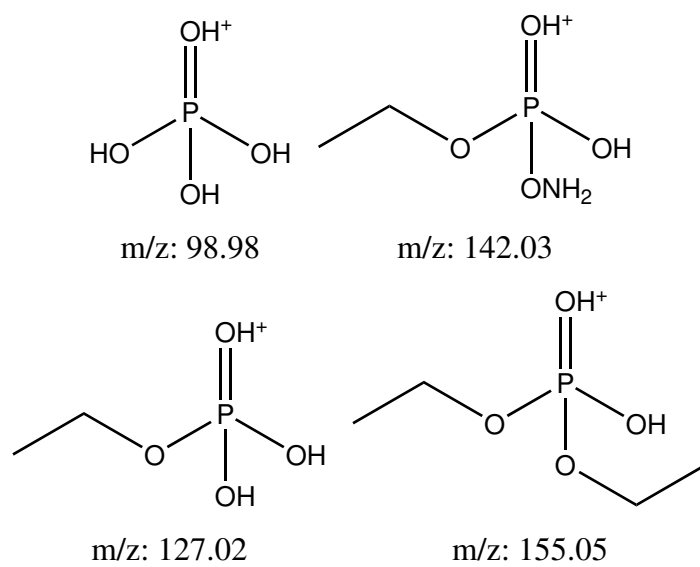
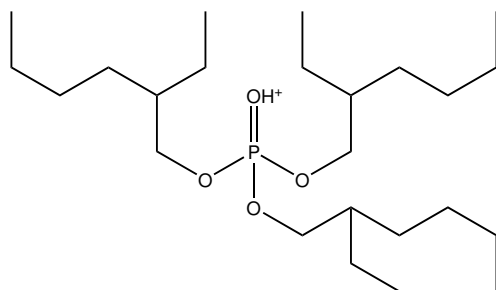**Figure 10:** TEP daughter ions with more than 80% abundance.

4.4.3 TnPP

TnPP follow the proposed mechanism of cleavage of one alkyl chain at C-O bond at the time. The collision energy requirement is relative to the other PFRs of medium strength for all peaks apart from the 81 m/z fragment, which is very high. The 81 m/z fragment might have a high collision energy due to the cleavage of the P-O bond. However, the structure of this proposed fragment is uncertain. IntelliStart also proposed a fragment at 85 m/z, however, this fragment had very low abundance at all collision energy spectra observed. IntelliStart did not, howevever propose 183 m/z as a fragment. Based on the observations of the daughter spectrum at 10 eV collision energy, 183 m/z should've been proposed as a daughter fragment. For TnPP 141 m/z is recommended as the quantification ion and 183 m/z as the confirmation ion in order to avoid using the general 99 m/z fragment. See figs. 11 to 15 for spectra and suggested daughter ion structures.
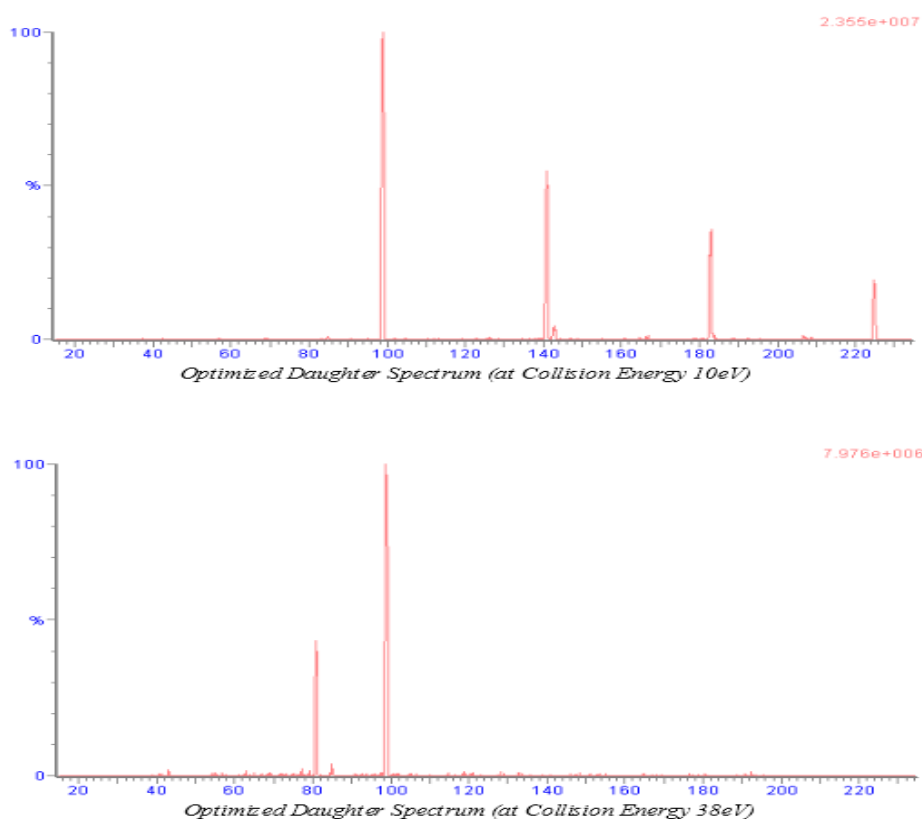
Compound	Formula/Mass		Parent m/z	Cone Voltage	Daughters	Collision Energy	Ion Mode
TnPP	C9H21O4P	1	224.89	10	98.83	16	ES+
		2	224.89	10	140.87	10	ES+
		3	224.89	10	84.80	18	ES+
		4	224.89	10	80.83	38	ES+

Figure 11: Spectrum and fragments generated with IntelliStart

m/z: 225.13
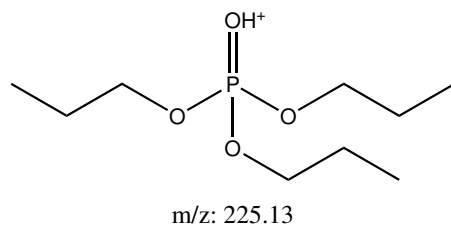
Figure 12: TnPP precursor ion

m/z: 98.98
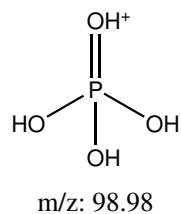
Figure 13: TnPP daughter ions with more than 80% abundance.

m/z: 141.03   m/z: 80.97   m/z: 80.97
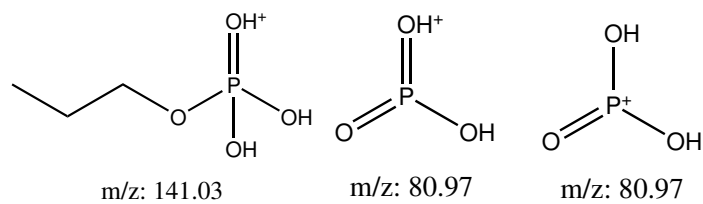
Figure 14: TMP daughter ions with more than 40% abundance.

m/z: 183.08
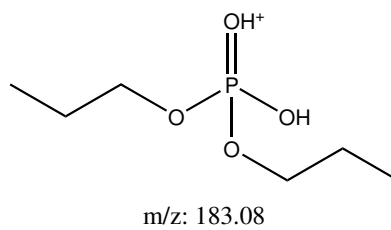
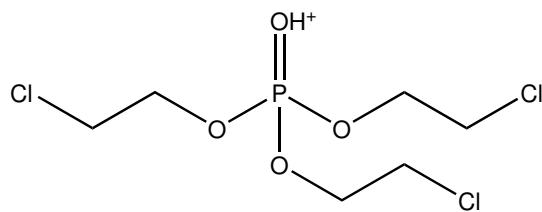**Figure 15:** TMP daughter ions with more than 20% abundance.

4.4.4 TnBP

TnBP follow the proposed mechanism of cleavage of one alkyl chain at the C-O bond at the time. The collision energy requirement is low/medium for all peaks apart from the 81 m/z fragment, which is very high. Just like TnPP the 81 m/z fragment might have a high collision energy due to the cleavage of the P-O bond. For TnBP the recommended fragments are 211 m/z as the quantification ion and 155 m/z as the confirmation ion in order to avoid using the general 99 m/z fragment, and preferably not use 155 as the quantification ion as this m/z is shared between a few other compounds as well. See figs. 16 and 18 to 20 for spectra and suggested structures of the daughter ions.
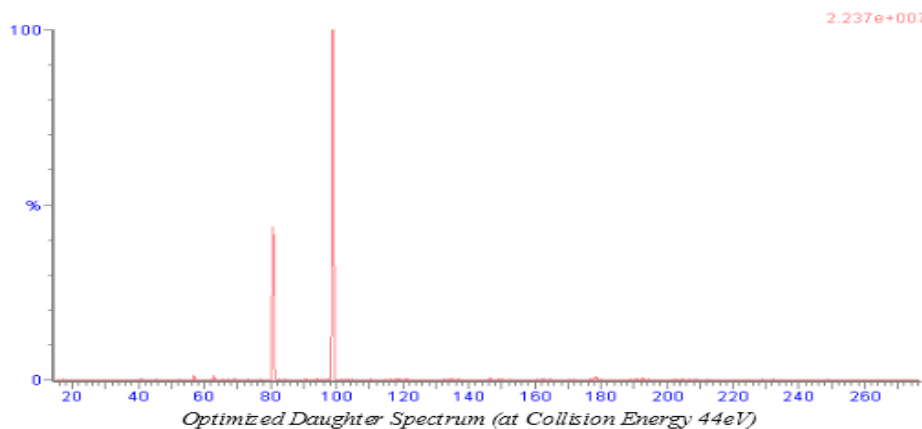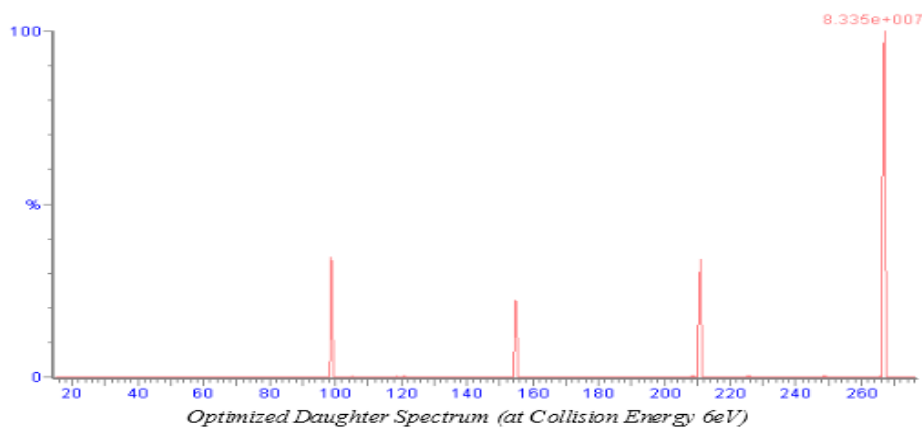
Compound	Formula/Mass		Parent m/z	Cone Voltage	Daughters	Collision Energy	Ion Mode
TnBP	C12H27O4P	1	266.88	10	98.76	14	ES+
		2	266.88	10	154.84	8	ES+
		3	266.88	10	210.92	6	ES+
		4	266.88	10	80.82	44	ES+

Figure 16: Spectrum and fragments generated with IntelliStart

m/z: 267.17
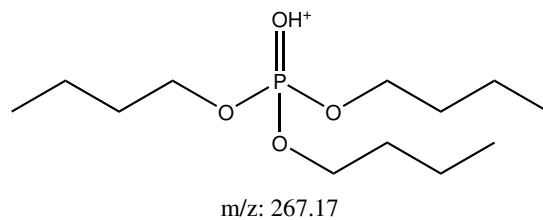
**Figure 17:** TnBP precursor ion

m/z: 98.98
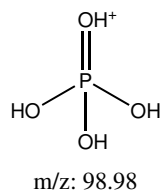
Figure 18: TnBP daughter ions with more than 80% abundance.

m/z: 80.97   m/z: 80.97
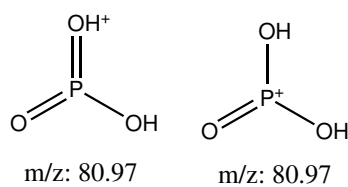
Figure 19: TnBP daughter ions with more than 40% abundance.

m/z: 211.11   m/z: 155.05
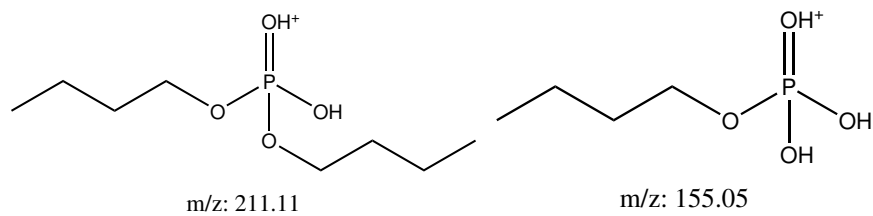
Figure 20: TnBP daughter ions with more than 20% abundance.

4.4.5   TiBP

The fragments generated in the spectra of TiBP are almost identical to the ones in the spectra of TnBP, and because the LC method used in the project can't separate TiBP and TnBP it is not possible to determine the concentration of them individually. Instead they will be combined. See section 4.4.4 for further discussion on the fragments, and figs. 21 to 25 for spectra and suggested daughter fragments structures for TiBP.
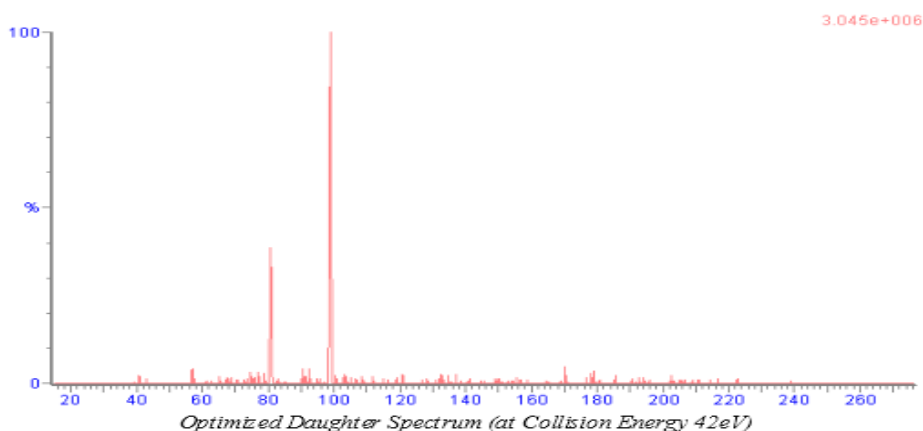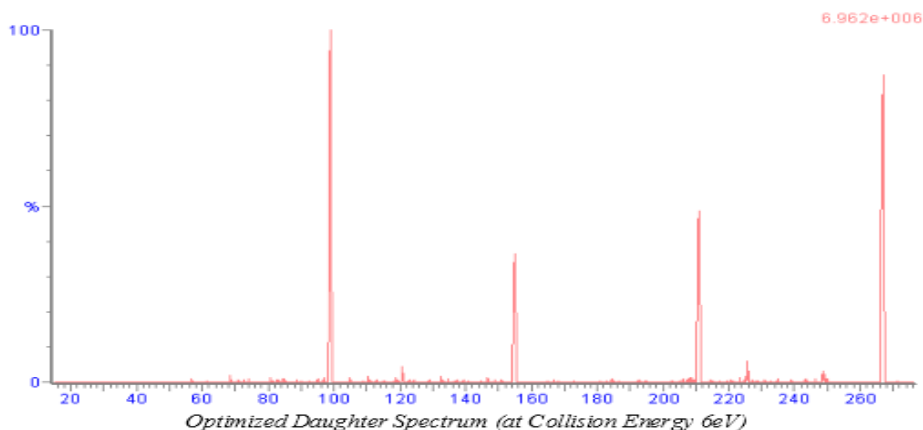
Compound	Formula/Mass		Parent m/z	Cone Voltage	Daughters	Collision Energy	Ion Mode
TiBP	C12H27O4P	1	266.88	14	98.82	14	ES+
		2	266.88	14	210.92	6	ES+
		3	266.88	14	154.84	6	ES+
		4	266.88	14	80.83	42	ES+

Figure 21: Spectrum and fragments generated with IntelliStart

m/z: 267.17
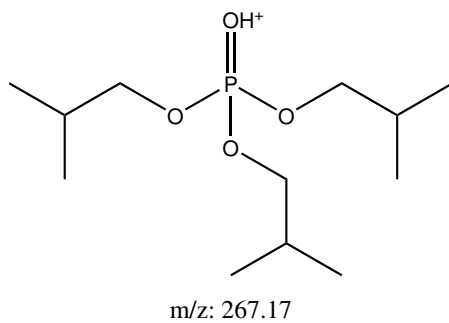
Figure 22: TiBP precursor ion

m/z: 98.98
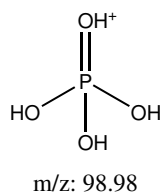
Figure 23: TiBP daughter ions with more than 80% abundance.

m/z: 211.11
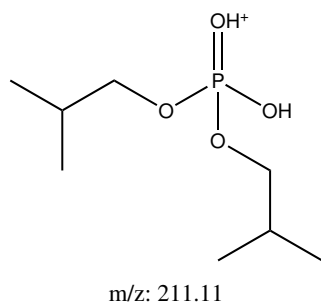
Figure 24: TiBP daughter ions with more than 40% abundance.
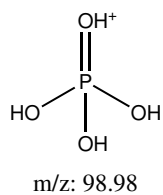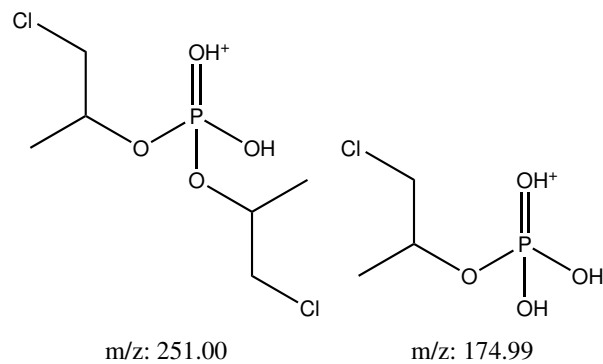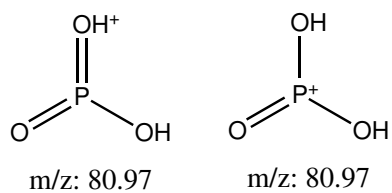

m/z: 155.05   m/z: 80.97   m/z: 80.97
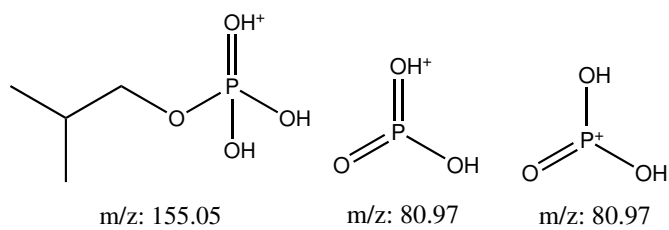
Figure 25: TiBP daughter ions with more than 20% abundance.

4.4.6 TBOEP

TBOEP follow the suggested mechanism of cleavage of one alkyl chain at the C-O bond at the time. The collision energy requirement is medium/high for all peaks. Any of the fragment daughters 299 m/z and 199 m/z can be suggested as quantification and confirmation ions with medium collision energy. 99 m/z daughter fragment should be avoided if possible. 142 m/z is not very abundant in any of the spectra and should therefore not only be regarded as an option if the other fragments show inconsistencies. See Figures 26 to 29 for spectra and suggested daughter ion structures.

Optimized Daughter Spectrum (at Collision Energy 14eV)
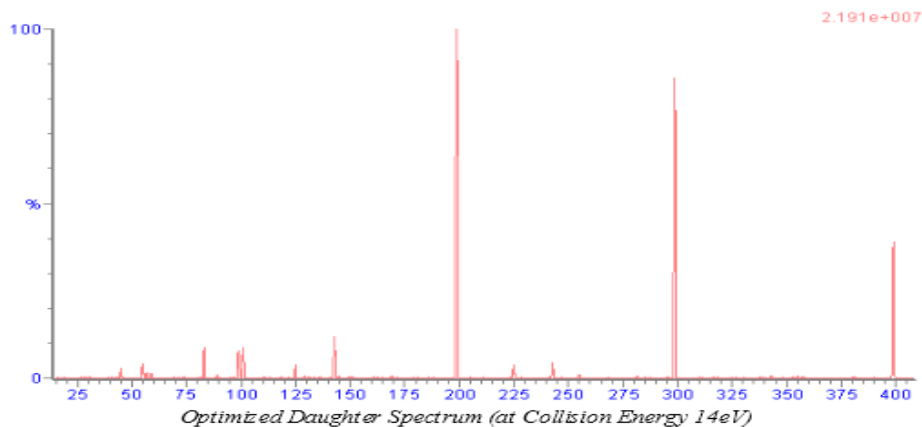
Compound	Formula/Mass		Parent m/z	Cone Voltage	Daughters	Collision Energy	Ion Mode
TBOEP	C18H39O7P	1	398.89	12	298.89	10	ES+
		2	398.89	12	198.82	14	ES+
		3	398.89	12	98.82	26	ES+
		4	398.89	12	142.81	16	ES+

Figure 26: Spectrum and fragments generated with IntelliStart

m/z: 399.25
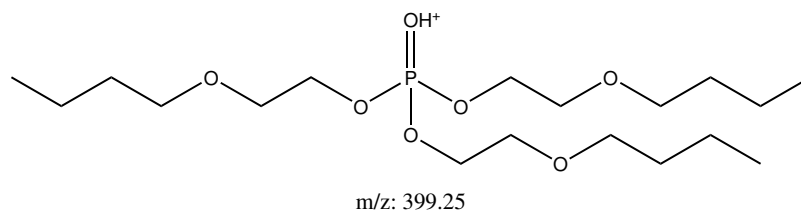
Figure 27: TBOEP precursor ion

m/z: 199.07

m/z: 299.16
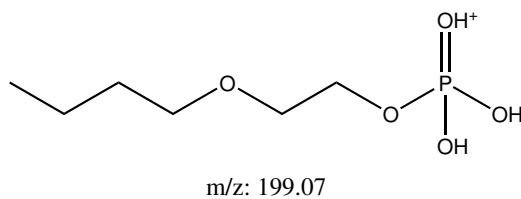
Figure 28: TBOEP daughter ions with more than 80% abundance.


m/z: 98.98   m/z: 143.01
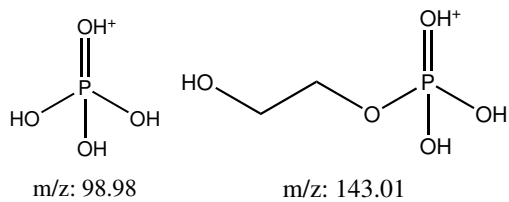
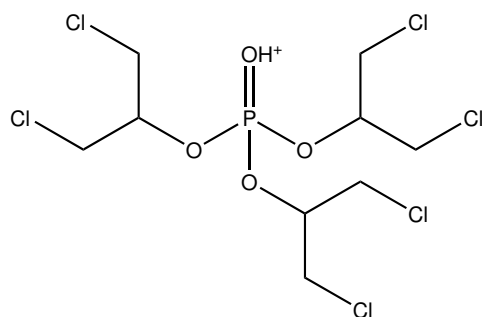**Figure 29:** TBOEP daughter ions with less than 20% abundance.

4.4.7 TEHP

TEHP follow the suggested mechanism of cleavage of one alkyl chain at the C-O bond at the time. The collision energy requirement is low/medium for all peak, however the abundance is also quite low on all daughter fragments apart from 99 m/z. Based on the abundance 323 m/z could be used as quantification and 99 m/z as confirmation ion as the unique 211 m/z fragment has a very low abundance. The suggested structure of the fragment at 71 m/z is based on cation stability and Alygizakis et al. (2019). See Figures 30 and 32 to 34.

Optimized Daughter Spectrum (at Collision Energy 6eV)
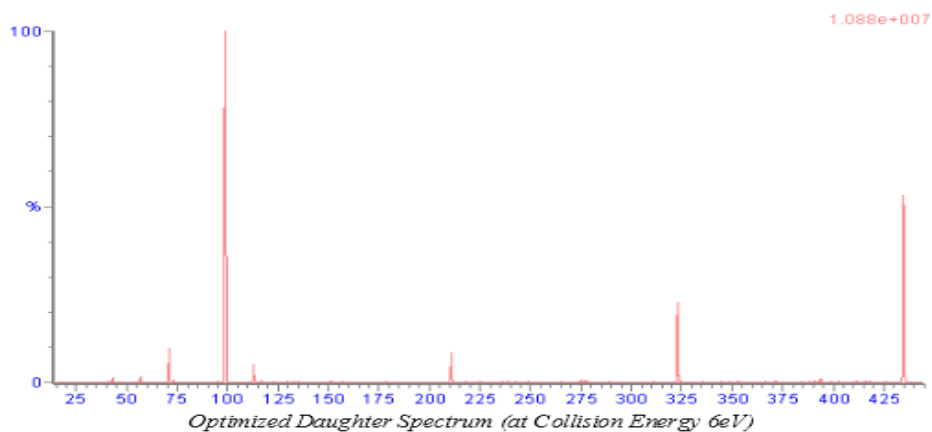
Compound	Formula/Mass		Parent m/z	Cone Voltage	Daughters	Collision Energy	Ion Mode
TEHP	C24H51O4P	1	434.94	24	98.82	12	ES+
		2	434.94	24	322.96	4	ES+
		3	434.94	24	70.95	8	ES+
		4	434.94	24	210.92	6	ES+

Figure 30: Spectrum and fragments generated with IntelliStart

m/z: 435.36

**Figure 31:** TEHP precursor ion
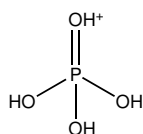
m/z: 98.98

Figure 32: TEHP daughter ions with more than 80% abundance.
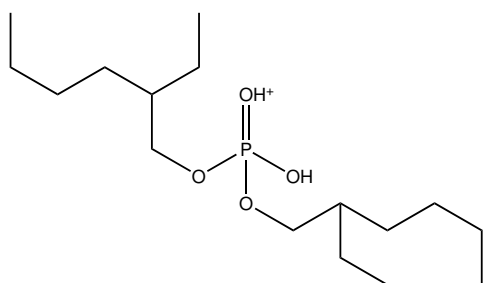
m/z: 323.24

**Figure 33:** TEHP daughter ions with more than 20% abundance.
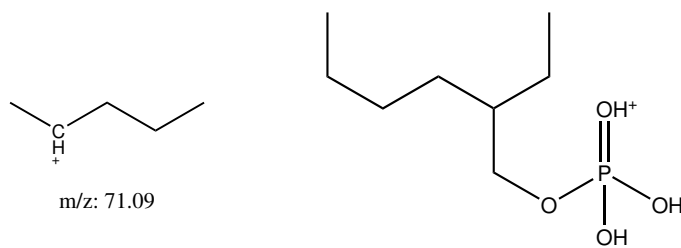
m/z: 71.09

m/z: 211.11

Figure 34: TEHP daughter ions with less than 20% abundance.

4.4.8 TCEP

TCEP follow the suggested mechanism of cleavage of one alkyl chain at the C-O bond at the time. The collision energy requirement is medium/high for all peak. Based on the abundance 223, 161 and 125 m/z can all be used as quantification and confirmation ion as they all are unique and of decent abundance. See Figures 35 to 39 for spectra and suggested daughter fragment structures.

Optimized Daughter Spectrum (at Collision Energy 12eV)
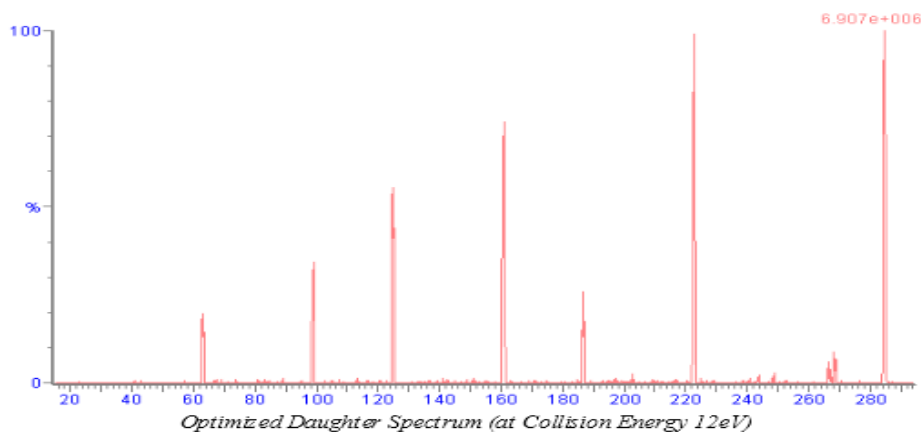
Compound	Formula/Mass		Parent m/z	Cone Voltage	Daughters	Collision Energy	Ion Mode
TCEP	C6H12Cl3O4P	1	284.67	16	98.82	22	ES+
		2	284.67	16	222.73	12	ES+
		3	284.67	16	160.74	14	ES+
		4	284.67	16	124.81	14	ES+

Figure 35: Spectrum and fragments generated with IntelliStart

m/z: 284.96

Figure 36: TCEP precursor ion
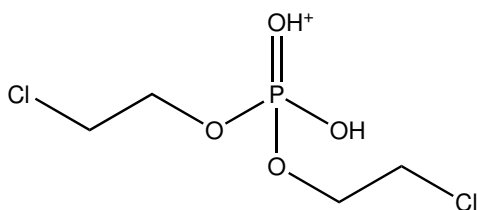
m/z: 222.97

Figure 37: TCEP daughter ions with more than 80% abundance.
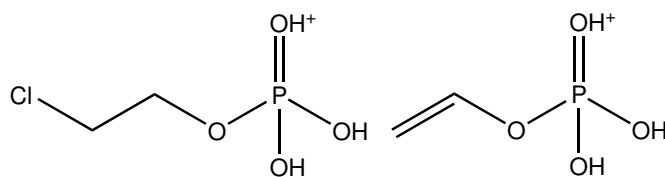
m/z: 160.98   m/z: 125.00

Figure 38: TCEP daughter ions with more than 40% abundance.
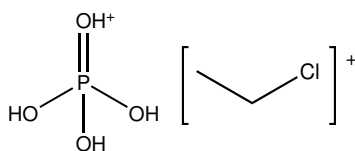
m/z: 98.98   m/z: 63.00

Figure 39: TCEP daughter ions with more than 20% abundance.

4.4.9 TCIPP

TCIPP follow the suggested mechanism of cleavage of one alkyl chain at the C-O bond at the time. The collision energy requirement is low to very high for the different peaks. Based on the abundance 175 and 251 m/z can be used as quantification and confirmation ion as they both are unique and of decent abundance. The 81 m/z fragment is interesting as the structure suggested shows a cleavage of a P-O bond, hence the very high collision energy of 50 eV. See Figures 40 to 44 for spectra and suggested daughter ion structures.

Optimized Daughter Spectrum (at Collision Energy 8eV)

Optimized Daughter Spectrum (at Collision Energy 50eV)
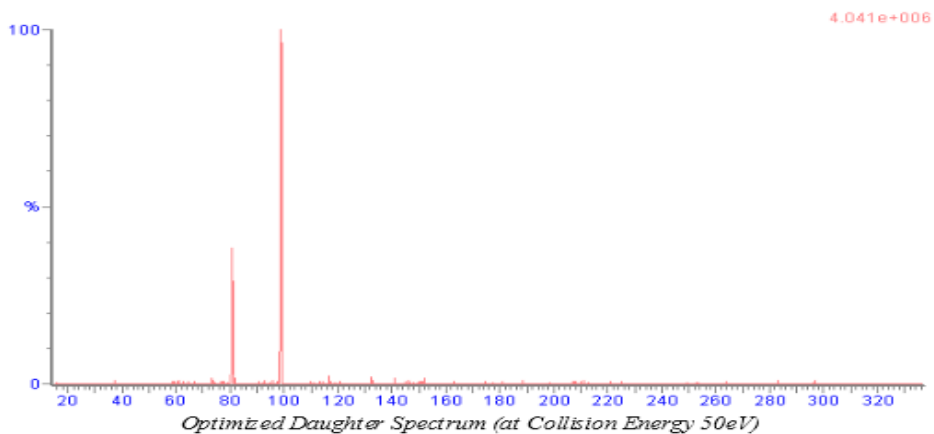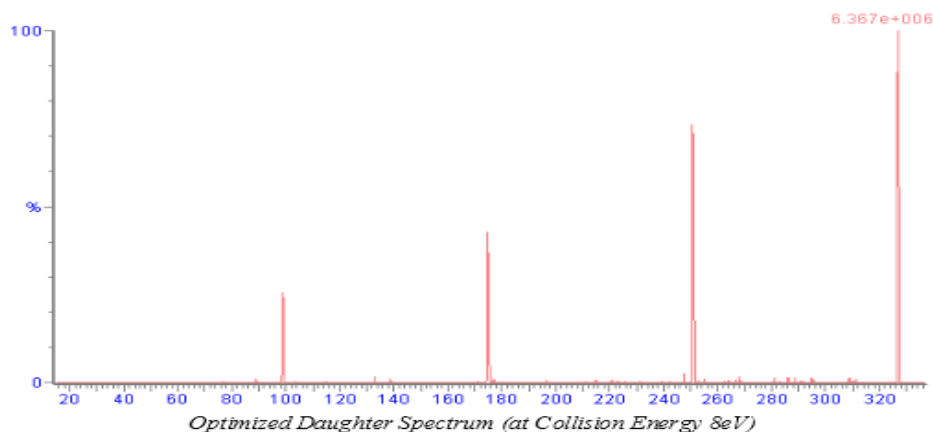
Compound	Formula/Mass		Parent m/z	Cone Voltage	Daughters	Collision Energy	Ion Mode
2020_TCIPP	326	1	327.10	2	98.94	20	ES+
		2	327.10	2	175.02	12	ES+
		3	327.10	2	251.01	8	ES+
		4	327.10	2	80.97	50	ES+

Figure 40: Spectrum and fragments generated with IntelliStart

m/z: 327.01
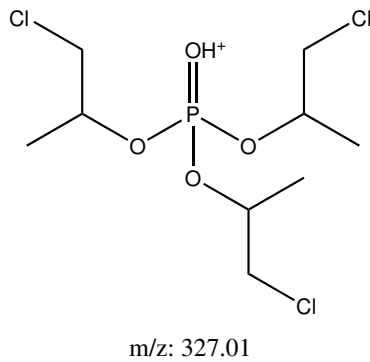
Figure 41: TCIPP precursor ion

m/z: 98.98

Figure 42: TCIPP daughter ions with more than 80% abundance.

m/z: 251.00   m/z: 174.99

Figure 43: TCIPP daughter ions with more than 40% abundance.

m/z: 80.97   m/z: 80.97

Figure 44: TCIPP daughter ions with more than 20% abundance.

4.4.10 TDCIPP

TCIPP follow the suggested mechanism of cleavage of one alkyl chain at the C-O bond at the time. The collision energy requirement is medium to very high for the different peaks. Based on the abundance 209 and 319 m/z can be used as quantification and confirmation ion as they both are unique and of decent abundance. The 75 m/z fragment is interesting as the structure suggested cleavage not at the C-O ester bond with a very high collision energy. See Figures 45 to 49 for spectra and suggested structure of daughter ions.
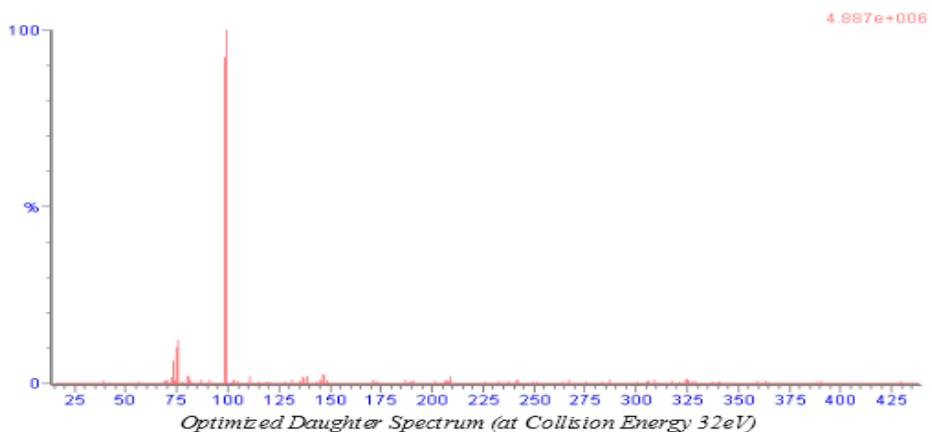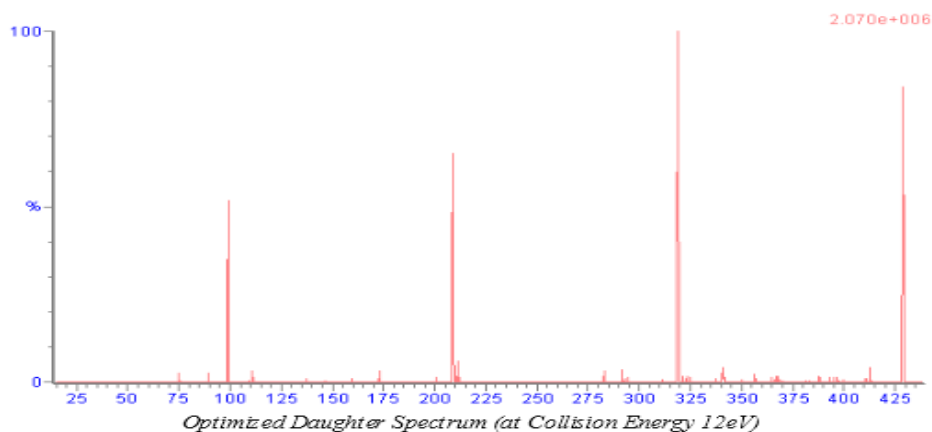
Compound	Formula/Mass		Parent m/z	Cone Voltage	Daughters	Collision Energy	Ion Mode
2020_TDCIPP	C9H15Cl6O4P	1	428.98	28	98.93	22	ES+
		2	428.98	28	208.96	16	ES+
		3	428.98	28	318.94	12	ES+
		4	428.98	28	74.98	32	ES+

Figure 45: Spectrum and fragments generated with IntelliStart

m/z: 428.89

Figure 46: TDCIPP precursor ion
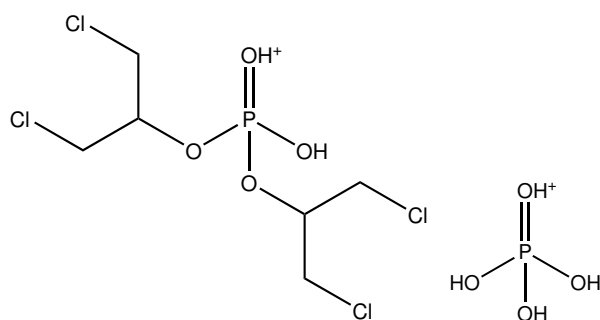
m/z: 318.92   m/z: 98.98

Figure 47: TDCIPP daughter ions with more than 80% abundance.
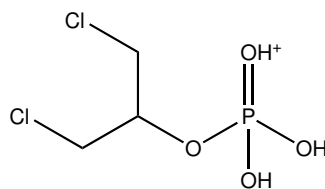
m/z: 208.95

Figure 48: TDCIPP daughter ions with more than 60% abundance.
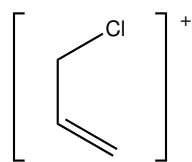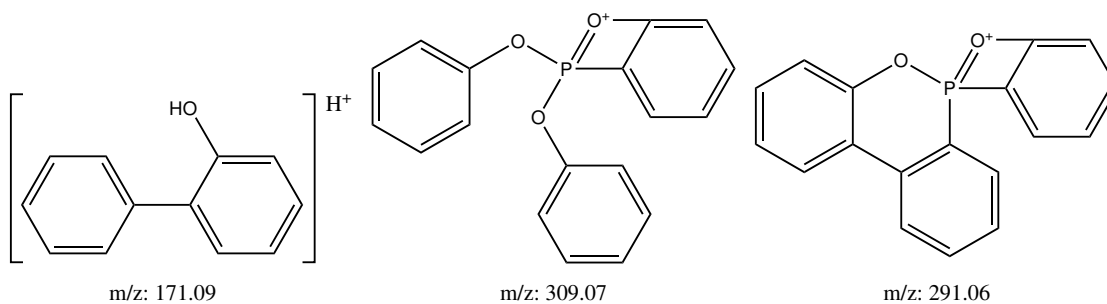

m/z: 75.00

Figure 49: TDCIPP daughter ions with less than 20% abundance.

4.4.11   TPP

TPP partly follow the suggested mechanism of cleavage of one alkyl chain at the C-O bond at the time. However, another phenomenon is observed as well. The spectrum shows several cases of H_2O (-18 m/z) and phenol (-94 m/z) cleavage, meaning breakage of the P-O bond is occurring. Multiple of the ions observed in the MS spectra support the rearrangement of the core phosphorus atom is bound to the aromatic ring both through a P-O bond, but also directly through a newly formed P-C bond. Even though some of the peaks have low abundance they are observed and support the structure. Observe the peaks in the spectrum Figure 50 with m/z values at 309, 291, 251, 233, 215, 171, 152, 94 and 77. It is uncertain whether there's a double bond between P=O or whether phosphorus goes through a change in oxidation number. These aromatic rearrangement structures will be repeating for other analytes as well and only one of the forms will be included, but it is uncertain which is more correct. See the suggested variations for the 215 m/z ion in fig. 52.

The collision energy requirement is high/very high for all the peaks found by IntelliStart. Based on the abundance and uniqueness of the observed peaks, 251 m/z should be used for the quantification. One peak is expected at 175 m/z as that would be the second branch C-O cleavage that the general fragmentation mechanism most PFRs follow. However, the abundance of this peak is very small on every tested spectra. Yet a variety of poly aromatic structures with high abundance are observed. Therefore the ion 215 m/z is proposed as the confirmation ion. See Figures 50 to 54 for spectra and suggested daughter ion structures.

Optimized Daughter Spectrum (at Collision Energy 24eV)
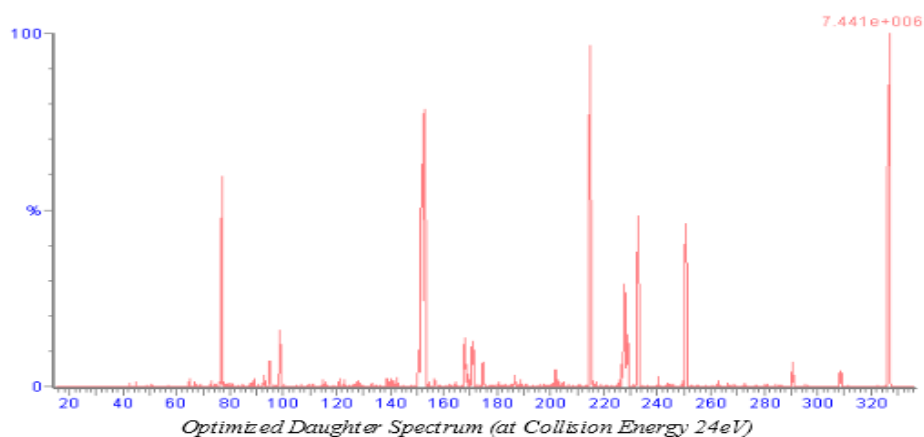
Compound	Formula/Mass		Parent m/z	Cone Voltage	Daughters	Collision Energy	Ion Mode
TPP	C18H15O4P	1	326.72	38	151.96	32	ES+
		2	326.72	38	76.92	32	ES+
		3	326.72	38	214.79	24	ES+
		4	326.72	38	250.79	28	ES+

Figure 50: Spectrum and fragments generated with IntelliStart

51
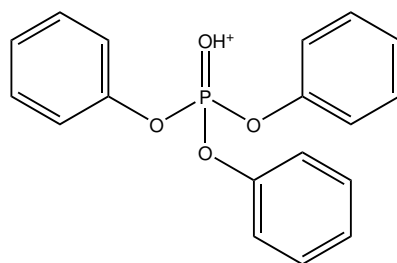
m/z: 327.08

Figure 51: TPP precursor ion

m/z: 215.03   m/z: 215.03   m/z: 152.06
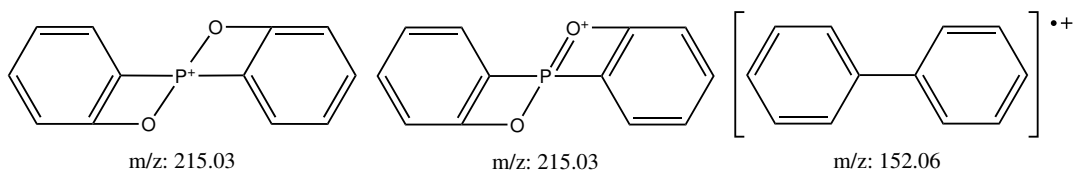
Figure 52: TPP daughter ions with more than 80% abundance.

m/z: 77.04   m/z: 233.04   m/z: 251.05
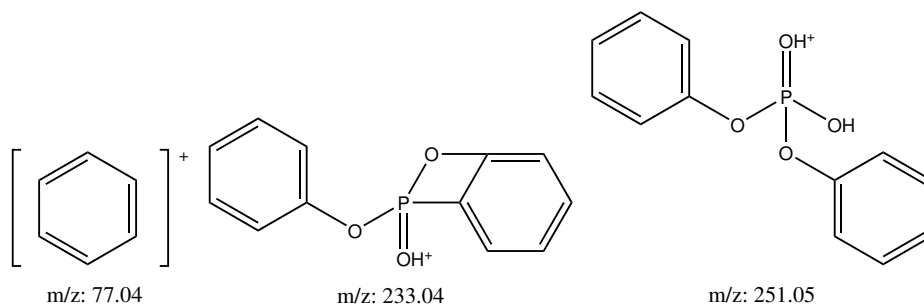
Figure 53: TPP daughter ions with more than 40% abundance.

m/z: 171.09   m/z: 309.07   m/z: 291.06

Figure 54: TPP daughter ions with less than 20% abundance.

4.4.12 TMPP

TMPP partly follow the suggested mechanism of cleavage of one alkyl chain at the C-O bond at the time. However, it also behaves similar to TPP in the cleave of P-O bonds, formation of P-C bonds and loss of H_2O. Fragments structures can again be found to support the rearrangement patterns introduced in section 4.4.11.

The collision energy requirement is like TPP high/very high for all the peaks found by IntelliStart. Based on the abundance and uniqueness of the observed peaks, 243 m/z should be used for the quantification. Large peaks are expected at 279 m/z and 189 m/z as suggested by the general mechanism for single branch cleavage fragments. These peaks are visible in the spectrum, but have significantly lower abundance than expected. 279 m/z still has enough abundance to be recommended as the confirmation ion. See Figures 55 to 60.
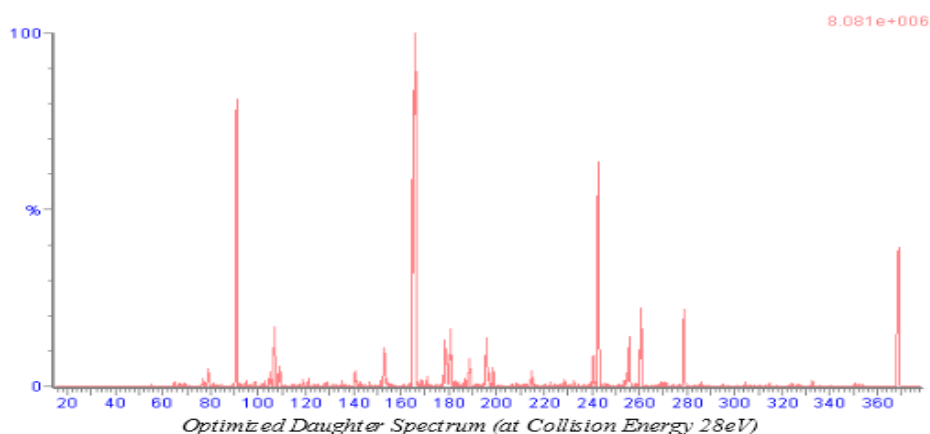
Optimized Daughter Spectrum (at Collision Energy 28eV)

Compound	Formula/Mass		Parent m/z	Cone Voltage	Daughters	Collision Energy	Ion Mode
		1	368.77	30	165.10	38	ES+
TMPP	C21H21O4P	2	368.77	30	90.90	38	ES+
		3	368.77	30	242.83	28	ES+

Figure 55: Spectrum and fragments generated with IntelliStart

m/z: 369.13
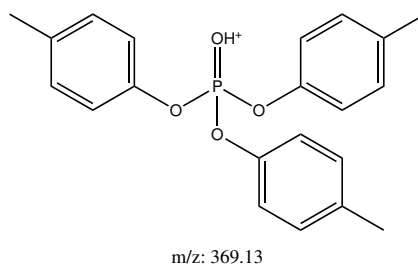
Figure 56: TMPP precursor ion
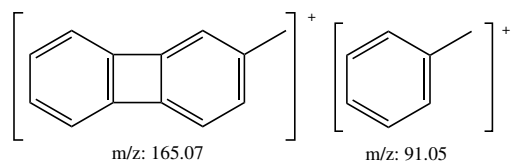
Figure 57: TMPP daughter ions with more than 80% abundance.
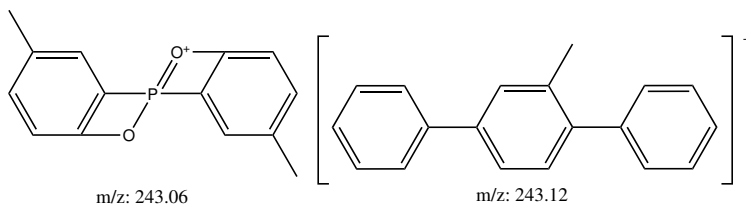
Figure 58: TMPP daughter ions with more than 60% abundance.
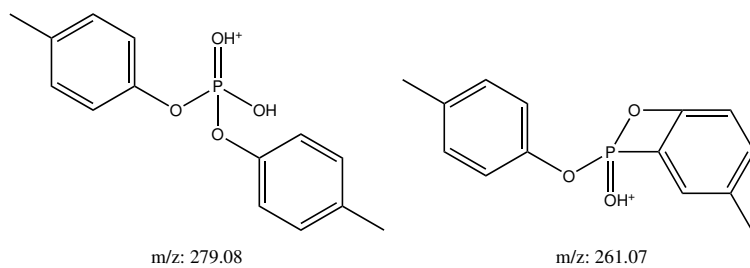
Figure 59: TMPP daughter ions with more than 20% abundance.
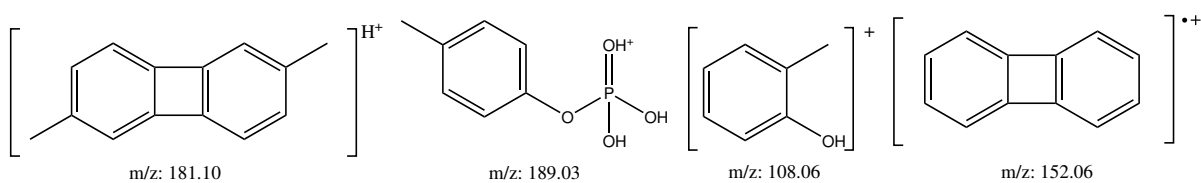
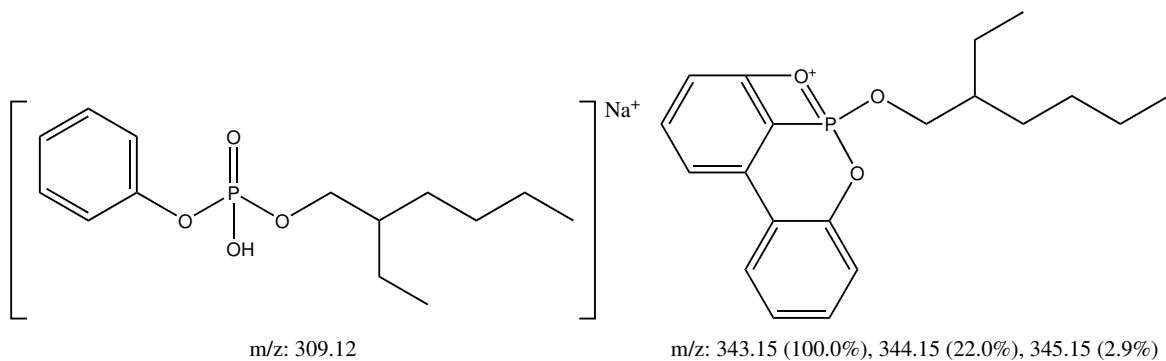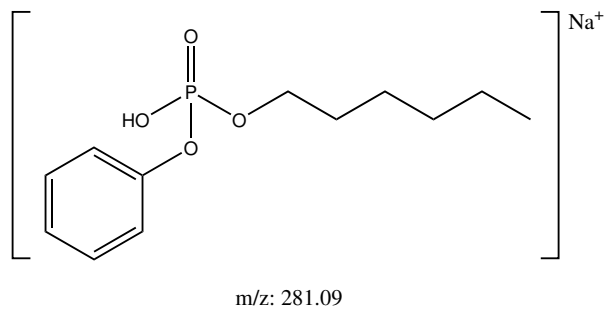**Figure 60:** TMPP daughter ions with less than 20% abundance.

4.4.13 DPMP

DPMP does not yield good daughter ion abundance for any parameters tested. The cone voltage optimization spectrum yields very equal results all the way from 3 to 50 V. The only clear peaks are the common fragments 77 m/z and 102 m/z which the parent compound can form several of. An Na adduct is formed as the $[M+Na]^+$ is the peak at 363 m/z. Recommending a daughter fragment to be used for quantification and confirmation based on these spectras can for these reasons not possible. However, several possible daughter ion strucutures are suggested. See Figures 61 to 64 for spectra and suggested daughter ion structures.

Optimized Daughter Spectrum (at Collision Energy 24eV)
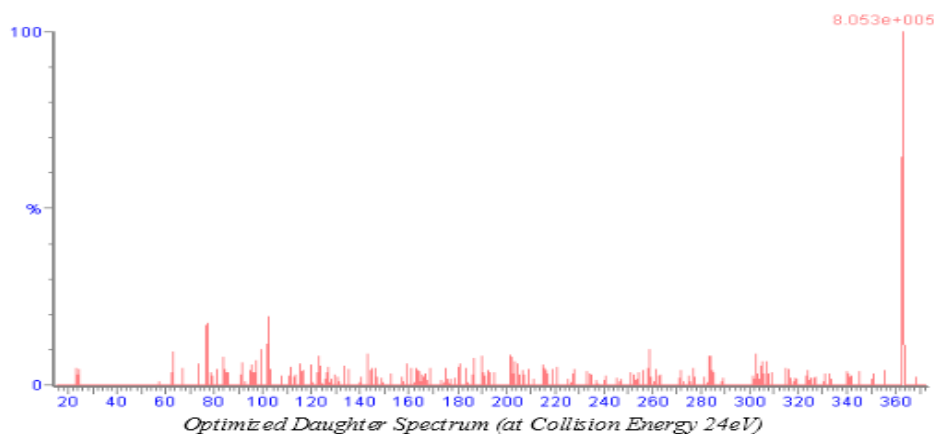
Compound	Formula/Mass		Parent m/z	Cone Voltage	Daughters	Collision Energy	Ion Mode
DPhP_DCrP	C19H17O4P	1	362.99	6	102.11	24	ES+
		2	362.99	6	77.06	22	ES+
		3	362.99	6	123.23	22	ES+
		4	362.99	6	84.22	22	ES+

Figure 61: Spectrum and fragments generated with IntelliStart

m/z: 363.08
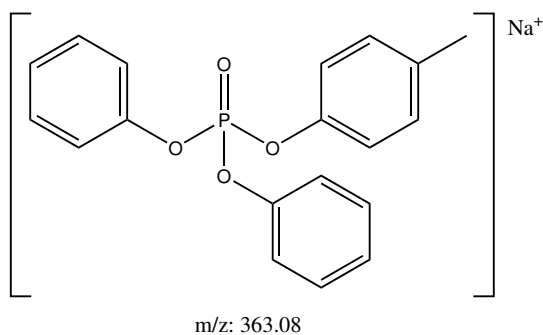
Figure 62: DPMP precursor ion

m/z: 77.04
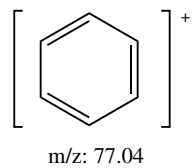
Figure 63: DPMP daughter ions with more than 20% abundance.

m/z: 175.02   m/z: 189.03   m/z: 215.03

m/z: 229.04   m/z: 233.04

m/z: 247.05   m/z: 247.05   m/z: 251.05

m/z: 265.06   m/z: 341.09
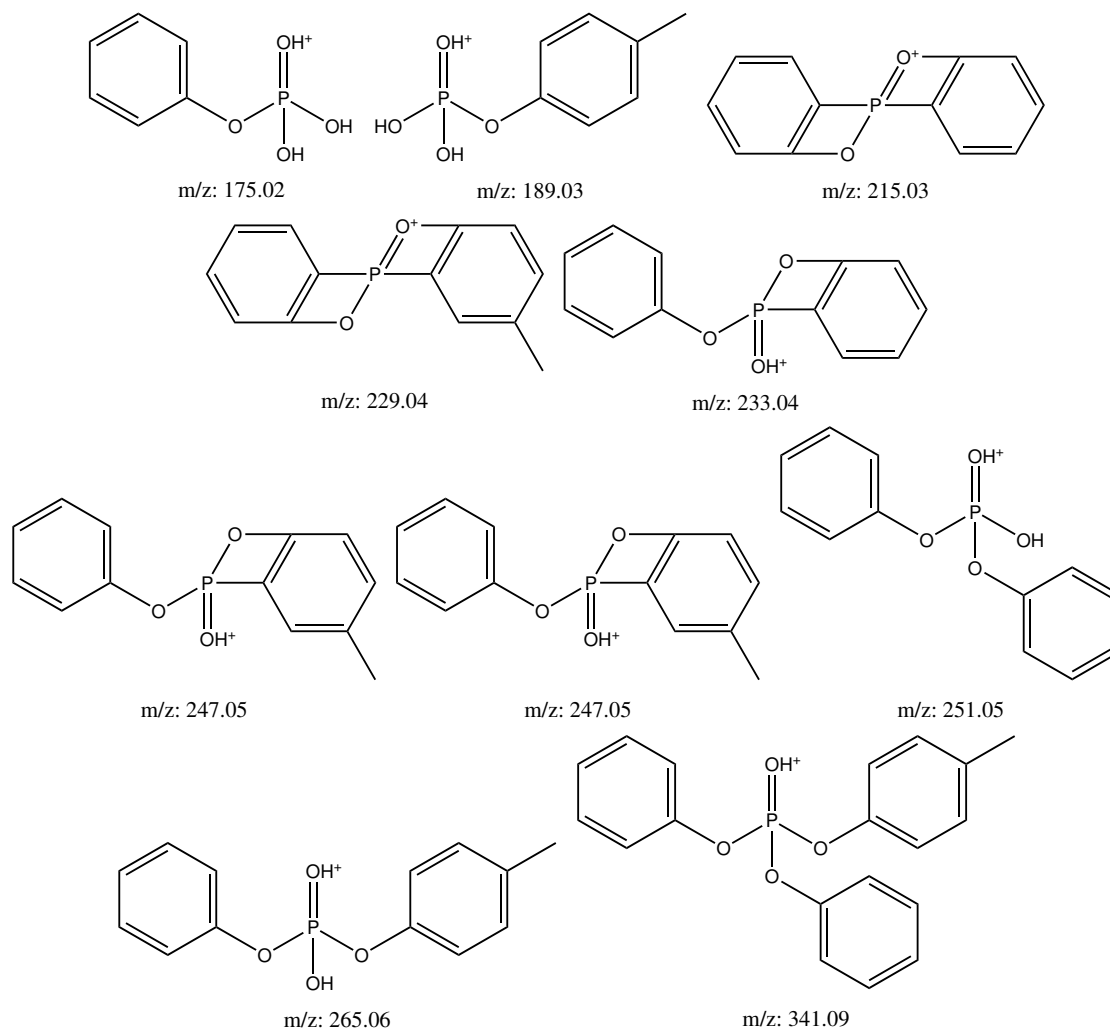
Figure 64: DPMP daughter ions with less than 20% abundance.

56

4.4.14 EHDP

An [M+Na]$^+$ adduct is formed for the parent ion at 385 m/z. Only the 273 m/z daughter ion yields a peak with decent abundance. Low abundance peaks are also observed at m/z 281 and 344. The 344 peak is also peculiar as no reasonable structure matched the m/z precisely see fig. 68. It is unclear why no further C-O bond cleavages are observed. Based on the abundance of the 273 m/z peak EHDP shouldn't be as problematic of a compound to analyze as it is. However, the fact that no other daughter ions have an abundance over even 5% is symptomatic of problematic quantification. Another interesting observation of the spectrum is that the aromatic 77 m/z peak is not visible, which it is for most other aromatic compounds. Based on these observations 273 m/z is recommended as the quantification ion and 281 m/z is recommended as the confirmation ion. See figs. 65 to 68 for spectra and suggested daughter structures.

Optimized Daughter Spectrum (at Collision Energy 20eV)
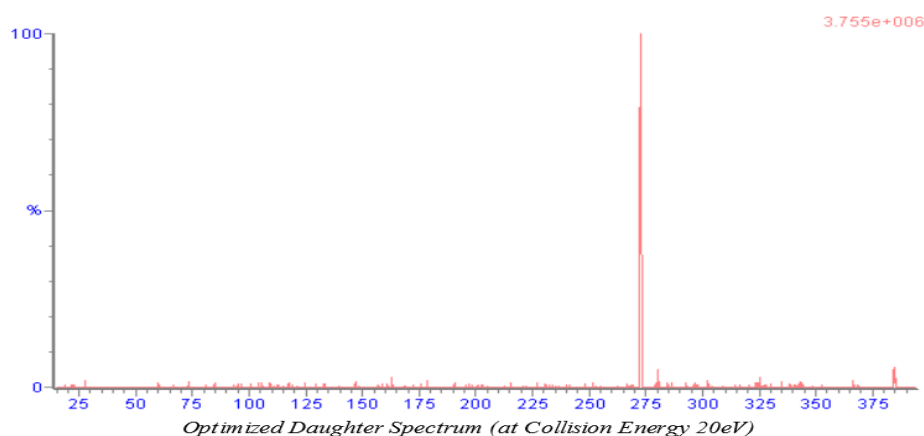
Compound	Formula/Mass		Parent m/z	Cone Voltage	Daughters	Collision Energy	Ion Mode
EHDP	362.4	1	384.73	40	272.71	14	ES+
		2	384.73	40	280.76	20	ES+
		3	384.73	40	343.61	10	ES+

Figure 65: Spectrum and fragments generated with IntelliStart

57

m/z: 385.15
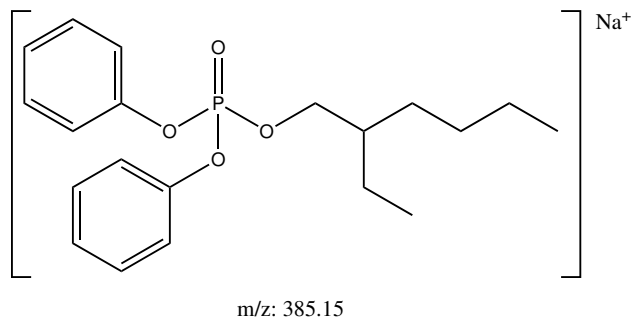
Figure 66: EHDP precursor ion

m/z: 273.03
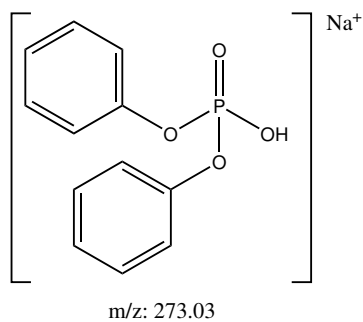
Figure 67: EHDP daughter ions with more than 20% abundance.

m/z: 281.09

m/z: 309.12

m/z: 343.15 (100.0%), 344.15 (22.0%), 345.15 (2.9%)

Figure 68: EHDP daughter ions with less than 20% abundance.

4.4.15 TTBPP

Due to the stability of tert-butyl cations the preferred cleavage bond seem to be the C-C bond between tert-butyl and the aromatic ring as seen by the loss of 56 amu between 495, 439, 383 and 327 m/z. There is also increasingly supporting evidence of what seem to be a common rearrangement for aromatic phosphates seen at lower abundance, i.e. 215 and 229 m/z. Based on these observations and of the 439, 383 and 327 m/z ions can be used as quantification and confirmation ions. See Figures 70 to 74 for spectra and suggested fragment ion structures.
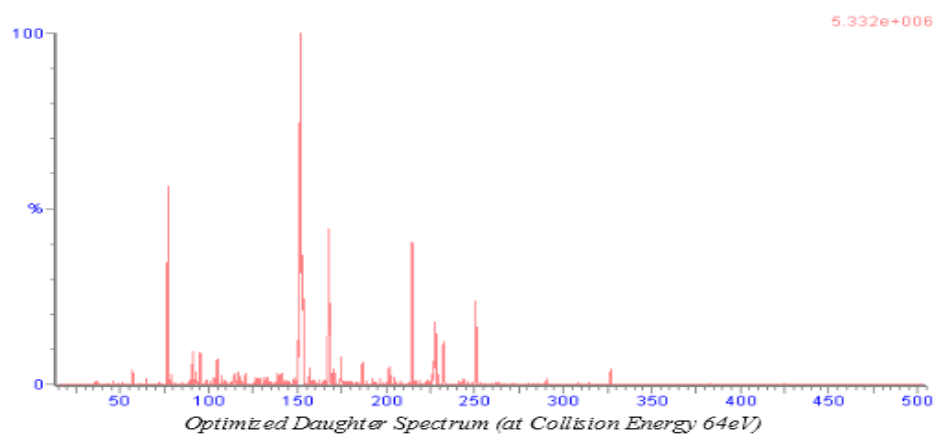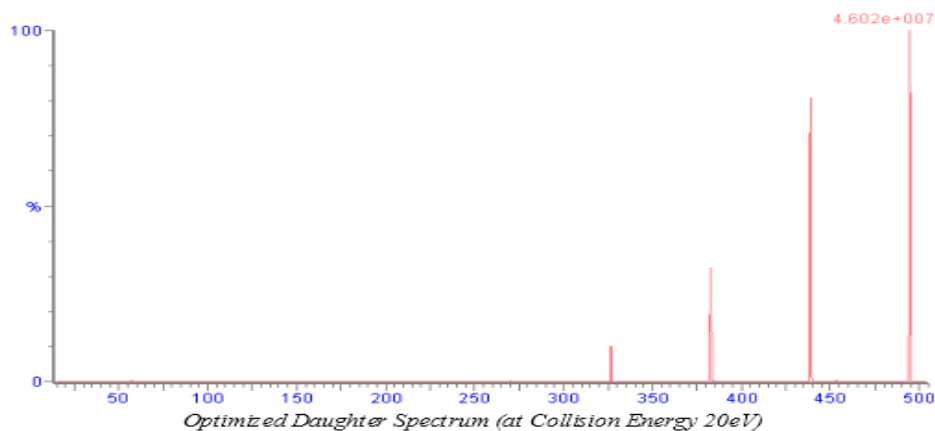
Compound	Formula/Mass		Parent m/z	Cone Voltage	Daughters	Collision Energy	Ion Mode
TTBPP	C30H39O4P	1	494.78	62	326.77	32	ES+
		2	494.78	62	438.82	20	ES+
		3	494.78	62	382.79	26	ES+
		4	494.78	62	151.97	64	ES+

Figure 69: Spectrum and fragments generated with IntelliStart
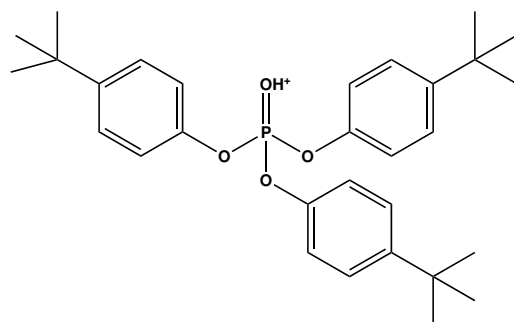
m/z: 495.27

Figure 70: TTBPP precursor ion
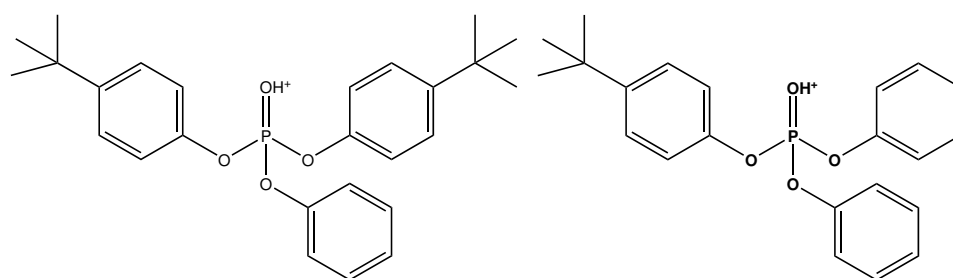
m/z: 439.20

m/z: 383.14
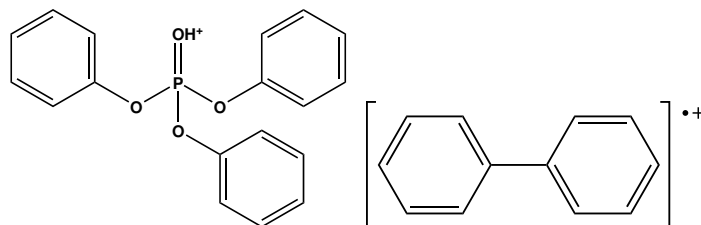
m/z: 327.08

m/z: 152.06

Figure 71: TTBPP daughter ions with more than 80% abundance.
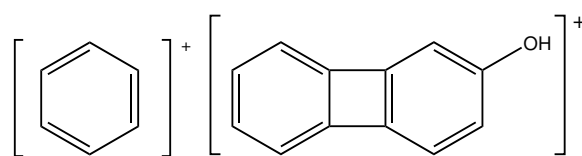
m/z: 77.04

m/z: 167.05

Figure 72: TTBPP daughter ions with more than 40% abundance.

m/z: 215.03
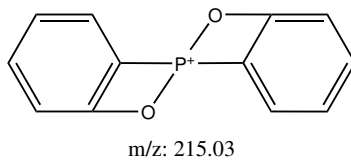
Figure 73: TTBPP daughter ions with more than 20% abundance.

m/z: 251.05   m/z: 171.09   m/z: 229.04

m/z: 233.04
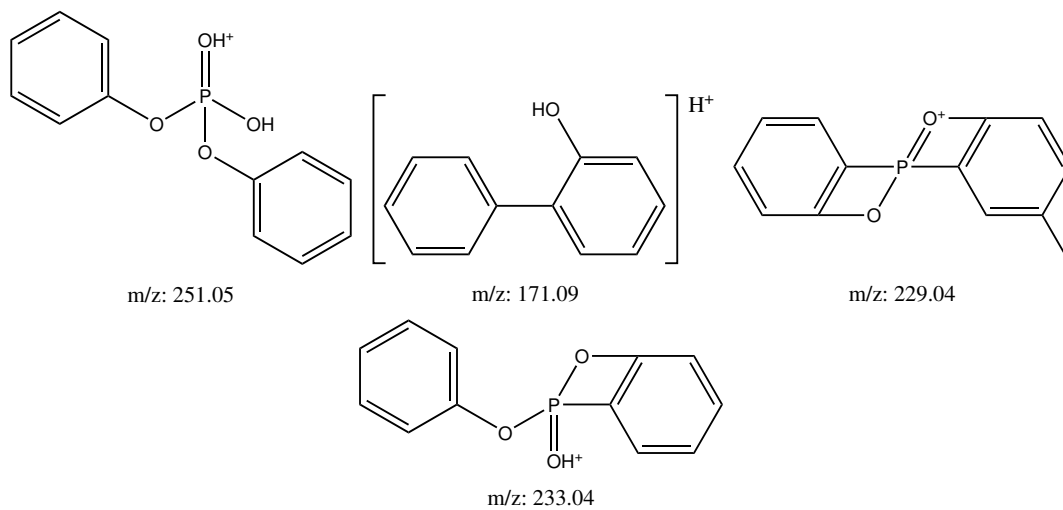
Figure 74: TTBPP daughter ions with less than 20% abundance.

4.4.16 RDP

RDP does not have any clear peaks with very distinguishable abundance, and the IntelliStart generated recommendations are either very common fragments, 77 and 23 m/z, or fragments that don't match fragmentation patterns seen in other PFRs, such as 441 m/z. Another interesting observation is the fact that the ion 521 m/z is not visible which would equal the first C-O ester bond cleavage for an aromatic ring. See figs. 75 to 78 for spectra and suggested fragment ion structures. Based on the low abundance of all the fragments, either another MS method should be applied or only a qualitative analysis seem possible.
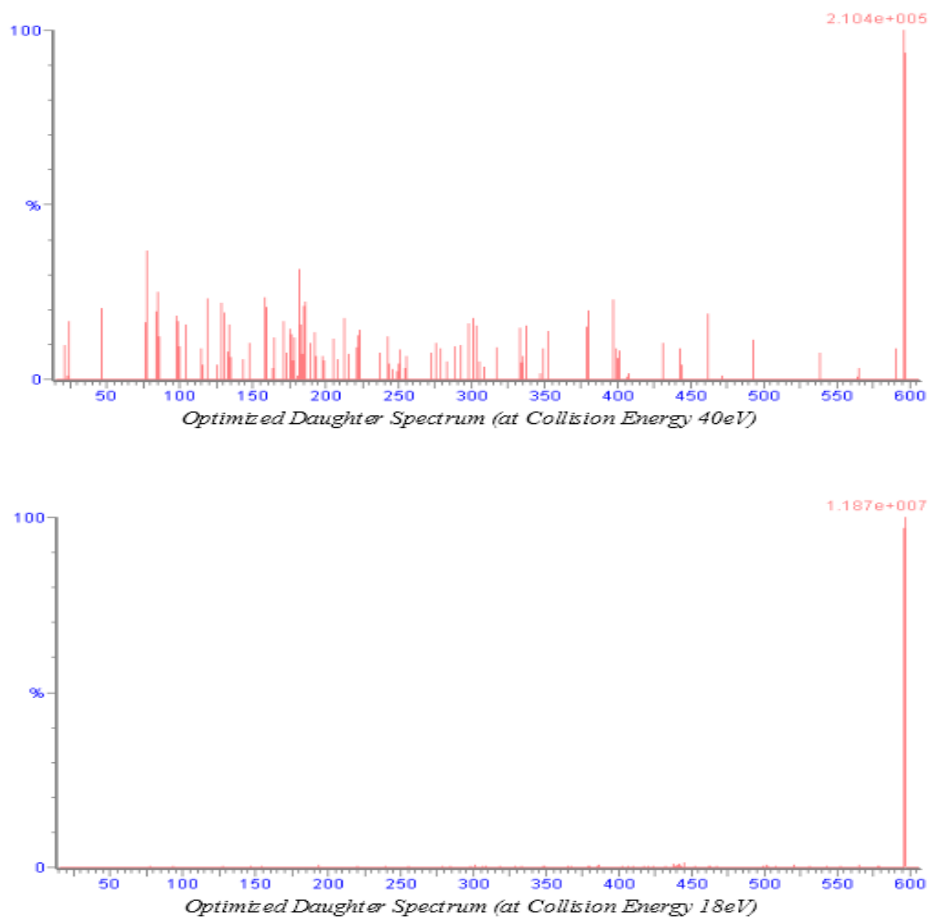
Compound	Formula/Mass		Parent m/z	Cone Voltage	Daughters	Collision Energy	Ion Mode
		1	597.00	10	441.21	18	ES+
TPRBDP_RDP	C30H24O8P2	2	597.00	10	23.14	30	ES+
		3	597.00	10	77.06	40	ES+

Figure 75: Spectrum and fragments generated with IntelliStart

m/z: 597.08
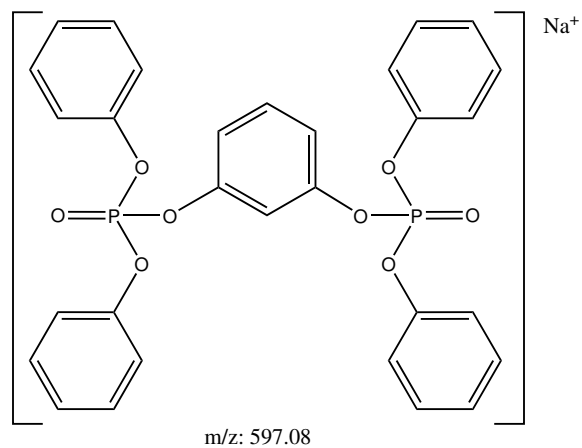
Figure 76: RDP precursor ion

m/z: 77.04
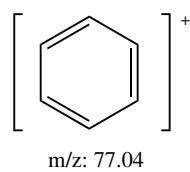
Figure 77: RDP daughter ions with more than 20% abundance.

Na
m/z: 22.99

m/z: 332.97

m/z: 445.02
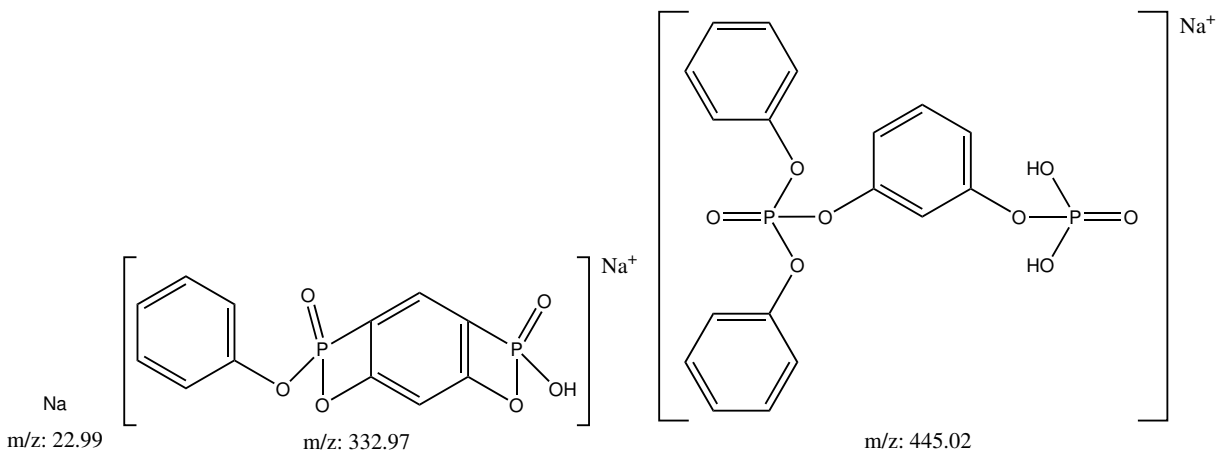
Figure 78: RDP daughter ions with less than 20% abundance.

4.4.17 V6

V6 seem to yield several fragment ions with high abundance. However, for several of the large abundance fragment ions, two structures have been suggested that both match the m/z and could potentially be stable enough. Even though the exact structure is not specifically elucidated does not mean quantitative analysis can't be performed. In fact due to the high abundance of 235, 297 and 389 m/z they all could potentially work as quantification and confirmation ion. See figs. 79 to 82 for spectra and suggested daughter ion structures.
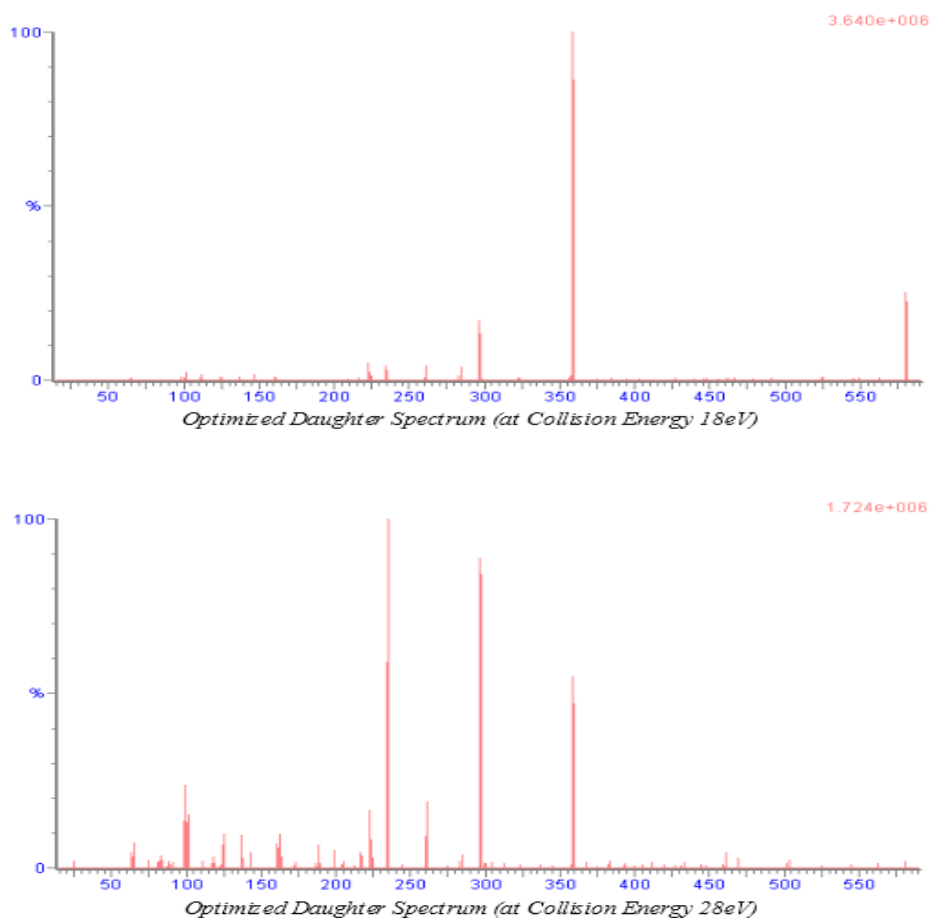
Compound	Formula/Mass		Parent m/z	Cone Voltage	Daughters	Collision Energy	Ion Mode
2020_V6	C13H24Cl6O8P2	1	581.00	4	358.99	18	ES+
		2	581.00	4	234.96	34	ES+
		3	581.00	4	297.01	28	ES+
		4	581.00	4	98.99	50	ES+

Figure 79: Spectrum and fragments generated with IntelliStart

m/z: 580.92
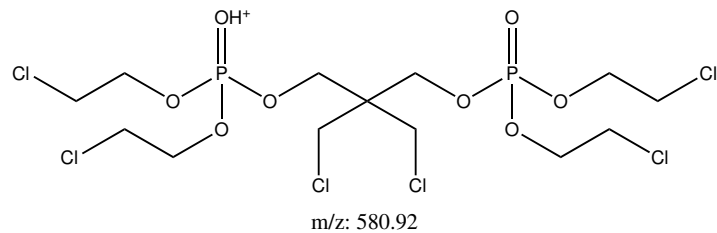
Figure 80: V6 precursor ion

m/z: 358.95   m/z: 234.97   m/z: 234.97

m/z: 296.96   m/z: 296.96
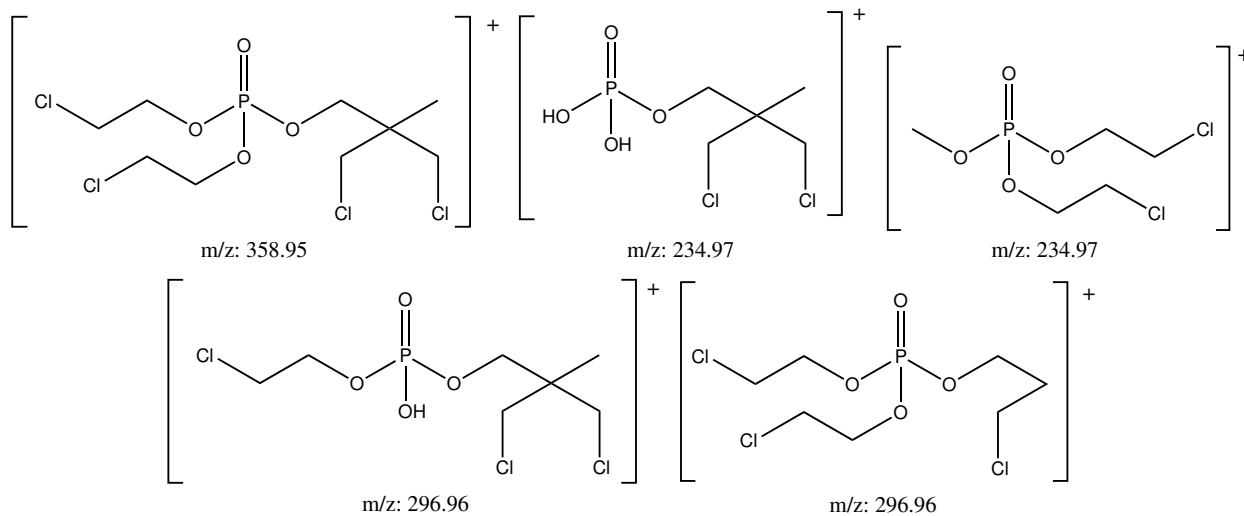
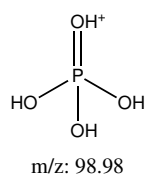**Figure 81:** V6 daughter ions with more than 80% abundance.

m/z: 98.98

Figure 82: V6 daughter ions with more than 20% abundance.

4.4.18 BPA-BDPP

All fragment ions seem to require very high collision energy for BPA-BDPP. The 367 m/z ion stands out as a high abundance ion requiring significantly less collision energy than the rest. This ion does not follow the common C-O bond breakage, instead a iso-propyl cation seem to be formed by breakage of C-C bond with an aromatic ring. The 215 m/z ion is also an interesting ion to observe as it has cleaved two C-O bonds, but also the iso-propyl-phenyl C-C bond. Another interesting peak observed in the same spectrum as 367 m/z is the 327 peak which equals the rest of the structure when the C-C iso-propyl-phenyl bond is broken. Using 367 and 327 m/z could work as a quantification and confirmation ion pair. See figs. 83 to 87 for suggested structures.
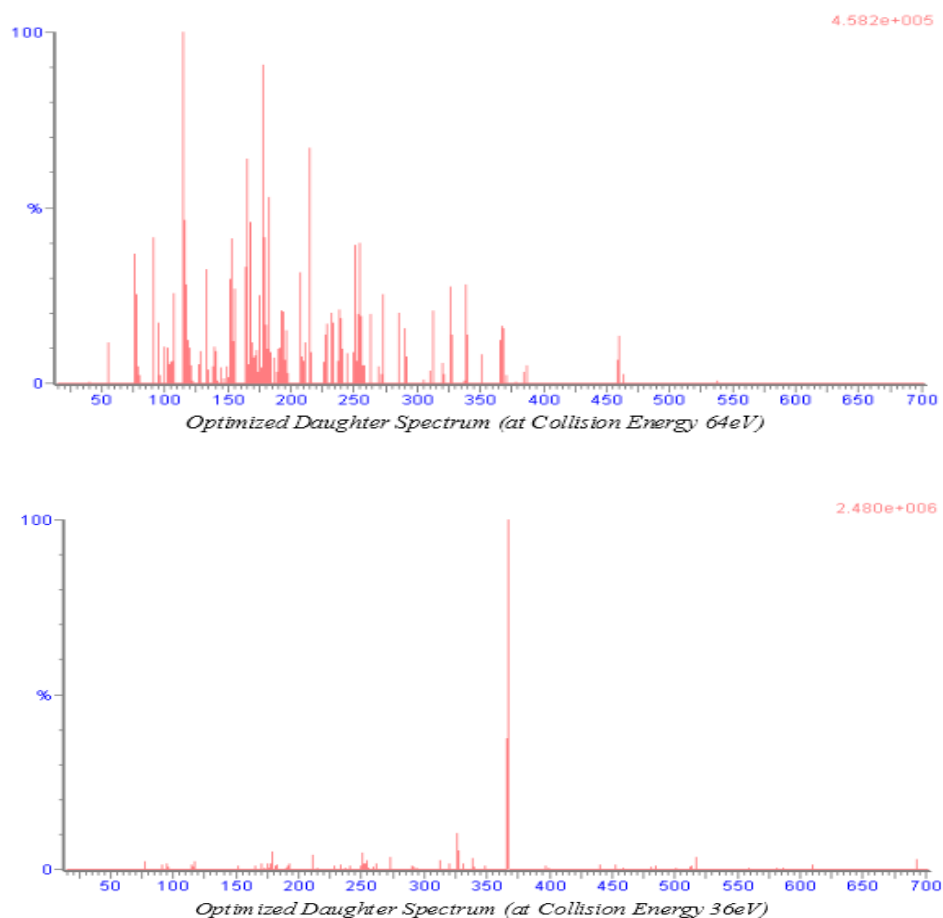
Compound	Formula/Mass		Parent m/z	Cone Voltage	Daughters	Collision Energy	Ion Mode
BPA_BDPP2020	692.6	1	693.25	80	367.14	36	ES+
		2	693.25	80	178.18	60	ES+
		3	693.25	80	115.07	70	ES+
		4	693.25	80	215.01	64	ES+

Figure 83: Spectrum and fragments generated with IntelliStart

m/z: 693.18
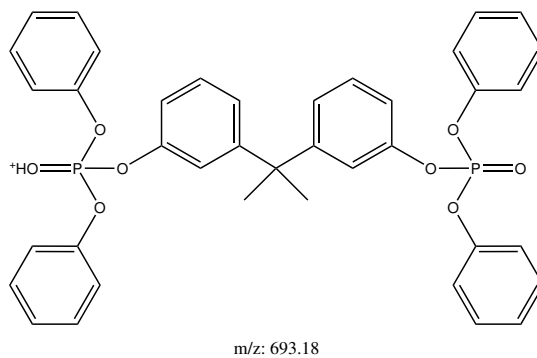
Figure 84: BPA-BDPP precursor ion

m/z: 367.11   m/z: 115.02

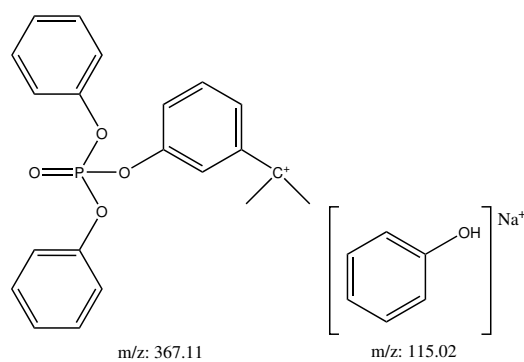**Figure 85:** BPA-BDPP daughter ions with more than 80% abundance.
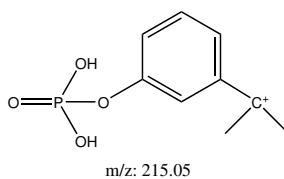

m/z: 215.05

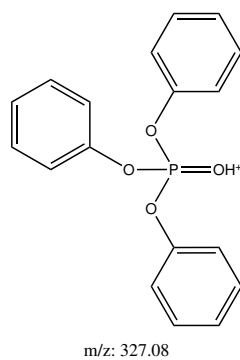**Figure 86:** BPA-BDPP daughter ions with more than 40% abundance.

m/z: 327.08

**Figure 87:** BPA-BDPP daughter ions with less than 20% abundance.

4.4.19 DnBP - Positive Mode

DnBP has medium abundance on several fragment ions with only low to medium collision energy required. However, some of the fragments show unfamiliar patterns. There seem to be formation of NH_2 adducts such as the 170 and 129 m/z fragments. Due to uniqueness among PFRs, 155 m/z is recommended as quantification while 99 m/z is recommended as confirmation ion to avoid the adducts. See figs. 88 to 91 for spectra and suggested structures of the daughter fragments.
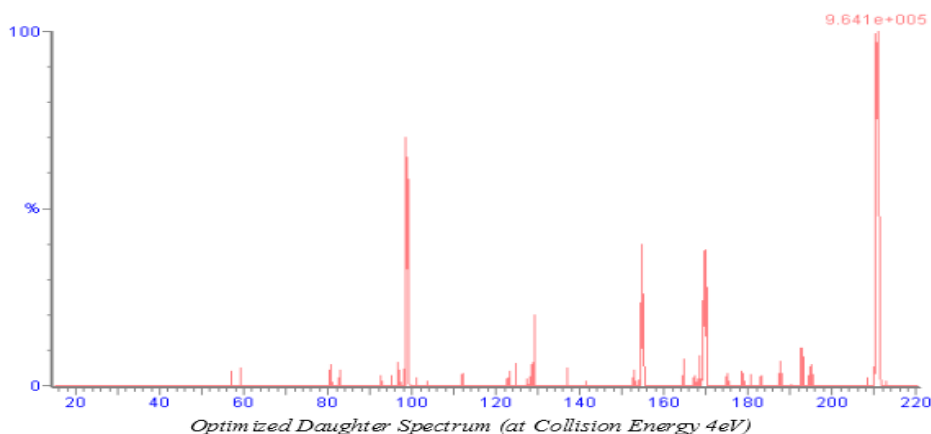
Compound	Formula/Mass		Parent m/z	Cone Voltage	Daughters	Collision Energy	Ion Mode
DnBP	C8H19O4P	1	210.88	12	98.78	12	ES+
		2	210.88	12	154.86	4	ES+
		3	210.88	12	169.75	4	ES+
		4	210.88	12	128.80	10	ES+

Figure 88: Spectrum and fragments generated with IntelliStart
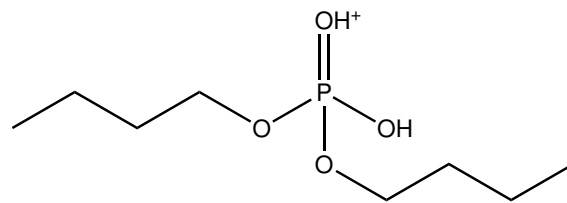
m/z: 211.11

Figure 89: DnBP precursor ion

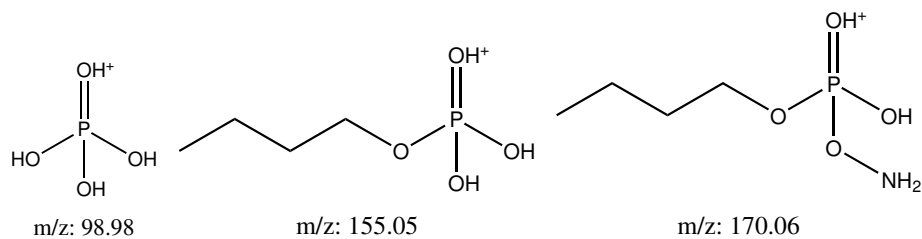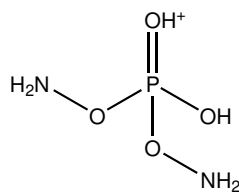m/z: 98.98   m/z: 155.05   m/z: 170.06

Figure 90: DnBP+ daughter ions with more than 40% abundance.


m/z: 129.01

Figure 91: DnBP+ daughter ions with more than 20% abundance.

4.4.20   DnBP - Negative Mode

Even though the mechanism in negative mode is not the same as in positive ESI mode with a bit higher collision energy requirement, the pattern seem to be similar. 153 m/z follows the same pattern as its positive pathway with 2 less hydrogens, and 97 m/z is also present, but with significantly lower abundance. Instead 79 m/z yields significant abundance. The 81 m/z positive analogue is not uncommon in positive mode. Thus, 153 m/z is recommended as the quantification ion, while 79 m/z is recommended as confirmation ion. See figs. 92 to 95 for spectra and suggested daughter ion structures.
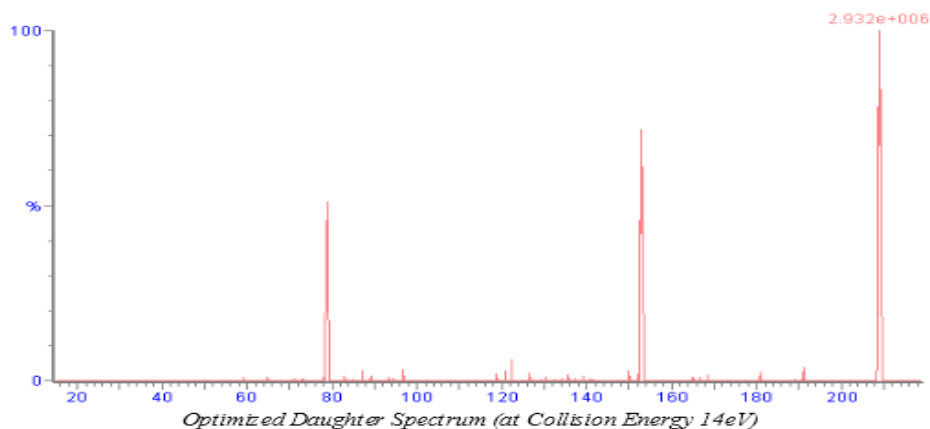
Optimized Daughter Spectrum (at Collision Energy 14eV)

Compound	Formula/Mass		Parent m/z	Cone Voltage	Daughters	Collision Energy	Ion Mode
		1	209.01	4	78.89	22	ES-
2020_DBP	C8H19O4P	2	209.01	4	153.01	14	ES-
		3	209.01	4	96.92	20	ES-

Figure 92: Spectrum and fragments generated with IntelliStart

m/z: 209.09
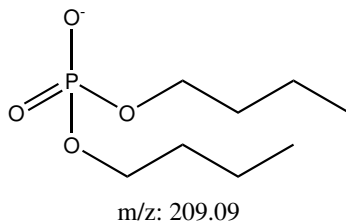
Figure 93: DnBP precursor ion

m/z: 153.03   m/z: 78.96 (100.0%)

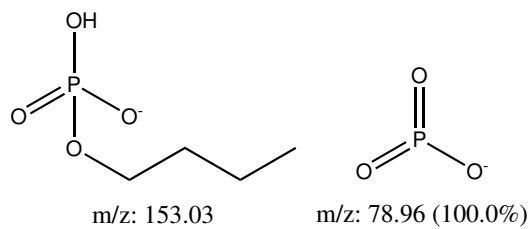**Figure 94:** TMP daughter ions with more than 40% abundance.
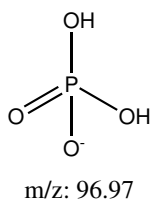

m/z: 96.97

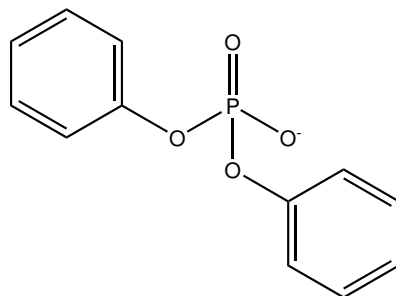**Figure 95:** DnBP- daughter ions with less than 20% abundance.

4.4.21 DPP - Negative Mode

All daughter ions required relatively high collision energy. An ion of special interest is the 93 m/z daughter ion with the largest abundance which is an ion not found in positive as this would suggest cleavage of the P-O bond instead of the C-O bond. The rest of the ions 79, 155 and 173 m/z follow the same pathway as it would've in positive mode. Since the 93 m/z ion is not unique to the compound it is initially not a fragment that should be used as the quantification ion. However, as the breakage of a second P-O bond would make the molecule become very unstable, this is therefore most probably not occur. Hence, 93 m/z is recommended as the quantification ion and 155 is recommended as the confirmation ion. See figs. 96 to 98 and 100 for spectra and suggested daughter ion structures.
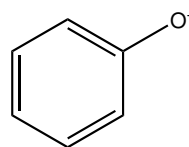

Optimized Daughter Spectrum (at Collision Energy 24eV)
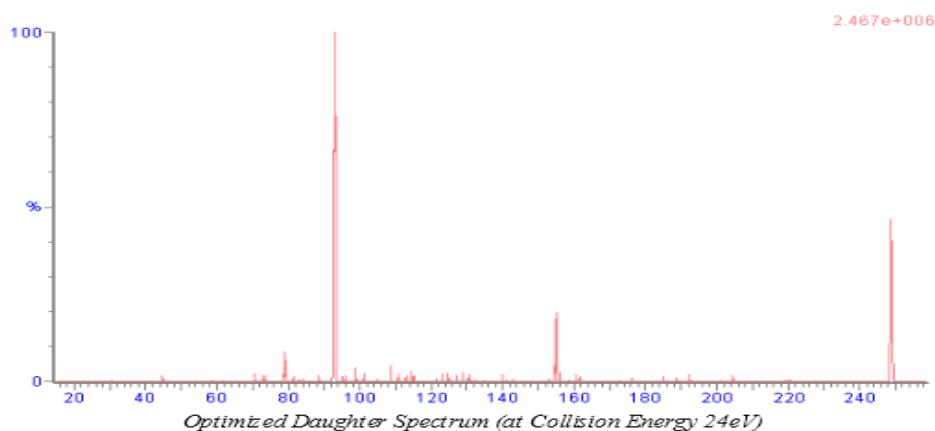
Compound	Formula/Mass		Parent m/z	Cone Voltage	Daughters	Collision Energy	Ion Mode
2020_DPhP	C12H11O4P	1	249.01	8	93.01	28	ES-
		2	249.01	8	154.97	20	ES-
		3	249.01	8	78.95	24	ES-
		4	249.01	8	173.00	20	ES-

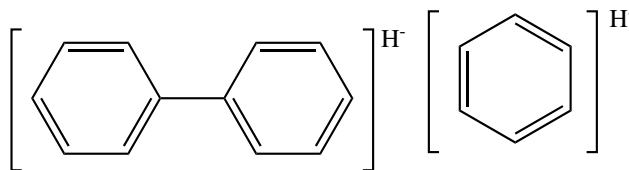**Figure 96:** Spectrum and fragments generated with IntelliStart

m/z: 249.03

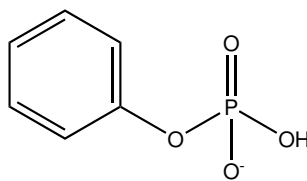**Figure 97:** DPP precursor ion

m/z: 93.03

Figure 98: DPP daughter ions with more than 80% abundance.

m/z: 155.09   m/z: 79.06

**Figure 99:** DPP daughter ions with more than 20% abundance.

m/z: 173.00

**Figure 100:** DPP daughter ions with less than 20% abundance.

4.4.22   BCEP

The collision energy required for the daughter fragments are medium to high. and only 191 and 207 *m/z* are of high abundance. However, the suggseted structure of both of these ions do not follow the common fragmentation pattern, as it seems as if alcohol groups have been replaced by hydrogen. This structure is based on the fact the loss at 207 and 191 *m/z* is less than the mass of chlorine. Instead it matches the loss of one and two oxygen atoms respectively. These two ions then follow their own pattern of P-O cleavage and P-H bond substitution. As they both follow the same fragmentation pattern these two ions are a good pair of quantification and confirmation ions. See figs. 101 to 105 for spectra and suggested daughter ion structures.
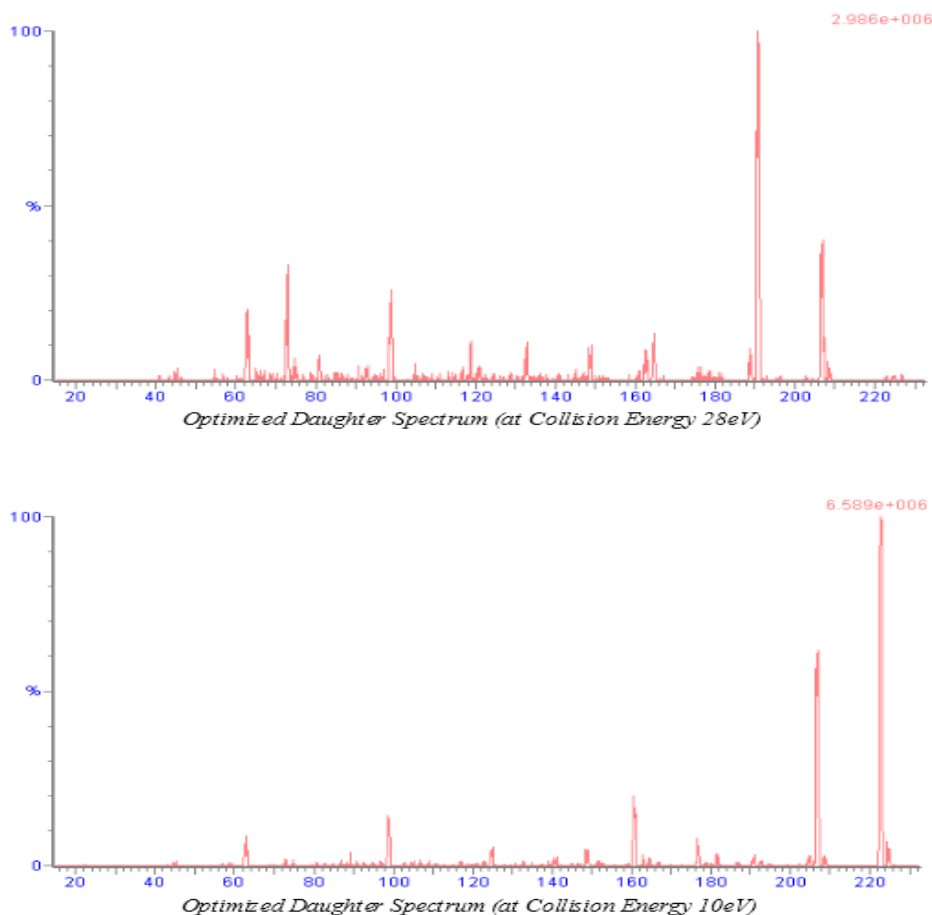
Compound	Formula/Mass		Parent m/z	Cone Voltage	Daughters	Collision Energy	Ion Mode
BCEP	C4H9Cl2O4P	1	222.87	76	190.78	28	ES+
		2	222.87	76	98.76	14	ES+
		3	222.87	76	160.75	10	ES+
		4	222.87	76	62.89	16	ES+

Figure 101: Spectrum and fragments generated with IntelliStart

74
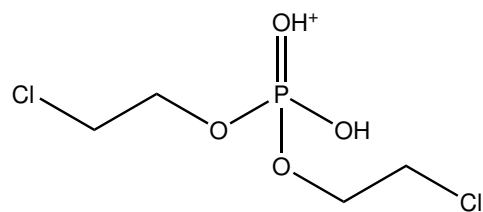
m/z: 222.97

Figure 102: BCEP precursor ion
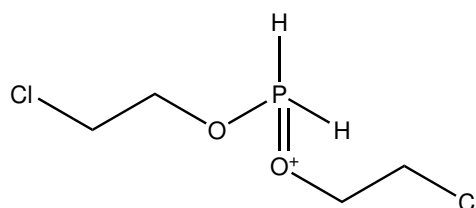
m/z: 190.98

Figure 103: BCEP daughter ions with more than 80% abundance.

m/z: 206.97

Figure 104: BCEP daughter ions with more than 40% abundance.
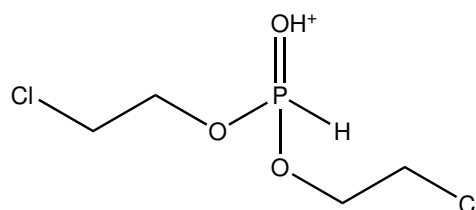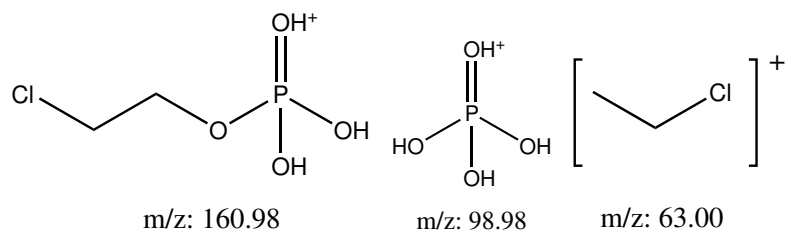
m/z: 160.98   m/z: 98.98   m/z: 63.00

Figure 105: BCEP daughter ions with more than 20% abundance.

4.4.23 BCIPP

The collision energy required for daughter fragments of BCIPP vary from low to high, where all ions follow the common fragmentation patern and the 99 m/z ion is the only with very high abundance. However, 175 and 77 m/z also yield acceptable abundance. As 175 m/z is the only unique PFR daughter ion this is the recommended quantification, while 99 m/z is the recommended confirmation ion. See figs. 106 to 109 for spectra and the suggested structures of the daughter ions.
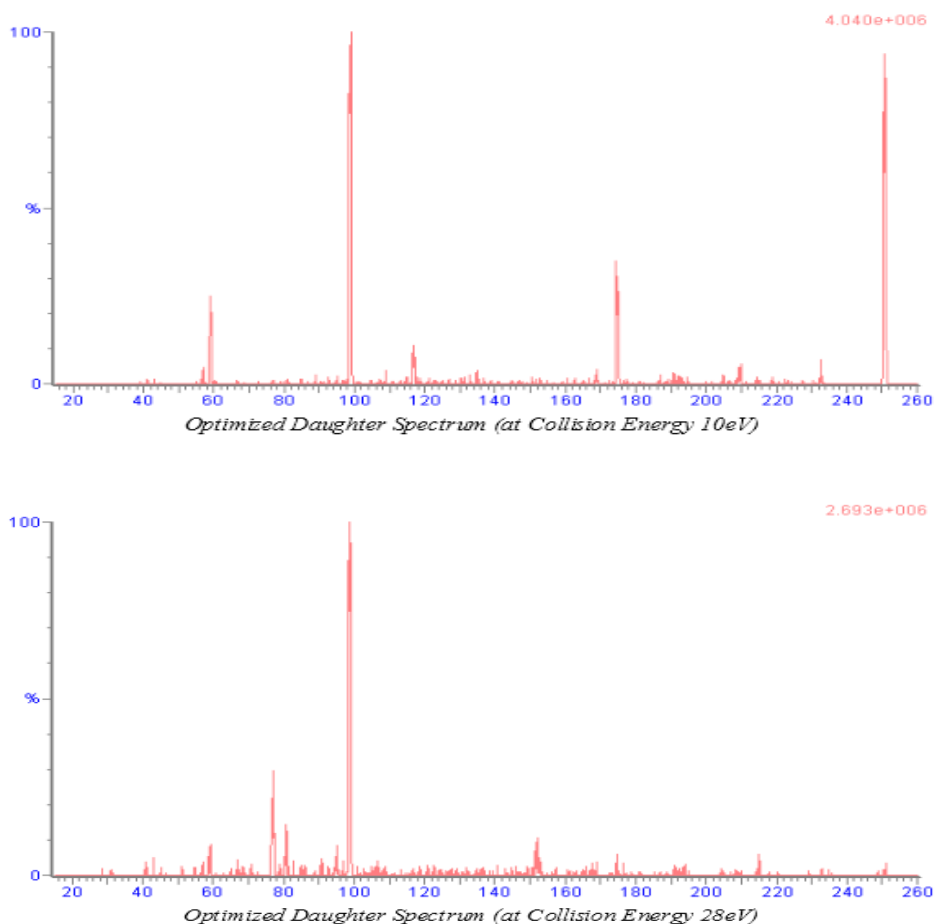
Compound	Formula/Mass		Parent m/z	Cone Voltage	Daughters	Collision Energy	Ion Mode
BCIPP	C6H13Cl2O4P	1	250.77	16	98.83	16	ES+
		2	250.77	16	174.79	6	ES+
		3	250.77	16	58.99	10	ES+
		4	250.77	16	76.93	28	ES+

Figure 106: Spectrum and fragments generated with IntelliStart

m/z: 251.00
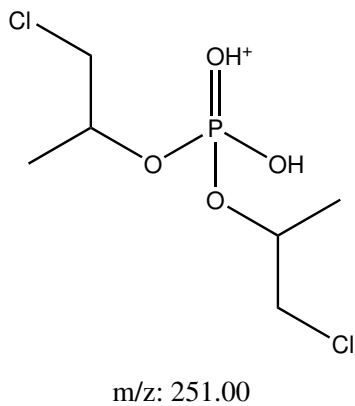
Figure 107: BCIPP precursor ion

m/z: 98.98
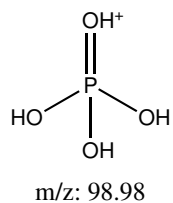
Figure 108: BCIPP daughter ions with more than 80% abundance.

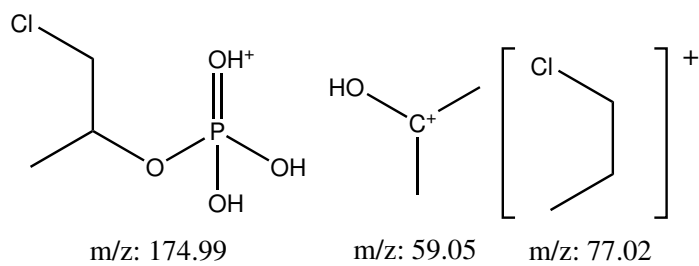m/z: 174.99   m/z: 59.05   m/z: 77.02

Figure 109: BCIPP daughter ions with more than 20% abundance.

77

4.4.24 BBOEP - Positive Mode

The collision energy required for the daughter fragments are all medium, and the most abundant daughter ion is 199 m/z. The ions 83, 101 and 283 m/z are also of decent abundance. However, it is worth to note that both 83 and 283 m/z follow the P-O to P-H substitution pattern. Even though the 101 m/z ion has a larger abundance than 83 and 283 m/z, it is not unique to the compound. Therefore 199 m/z is recommended as the quantification ion and 83 or 283 are recommended as the confirmation ion. See figs. 110 to 114 for spectra and suggested structures of the daughter ions.
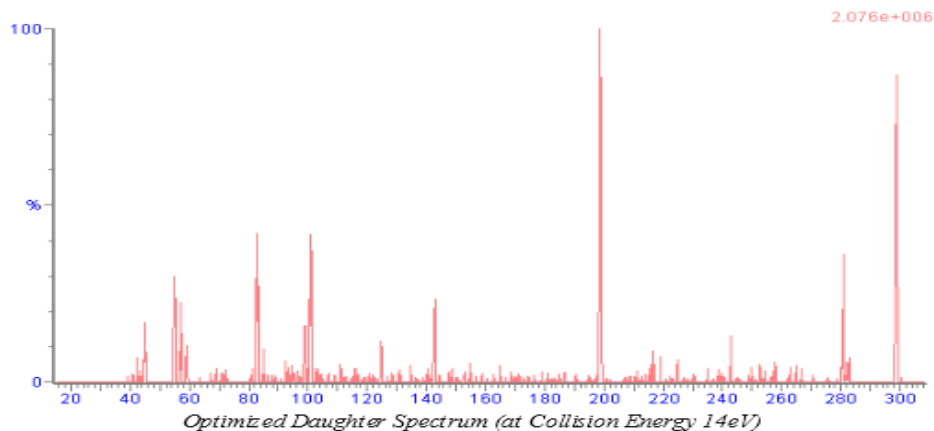
Compound	Formula/Mass		Parent m/z	Cone Voltage	Daughters	Collision Energy	Ion Mode
BBOEP	C12H27O6P	1	298.87	16	198.83	10	ES+
		2	298.87	16	82.90	14	ES+
		3	298.87	16	100.96	14	ES+
		4	298.87	16	54.96	14	ES+

Figure 110: Spectrum and fragments generated with IntelliStart

m/z: 299.16
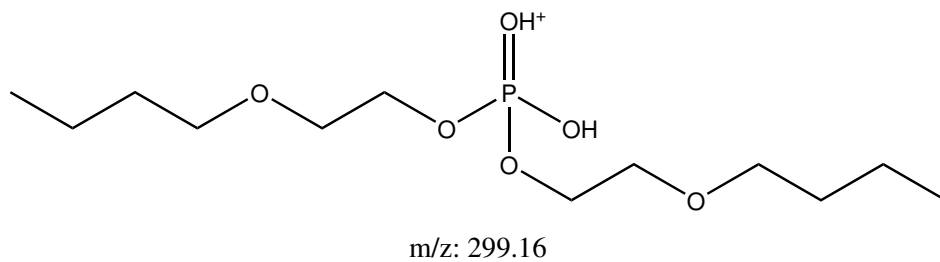
Figure 111: BBOEP precursor ion

m/z: 199.07
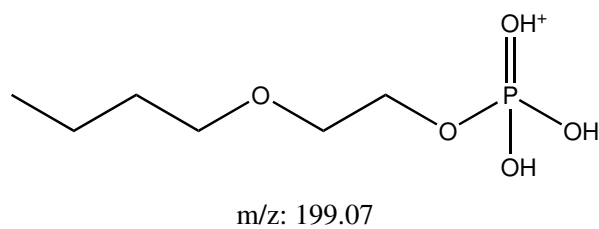
Figure 112: BBOEP+ daughter ions with more than 80% abundance.

m/z: 82.99   m/z: 101.10
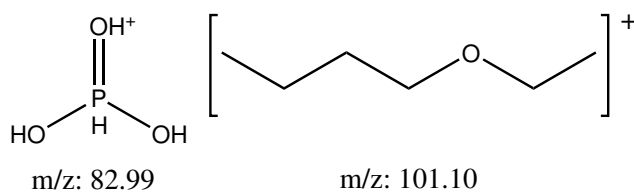
Figure 113: BBOEP+ daughter ions with more than 40% abundance.

m/z: 55.05   m/z: 283.17
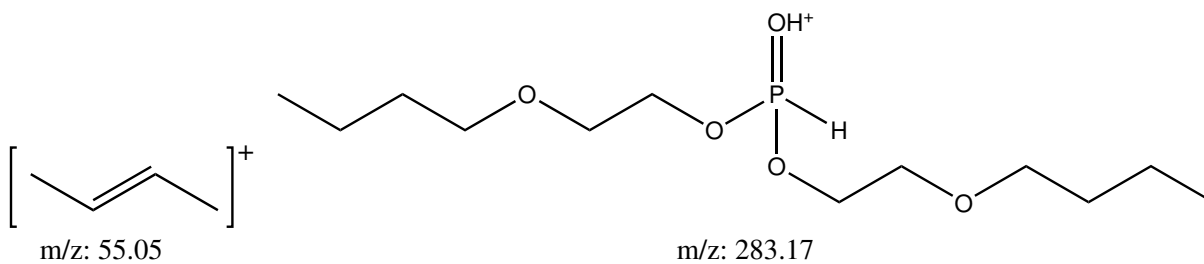
**Figure 114:** BBOEP+ daughter ions with more than 20% abundance.

4.4.25 BBOEP - Negative Mode

The collision energy required for the daughter fragments of BBOEP is medium to very large in negative mode. Like in positive mode there there seem to be sequential oxygen loss in negative mode as well, such as 281 and 265 m/z. As 197 m/z follows the general pattern and has a significant abundance this is recommended as the quantification ion while 79 m/z is recommended as the confirmation ion. See figs. 115 to 119 for spectra and the suggested daughter ion structures.

Optimized Daughter Spectrum (at Collision Energy 20eV)
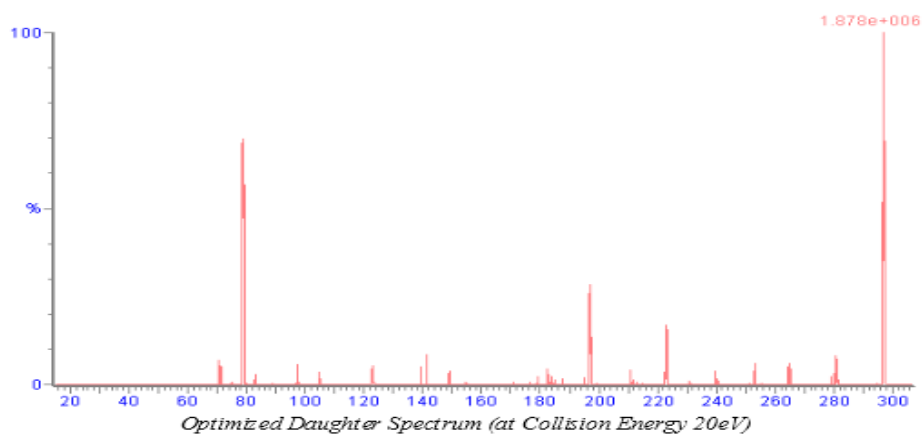
Compound	Formula/Mass		Parent m/z	Cone Voltage	Daughters	Collision Energy	Ion Mode
2020_BBOEP	C12H27O6P	1	297.12	60	78.95	26	ES-
		2	297.12	60	197.07	16	ES-
		3	297.12	60	183.02	32	ES-
		4	297.12	60	223.10	20	ES-

Figure 115: Spectrum and fragments generated with IntelliStart

m/z: 297.15
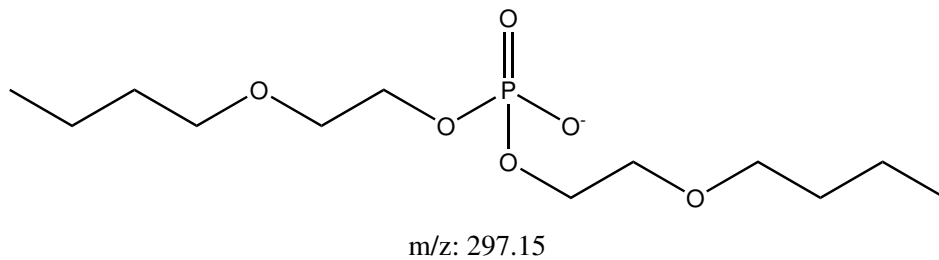
Figure 116: BBOEP- precursor ion

m/z: 78.96 (100.0%)
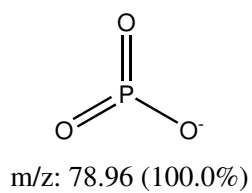
Figure 117: BBOEP- daughter ions with more than 60% abundance.

m/z: 197.06
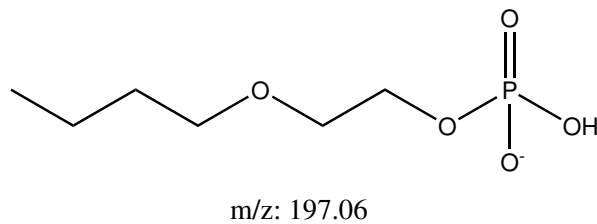
Figure 118: BBOEP- daughter ions with more than 20% abundance.

m/z: 183.08
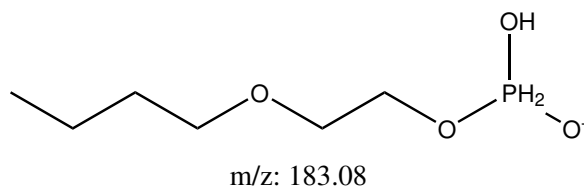
Figure 119: BBOEP- daughter ions with less than 20% abundance.

4.4.26 BBOEHEP

The optimized collision energy requirement ranges from medium to high for the abundance of the daughter ions of BBOEHEP where the ion with the highest abundance is 243 m/z. It is worth noting that the larger ester groups are cleaved before the smaller ester group as they have larger abundances than those cleaving the smaller ester group first. However, it is important to keep in mind that there are two larger groups and only one smaller group and that cleavage of the ether bond is possible, making two smaller ester groups. Yet this ether cleavage was not really observed in BBOEP signaling that it will most likely won't occur in BBOEHEP either. Based on abundance 243 m/z is recommended as quantification ion and 143 is recommended as confirmation ion. See figs. 120 to 123 for spectra and suggested daughter ion structures.
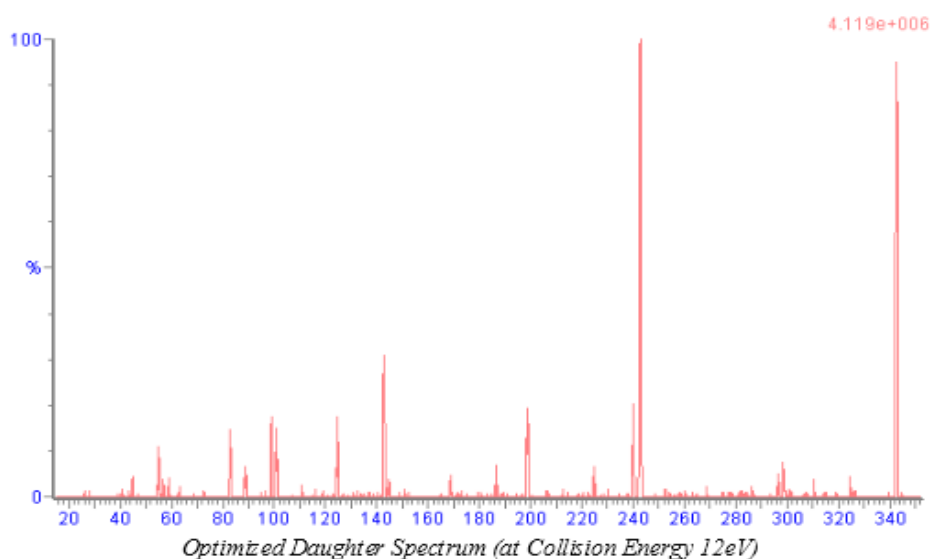
Compound	Formula/Mass		Parent m/z	Cone Voltage	Daughters	Collision Energy	Ion Mode
BBOEHEP	C14H31O7P	1	342.83	8	242.84	10	ES+
		2	342.83	8	142.82	12	ES+
		3	342.83	8	98.76	26	ES+
		4	342.83	8	198.84	12	ES+

Figure 120: Spectrum and fragments generated with IntelliStart

82

m/z: 343.19
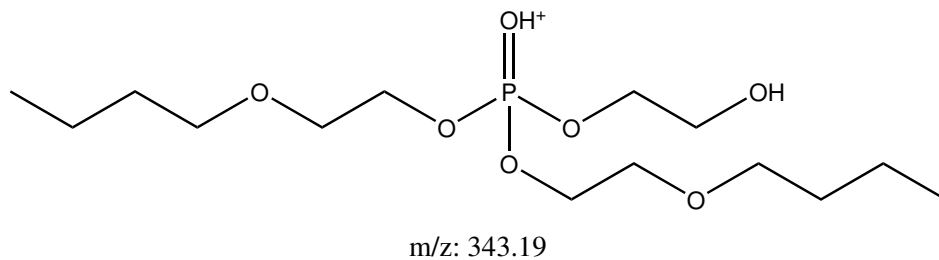
Figure 121: BBOEHEP precursor ion

m/z: 243.10
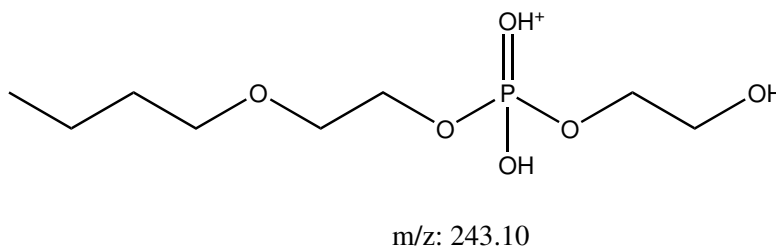
Figure 122: BBOEHEP daughter ions with more than 80% abundance.

m/z: 143.01   m/z: 199.07   m/z: 98.98
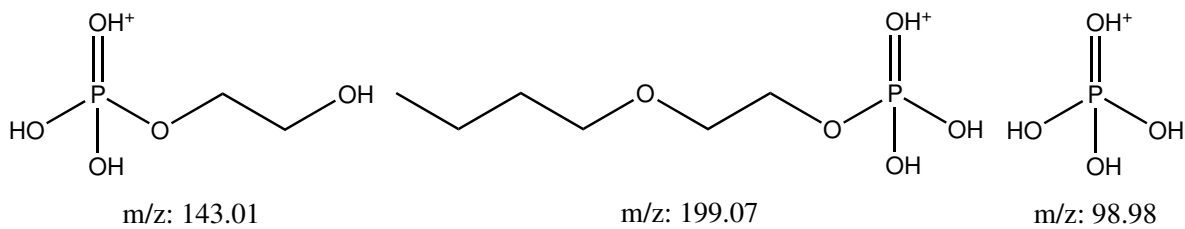
Figure 123: BBOEHEP daughter ions with more than 20% abundance.

4.4.27   3OH-TBOEP

The optimized collision energy requirement is medium for the abundance of all the daughter ions of 3OH-TBOEP, where the highest abundance is 243 m/z. The issue with metabolites is that they are going to overlap in m/z as they are similar in structure. Therefore separation of metabolites in the LC in order to avoid overlap of signals is recommended. Assuming no overlap occur for these metabolites 243 m/z is recommended as the quantification ion and 299 is recommended as the confirmation ion. See figs. 124 to 128 for spectra and suggested daughter ion structures.

Optimized Daughter Spectrum (at Collision Energy 14eV)
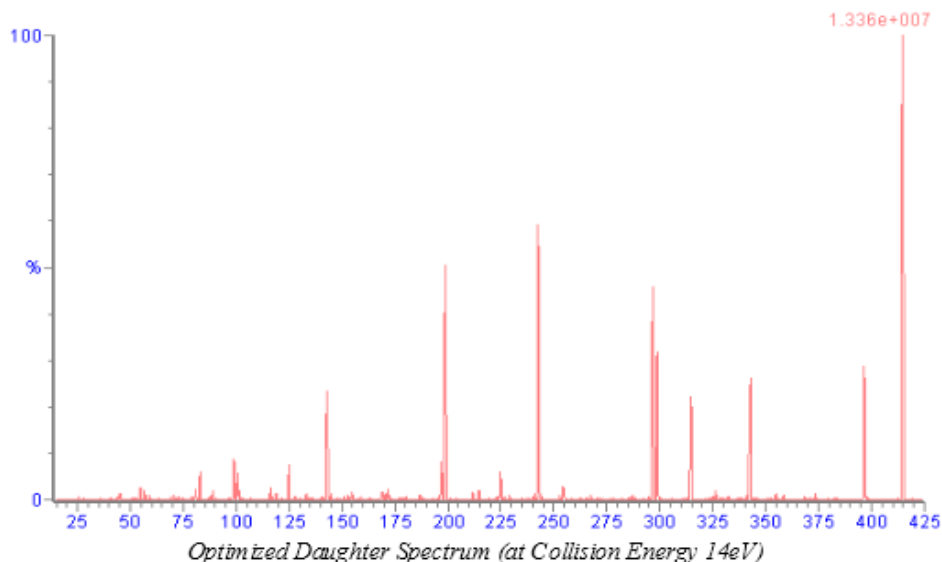
Compound	Formula/Mass		Parent m/z	Cone Voltage	Daughters	Collision Energy	Ion Mode
3OH-TBOEP	C18H39O8P	1	414.82	28	242.87	14	ES+
		2	414.82	28	299.16	14	ES+
		3	414.82	28	198.82	14	ES+
		4	414.82	28	142.81	18	ES+

Figure 124: Spectrum and fragments generated with IntelliStart

m/z: 415.25
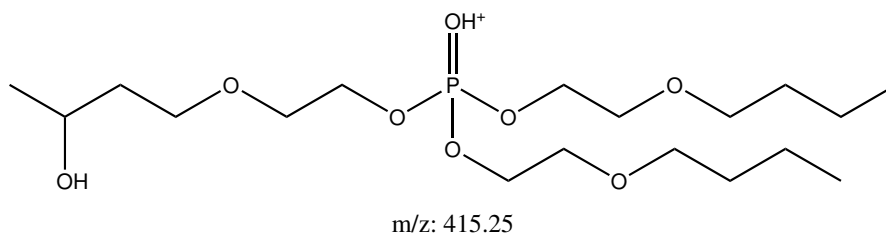
Figure 125: 3OH-TBOEP precursor ion

m/z: 243.10
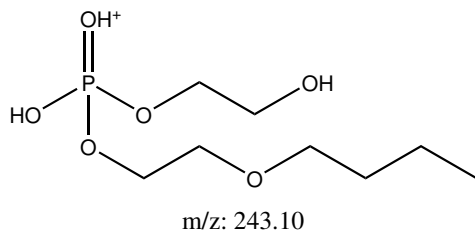
Figure 126: 3OH-TBOEP daughter ions with more than 60% abundance.

m/z: 199.07

m/z: 299.16
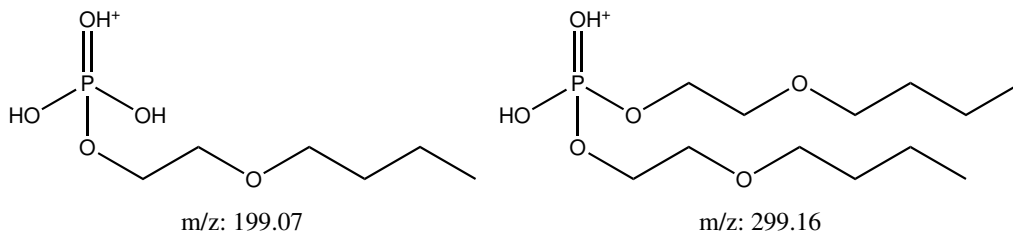
Figure 127: 3OH-TBOEP daughter ions with more than 40% abundance.

m/z: 143.01
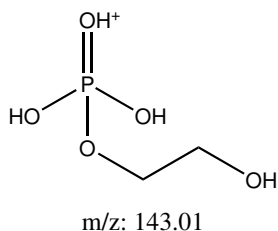
Figure 128: 3OH-TBOEP daughter ions with more than 20% abundance.

4.4.28 Comparison of Daughter Ions

As TnPP, TCIPP and BBOEHEP all shared the same daughter and eluted approximately at the same time this can be the reason the analytical parameters for their 99 m/z ion were not optimal. Being aware of overlapping retention time and daughter fragments is very important when developing methods in analytical chemistry. Therefore table 10 includes recommendations for several what quantification and confirmation ions to chose in further studies of PFRs. It is clear that many literature studies prefer to use the 99 m/z ion, however, as high throughput is important in analytical studies, this project would recommended further studies to abstain from using this fragment so analytes can co-elute without causing confounding problems.

Table 10: Combined tables 2 and 5 with information about experimentally used transitions for analyzation with ethylacetate and literature used transitions with the recommendations for quantification ion (QI) and confirmation ion (CI) for comparison. m/z analyzed in negative mode are marked with "-". "," separates ESI positive from negative mode. Fragments separated by "/" are considered equal and either are recommended. When multiple are recommended as QI, any combination of QI and CI can be used.

Compound	RT	QI Used	CI Used	QI Recommended	CI Recommended	QI Literature	CI Literature
TMP	0.29	79	109	109	79	110	79
TEP	0.59	127	155	127	155	155	127/138
TnPP	1.87	99		141	183	99	183/141
TnBP	2.28	155	211	211	155	99	155/210
TiBP	2.28	211	155	211	155		
TBOEP	2.38	299	199	299	199	299	199
TEHP	3.29	99	71	323	99	99	80/133
TCEP	1.52	99	223	223/161/125		223	99/63
TCIPP	1.89	99		251/175		99	250/175/125
TDCIPP	2.22	99		319/209		99	320/209
TPP	2.28	152	215	251	215	377	152/215
TMPP	2.54	91	165	243	279	165	99
DPMP	2.37	152	229			152	99/228
EHDPP	2.64	273		273	281	251	151/77
IDPP	2.79	153	77			251	151/77
BPDP							
TTBPP	3.04	152	439	439/383/327		479	367
RDP	2.54	419	481			481	419
V6	2.06	359		359/297/235		361	235
BPA-BDPP	2.76	367	327	367	327	367	327
DnBP				155, 153-	99, 79-	79	153
DPP				93-	155-	93	155
BCEP				207/191		35	37
BCIPP				175	99	35	37
BBOEP				190, 197-	283/83, 79-	79	197
BBOEHEP	1.82	243	99	243	143		
3OH-TBOEP	1.97	199	243	243	299		
TEP-d15	0.57	134	102			135	167
TnBP-d27	2.26	102				102	166/82
TCEP-d12	1.50	102	130			102	82
TDICPP-d15	2.21	216	102			102	331/201

5 Conclusion and Further Work

This project was initially intended to finish the second phase of a two part project to first develop a rapid method to analyze PFRs and secondly perform a quantitative analysis to determine their presence in harbor porpoises. However, due to COVID-19, major sections of the second part was cancelled which would've significantly increased the certainty of the results obtained. Still, this project did yield other sorts of results. A very thorough analyzation of fragmentation pathways and patterns by studying possible daughter structures based on MS/MS results will hopefully assist future high throughput PFR analysis.

This project also offers insights in the possibility that TnBP, TPP and BBOEHEP, a metabolite of TBOEP, are present in the liver of porpoises from the Norwegian coast. There's also some weak indication that IDPP, TCIPP, TBOEP and BPA-BDPP could be present in the liver. TEHP, TDCIPP and EHDP seem to be present in the analyzation instrument and should be investigated following the same protocol on another instrument in order to test this hypothesis. During the extraction process it seems possible that pollution of TMP, TEP, RDP, TTBPP, DPMP and maybe TBOEP occur during extraction. A non-contact with plastic could test this hypothesis such as using glassware. Another possible source of contamination is that pollution occurs during the evaporation.

All of the claims above should be further investigated as the certainty of the results are low due to few tested samples.

6 Acknowledgement

References

Al-Jitan, S., Alkhoori, S. A., and Yousef, L. F. (2018). Chapter 13 - phenolic acid from plants: Extraction and application to human health. In ur Rahman, A., editor, *Studies in Natural Products Chemistry*, volume 58 of *Studies in Natural Products Chemistry*, pages 389 – 417. Elsevier.

Alygizakis, N., Galani, K., and Thomaidis, N. (2019). Tris(2-ethylhexl)phosphate; lc-esi-qtof; ms2; ce: Ramp 24.3-36.5 ev; r=35000; [m+h]+. MassBank EU. MS splash splash10-0002-9630000000-04626de08b9fd0ba65f7.

Alzualde, A., Behl, M., Sipes, N. S., Hsieh, J.-H., Alday, A., Tice, R. R., Paules, R. S., Muriana, A., and Quevedo, C. (2018). Toxicity profiling of flame retardants in zebrafish embryos using a battery of assays for developmental toxicity, neurotoxicity, cardiotoxicity and hepatotoxicity toward human relevance. *Neurotoxicology and Teratology*, 70:40 – 50.

Banerjee, B., Seth, V., Bhattacharya, A., Pasha, S., and Chakraborty, A. (1999). Biochemical effects of some pesticides on lipid peroxidation and free-radical scavengers. *Toxicology Letters*, 107(1):33 – 47.

Berendsen, B. J. A., Stolker, L. A. M., and Nielen, M. W. F. (2013). The (un)certainty of selectivity in liquid chromatography tandem mass spectrometry. *Journal of The American Society for Mass Spectrometry*, 24(1):154–163.

Bermejo, P., Capelo, J., Mota, A., Madrid, Y., and Cámara, C. (2004). Enzymatic digestion and ultrasonication: a powerful combination in analytical chemistry. *TrAC Trends in Analytical Chemistry*, 23(9):654 – 663.

Bjørge, A. and Tolley, K. A. (2018). Harbor porpoise: Phocoena phocoena. In Würsig, B., Thewissen, J., and Kovacs, K. M., editors, *Encyclopedia of Marine Mammals (Third Edition)*, pages 448 – 451. Academic Press, third edition edition.

Blum, A., Behl, M., Birnbaum, L. S., Diamond, M. L., Phillips, A., Singla, V., Sipes, N. S., Stapleton, H. M., and Venier, M. (2019). Organophosphate ester flame retardants: Are they a regrettable substitution for polybrominated diphenyl ethers? *Environmental Science & Technology Letters*, 6(11):638–649.

Bolgar, M., Hubball, J., Groeger, J., and Meronek, S. (2015). *Handbook, For the Chemical Analysis of Plastic and Polymer Additives, 2nd Edition*, chapter Additives as Possible Hazards: Extractable and Leachable Compounds, page xii. CRC Press.

Brandsma, S. H., de Boer, J., van Velzen, M. J., and Leonards, P. E. (2014). Organophosphorus flame retardants (pfrs) and plasticizers in house and car dust and the influence of electronic equipment. *Chemosphere*, 116:3 – 9. Flame Retardants in the Environment - Papers presented at 6th International Symposium on Flame Retardants (BFR2013), San Francisco from April 7-10.

Brandsma, S. H., Leonards, P. E., Leslie, H. A., and de Boer, J. (2015). Tracing organophosphorus and brominated flame retardants and plasticizers in an estuarine food web. *Science of The Total Environment*, 505:22 – 31.

Brandsma, S. H., Sellström, U., de Wit, C. A., de Boer, J., and Leonards, P. E. G. (2013). Dust measurement of two organophosphorus flame retardants, resorcinol bis(diphenylphosphate) (rbdpp) and bisphenol a bis(diphenylphosphate) (bpa-bdpp), used as alternatives for bde-209. *Environmental Science & Technology*, 47(24):14434–14441.

Bruins, A. P. (1998). Mechanistic aspects of electrospray ionization. *Journal of Chromatography A*, 794(1-2).

Castorina, R., Bradman, A., Stapleton, H. M., Butt, C., Avery, D., Harley, K. G., Gunier, R. B., Holland, N., and Eskenazi, B. (2017). Current-use flame retardants: Maternal exposure and neurodevelopment in children of the chamacos cohort. *Chemosphere*, 189:574 – 580.

Chen, D., Letcher, R. J., and Chu, S. (2012). Determination of non-halogenated, chlorinated and brominated organophosphate flame retardants in herring gull eggs based on liquid chromatography–tandem quadrupole mass spectrometry. *Journal of Chromatography A*, 1220:169 – 174.

Chu, S., Chen, D., and Letcher, R. J. (2011). Dicationic ion-pairing of phosphoric acid diesters post-liquid chromatography and subsequent determination by electrospray positive ionization-tandem mass spectrometry. *Journal of Chromatography A*, 1218(44):8083 – 8088.

Cristale, J., Ramos, D. D., Dantas, R. F., Junior, A. M., Lacorte, S., Sans, C., and Esplugas, S. (2016). Can activated sludge treatments and advanced oxidation processes remove organophosphorus flame retardants? *Environmental Research*, 144:11 – 18.

D'Agostino, P. A. and Provost, L. R. (1994). Capillary column gas chromatographic-tandem mass spectrometric analysis of phosphate esters in the presence of interfering hydrocarbons. *Journal of Chromatography A*, 670(1):127 – 134.

Dams, R., Huestis, M. A., Lambert, W. E., and Murphy, C. M. (2003). Matrix effect in bioanalysis of illicit drugs with lc-ms/ms: Influence of ionization type, sample preparation, and biofluid. *Journal of the American Society for Mass Spectrometry*, 14.

Dass, C. (2007). *Fundamentals of Contemporary Mass Spectrometry*, chapter 14. Wiley-Interscience.

Dodson, R. E., Perovich, L. J., Covaci, A., Van den Eede, N., Ionas, A. C., Dirtu, A. C., Brody, J. G., and Rudel, R. A. (2012). After the pbde phase-out: A broad suite of flame retardants in repeat house dust samples from california. *Environmental Science & Technology*, 46(24):13056–13066. PMID: 23185960.

Ettre, L. (1980). Relative retention expressions in chromatography. *Journal of Chromatography A*, 198(3):229 – 234.

Freedonia (2011). *Global demand for flame retardants to rise 6.1% per year through 2014*, pages 9–10. Elsevier BV.

Freiser, H. and Jiang, Q. (2009). Optimization of the enzymatic hydrolysis and analysis of plasma conjugated gamma-cehc and sulfated long-chain carboxychromanols, metabolites of vitamin e. *Analytical biochemistry*, 388(2):260—265.

García-López, M., Rodríguez, I., and Cela, R. (2010). Mixed-mode solid-phase extraction followed by liquid chromatography–tandem mass spectrometry for the determination of tri- and di-substituted organophosphorus species in water samples. *Journal of Chromatography A*, 1217(9):1476 – 1484.

Giulivo, M., Capri, E., Eljarrat, E., and Barceló, D. (2016). Analysis of organophosphorus flame retardants in environmental and biotic matrices using on-line turbulent flow chromatography-liquid chromatography-tandem mass spectrometry. *Journal of Chromatography A*, 1474:71 – 78.

Giulivo, M., Capri, E., Kalogianni, E., Milacic, R., Majone, B., Ferrari, F., Eljarrat, E., and Barceló, D. (2017). Occurrence of halogenated and organophosphate flame retardants in sediment and fish samples from three european river basins. *Science of The Total Environment*, 586:782 – 791.

Guo, X., Mu, T., Xian, Y., Luo, D., and Wang, C. (2016). Ultra-performance liquid chromatography tandem mass spectrometry for the rapid simultaneous analysis of nine organophosphate esters in milk powder. *Food Chemistry*, 196:673 – 681.

Gustavsson, J., Ahrens, L., Nguyen, M. A., Josefsson, S., and Wiberg, K. (2017). Development and comparison of gas chromatography–mass spectrometry techniques for analysis of flame retardants. *Journal of Chromatography A*, 1481:116 – 126.

Hallanger, I. G., Sagerup, K., Evenset, A., Kovacs, K. M., Leonards, P., Fuglei, E., Routti, H., Aars, J., Strøm, H., Lydersen, C., and Gabrielsen, G. W. (2015). Organophosphorous flame retardants in biota from svalbard, norway. *Marine Pollution Bulletin*, 101(1):442 – 447.

Hammond, P., Bearzi, G., Bjørge, A., Forney, K., Karczmarski, L., Kasuya, T., Perrin, W., Scott, M., Wang, J., Wells, R., and Wilson, B. (2008). Phocoena phocoena, harbour porpoise. *The IUCN Red List of Threatened Species 2008: e.T17027A6734992.*

Ho, C. S., Lam, C. W. K., Chan, M. H. M., Cheung, R. C. K., Law, L. K., Lit, L. C. W., Ng, K. F., Suen, M. W. M., and Tai, H. L. (2003). Electrospray ionisation mass spectrometry: Principles and clinical applications. *The Clinical biochemist. Reviews*, 24(1):3–12.

Hoffman, K., Stapleton, H. M., Lorenzo, A., Butt, C. M., Adair, L., Herring, A. H., and Daniels, J. L. (2018). Prenatal exposure to organophosphates and associations with birthweight and gestational length. *Environment International*, 116:248 – 254.

Hunt, T. (2000). Polymer additives: Supercritical fluid chromatography. In Wilson, I. D., editor, *Encyclopedia of Separation Science*, pages 3901 – 3906. Academic Press, Oxford.

Ionas, A. C. (2016). *Migration of hazardous chemicals to the indoor environment - "Horizon Scanning" for flame retardants present in consumer goods.* PhD thesis, University of Antwerp and VU University Amsterdam.

Kazakevich, Y., LoBrutto, R., Chen, G., Zhang, L.-K., and Pramanik, B. N. (2007). *HPLC for Pharmaceutical Scientists*, chapter LC/MS: Theory, Instrumentation, and Application to Small Molecules, pages 300–304. John Wiley & Sons, Inc.

Liu, L.-Y., Salamova, A., He, K., and Hites, R. A. (2015). Analysis of polybrominated diphenyl ethers and emerging halogenated and organophosphate flame retardants in human hair and nails. *Journal of Chromatography A*, 1406:251 – 257.

Liu, Z., Zhao, X., Wu, L., Zhou, S., Gong, Z., Zhao, Y., and Wu, Y. (2020). Development of a sensitive and reliable uhplc-ms/ms method for the deteremination of multiple urinary biomarkers of mycotoxin exposure. *Toxins*, 12(3).

Lundanes, E., Reubsaet, L., and Breibokk, T. (2014). *Chromatography*, chapter 3. Wiley-VCH.

Mariani, G., S, T., Comero, S., Buttiglieri, G., Paracchini, B., Skejo, H., Sanz, L. A., and Gawlik, B. (2017). Short-term isochronous stability study of contaminants of emerging concern in environmental water samples. Technical report, Join Research Center, the European Commission's science and knowledge service.

Marklund, A., Andersson, B., and Haglund, P. (2003). Screening of organophosphorus compounds and their distribution in various indoor environments. *Chemosphere*, 53(9):1137 – 1146.

Matuszewski, B. K., Constanzer, M. L., and Chavez-Eng, C. M. (2003). Strategies for the assessment of matrix effect in quantitative bioanalytical methods based on hplc-ms/ms. *Analytical Cemistry*, 75(13).

McWilliams, A. (2018). *Flame Retardant Chemicals: Technologies and Global Markets*, pages 1–5. BCC Publishing.

Meyer, J. and Bester, K. (2004). Organophosphate flame retardants and plasticisers in wastewater treatment plants. *J. Environ. Monit.*, 6:599–605.

Mortier, K. A., Zhang, G.-F., Van Peteghem, C. H., and Lambert, W. E. (2004). Adduct formation in quantitative bioanalysis: Effect of ionization conditions on paclitaxel. *Journal of the American Society for Mass Spectrometry*, 15(4).

Nygård, E. H. (2019). Method Development for Rapid Determination of Organophosphorus Flame Retardants Exposure using UHPLC-MS/MS. Pre-project, Norwegian University of Science and Technology, Trondheim, Norway.

Papachlimitzou, A., Barber, J. L., Losada, S., Bersuder, P., Deaville, R., Brownlow, A., Penrose, R., Jepson, P. D., and Law, R. J. (2015). Organophosphorus flame retardants (pfrs) and plasticisers in harbour porpoises (phocoena phocoena) stranded or bycaught in the uk during 2012. *Marine Pollution Bulletin*, 98(1):328 – 334.

Pierce, G., Santos, M., Murphy, S., Learmonth, J., Zuur, A., Rogan, E., Bustamante, P., Caurant, F., Lahaye, V., Ridoux, V., Zegers, B., Mets, A., Addink, M., Smeenk, C., Jauniaux, T., Law, R., Dabin, W., López, A., Farré, J. A., González, A., Guerra, A., García-Hartmann, M., Reid, R., Moffat, C., Lockyer, C., and Boon, J. (2008). Bioaccumulation of persistent organic pollutants in female common dolphins (delphinus delphis) and harbour porpoises (phocoena phocoena) from western european seas: Geographical trends, causal factors and effects on reproduction and mortality. *Environmental Pollution*, 153(2):401 – 415.

POPRC (2008). Risk management evaluation for commercial octabromodiphenyl ether. In *Report of the Persistent Organic Pollutants Review Committee on the work of its fourth meetnig*. UN Environment Programme.

Quintana, J., Rodil, R., and Reemtsma, T. (2006). Determination of phosphoric acid mono- and diesters in municipal wastewater by solid-phase extraction and ion-pair liqid chromatography-tandem mass spectrometry. *Analytical Chemistry*, 78(5):1644–1650.

Sala, B., Giménez, J., de Stephanis, R., Barceló, D., and Eljarrat, E. (2019). First determination of high levels of organophosphorus flame retardants and plasticizers in dolphins from southern european waters. *Environmental Research*, 172:289 – 295.

Santín, G., Eljarrat, E., and Barcelåó, D. (2016). Simultaneous determination of 16 organophosphorus flame retardants and plasticizers in fish by liquid chromatography-tandem mass spectrometry. *Journal of Chromatography A*, 1441:34 – 43.

Schulze, T. (2020). Massbank europe mass spectral database.

Schwarzenberg, A., Ichou, F., Cole, R. B., Machuron-Manda, X., Junot, C., Lesagea, D., and Tabet, J.-C. (2013). Identification tree based on fragmentationrules for structure elucidation oforganophosphorus esters by electrospraymass spectrometry. *Jorunal of Mass Spectrometry*, 48(5).

Soltaninejad, K., Shadnia, S., Afkhami-Taghipour, M., Saljooghi, R., Mohammadirad, A., and Abdollahi, M. (2007). Blood β-glucuronidase as a suitable biomarker at acute exposure of severe organophosphorus poisoning in human. *Human & Experimental Toxicology*, 26.

Strand, J., Larsen, M. M., and Lockyer, C. (2005). Accumulation of organotin compounds and mercury in harbour porpoises (phocoena phocoena) from the danish waters and west greenland. *Science of The Total Environment*, 350(1):59 – 71.

Supelco (1998). Guide to solid phase extraction.

ThermoFisher-Scientific (2020). Mass analyzer technology overview | thermo fisher scientific.

Thomas, M., Stapleton, H., Dills, R., Violette, H., Christakis, D., and Sathyanarayana, S. (2017). Demographic and dietary risk factors in relation to urinary metabolites of organophosphate flame retardants in toddlers. *Chemosphere*, 185:918 – 925.

Thornton, J. D. (2011). Extraction, liquid-liquid.

UNEP/POPS/POPRC (2015). Risk management evalutation on decabromodiphenyl ether (commercial mixture, c-decabde). In *Report of the Persistant Organic Pollutats Review Committee on the work of its eleventh meeting*. UNEP.

van der Veen, I. and de Boer, J. (2012). Phosphorus flame retardants: Properties, production, environmental occurrence, toxicity and analysis. *Chemosphere*, 88(10):1119 – 1153.

Verplaetse, R. and Tytgat, J. (2011). Lc-ms/ms in forensic toxicology: what about matrix effects? *TIAFT Bulletin*, 41:8–16.

Wang, S., Cyronak, M., and Yang, E. (2007). Does a stable isotopically labeled internal standard always correct analyte response?: A matrix effect study on a lc/ms/ms method for the determination of carvedilol enantiomers in human plasma. *Journal of Pharmaceutical and Biomedical Analysis*, 43(2):701 – 707.

Wang, X.-W., Liu, J.-F., and Yin, Y.-G. (2011). Development of an ultra-high-performance liquid chromatography–tandem mass spectrometry method for high throughput determination of organophosphorus flame retardants in environmental water. *Journal of Chromatography A*, 1218(38):6705 – 6711.

Waters (2008). A guide to bioanalytical method development. Application Note: 720002710en.

Waters (2020). Beginner's guide to spe - sold-phase extraction.

Waters-Corporation (2020). What types of instruments are used? : Waters.

Wensing, M., Uhde, E., and Salthammer, T. (2005). Plastics additives in the indoor environment—flame retardants and plasticizers. *Science of The Total Environment*, 339(1):19 – 40.

Zhu, J. and Cole, R. B. (2000). Formation and decompositions of chloride adduct ions, [m + cl]-, in negative ion electrospray ionization mass spectrometry. *Journal of the American Society for Mass Spectrometry*, 11(11).